Title: Ocean mixing and ice-sheet control of last deglacial seawater $^{234}U/^{238}U$ evolution

Authors: Tianyu Chen[1*], Laura F. Robinson[1], Matthew P. Beasley[1], Louis M. Claxton[1], Morten B. Andersen[2,3], Lauren J. Gregoire[4], Jemma Wadham[5], Daniel J. Fornari[6], Karen S. Harpp[7]

Affiliations:

[1]Bristol Isotope Group, School of Earth Sciences, University of Bristol, Bristol, UK.

[2]Institute of Geochemistry and Petrology, Department of Earth Sciences, ETH Zürich, Zürich, Switzerland.

[3]School of Earth & Ocean Sciences, Cardiff University, UK

[4]School of Earth and Environment, University of Leeds, Leeds, UK

[5]Bristol Glaciology Centre, School of Geographical Sciences, University of Bristol, Bristol, UK

[6]Department of Geology and Geophysics, Woods Hole Oceanographic Institution

Woods Hole, MA, USA

[7]Geology Department, Colgate University, 13 Oak Drive, Hamilton, NY, USA

* Correspondence to: tc14502@bristol.ac.uk

Abstract: Seawater $^{234}U/^{238}U$ provides global-scale information on continental weathering and is vital for marine U-series geochronology. Previous evidence supports an increase in $^{234}U/^{238}U$ since the last glacial, but the timing and amplitude of its variability was poorly constrained. Here we report two seawater $^{234}U/^{238}U$ records based on well-preserved deep-sea corals from the low latitude Atlantic and Pacific. The Atlantic $^{234}U/^{238}U$ starts to increase before major sea level rise and overshoots the modern value by 3‰ in the early deglaciation. Deglacial $^{234}U/^{238}U$ of the Pacific converges with the Atlantic after the abrupt resumption of Atlantic meridional overturning. We suggest that ocean mixing and early deglacial release of excess ^{234}U from enhanced subglacial melt activity of the Northern Hemisphere ice sheets have driven the observed $^{234}U/^{238}U$ evolution.

One Sentence Summary: Well constrained seawater $^{234}U/^{238}U$ evolution provides evidence of less efficient inter-ocean mixing and enhanced subglacial melt activity early in the last deglaciation.

Main Text: The last deglaciation (18.0-10.5 ka, thousand years ago) saw massive changes in the Earth's surficial environments including temperature and precipitation, as well as the retreat of the Northern Hemisphere (NH) ice sheets and sea-level rise (*1, 2*). These processes have the potential to induce large variability of weathering of the upper continents and the composition of chemical fluxes to the ocean. The ratio $^{234}U/^{238}U$ is one of the isotopic signatures with potential to record global changes in continental weathering during this critical climate transition (*3*).

The activity ratio of ^{234}U to ^{238}U in the modern seawater is ~15% higher than secular equilibrium (*4*), due to the relative mobile nature of ^{234}U induced by α-recoil effects (*5*) in the weathered host rocks. ^{234}U is enriched relative to ^{238}U at particle boundaries or damaged lattices, and is expected to be preferentially released in the initial phases of weathering (*6*). Leaching experiments (*7*) support that the early fraction of granite leachates is high in both U concentration and $\delta^{234}U$ ($\delta^{234}U = (^{234}U/^{238}U_{activity\ ratio}-1)*1000$)). In the last glacial period, subglacial drainage of meltwaters from a limited area of ice sheet interior to the margins may have been possible (*8*), analogous to the Antarctic Ice Sheet today where basal meltwater is routed to the margins via subglacial channels (*9*). Nevertheless, a large fraction of the glaciated NH continents likely had very limited chemical weathering flux to the ocean due to widespread freezing conditions of the ice-sheet base (*10*). It is reasonable to assume that a labile pool of excess ^{234}U due to α-recoil would have accumulated in the frozen sediments or isolated subglacial lakes/ponds in the wet-based zones under these ice-sheets. In fact, high dissolved $\delta^{234}U$ of up to ~4000‰ has been observed in the Antarctic Taylor Valley (*11*), a region thought to be hydrologically connected to the nearby ice sheets (*12*). In the non-glaciated regions, $\delta^{234}U$ released from weathering would also respond to tectonic and precipitation changes (*3*). A reliable reconstruction of oceanic $\delta^{234}U$ thus offers a potentially important route for tracing global scale weathering variability during climate transitions.

The long residence time of U in seawater (~400 ky, thousand years (*13, 14*)) would lead to the expectation that any equilibrium response to external inputs should be more than an order of magnitude longer than the deglacial time scale (~10 ky). However, a growing number of studies have inferred that seawater $\delta^{234}U$ might have been lower during the last glacial than

the Holocene and previous interglacials (*3, 15-17*), and might have also changed on millennial time scales (*18*). These observations imply that there have been large, relatively rapid changes in the U isotope budget of the ocean, and are supported by an updated compilation of published coral initial $\delta^{234}U$ data over the last 30 ka (Fig. 1a). However the extensive scatter in the data which is likely due to diagenesis (*19*) has limited the ability to constrain the timing and magnitude of $\delta^{234}U$ variations through time.

To put more robust limits on seawater $\delta^{234}U$ evolution and infer past changes in chemical weathering, we report two well-constrained U isotope records based on well-preserved deep-sea corals recovered from the low latitude North Atlantic and the Pacific Galápagos platform over the last 30 ka (Fig. 1b, S1, S2), with additional samples for reference from 50-30 ka (*19*) (Fig. S3). The general trend of $\delta^{234}U$ evolution agrees with previous studies (*3, 15-17*), although the new glacial deep-water corals tend to exhibit higher $\delta^{234}U_i$ than the surface corals in each ocean basin (Fig. S3). Our data thus suggest a somewhat smaller glacial-Holocene $\delta^{234}U$ difference of only 3-4‰ (Fig 1). Atlantic $\delta^{234}U$ started to increase at around 22-20 ka (Fig. 1b), followed by a rapid increase of ~6‰ up to 150‰ during Heinrich Stadial 1 (HS1, 18.0-14.6 ka). Available Pacific data are less well resolved, but exhibit lower $\delta^{234}U$ values than the Atlantic during early HS1. The $\delta^{234}U$ of Atlantic and Pacific records converged to the modern level during the Bølling-Allerod (B-A: 14.6 – 12.9 ka). Prior to the last glacial maximum (25-50 ka) our dataset is consistent with a lower $\delta^{234}U$ than the Holocene (Fig. S3), but it is not well enough resolved to identify potential millennial scale changes (*18*).

There are several possible causes for the observed deglacial seawater $\delta^{234}U$ increase. Coastal regions have been inferred to retain U with high $\delta^{234}U$ during sea-level highstands (*16*). Re-dissolution of the coastal U has been hypothesized to drive $\delta^{234}U$ increase when sea level rises (*16*). If so, seawater $\delta^{234}U$ is expected to increase closely following sea-level rise. The increase in Atlantic $\delta^{234}U$ does appear to coincide with the initiation of the sea level rise (Fig. 2), but most of the $\delta^{234}U$ increase occurred before the major sea-level rise in the late deglaciation. Hence we suggest that although U stored in the coastal areas could be important for $\delta^{234}U$ variability in other situations (*18*), it was probably not the main driver of the deglacial $\delta^{234}U$ evolution. An increase in deep water oxygenation may release redox sensitive U from the seafloor sediments, possibly affecting seawater U budget during deglaciation. The early deglaciation is thought to have had lower oxygen concentrations than the modern day in the upper ocean (e.g., <1.5 km) (*20*). Increased bottom water oxygenation in the Atlantic and

deep Pacific only occurred after HS1 (*20*) with resumption of North Atlantic deep overturning (*21*), which occurred later than the observed increase in $\delta^{234}U$. Together, these results suggest that external sources with excess ^{234}U or ocean mixing have to be involved to explain the observed $\delta^{234}U$ variability.

Models (*22*) and proxies such as $^{231}Pa/^{230}Th$ (*21, 23*) support a reduced deep Atlantic Meridional Overturning Circulation (AMOC) (Fig. 2) as well as reduced surface Gulf Stream (*24*) and Agulhas leakage (*25*) during HS1. These processes likely resulted in an upper Atlantic that was more isolated from the rest of the ocean than it is today (*19*). Increased isolation of the upper Atlantic (~2.0 km, including the depth range of the deep sea corals in this study) would act to reduce the effective uranium residence time, and allow its $\delta^{234}U$ to change more rapidly than in the Pacific. We applied a two-box model, consisting of an upper Atlantic-Arctic box and a 'rest-of-the-ocean' box, to study the influence of changing external sources and changing ocean circulation on seawater $\delta^{234}U$ (*19*). Modern high-latitude riverine inputs have significantly higher $\delta^{234}U$ than middle to low latitude inputs and mainly supply the Arctic and polar North Atlantic (*19*). If the $\delta^{234}U$ and U fluxes of all external sources are kept constant throughout the last 25 ky, our model result (Fig. 3a) shows that a slowdown of ocean circulation during HS1 can result in a resolvable difference of $\delta^{234}U$ between the upper Atlantic and the rest of the ocean, depending on the degree of reduction in exchange flux. This result is consistent with the difference in $\delta^{234}U$ between the Pacific and Atlantic $\delta^{234}U$ records (Fig. 1) and contrasts with the general assumption that U isotopes are homogenous throughout the global ocean (i.e., difference no larger than 0.4‰ (*4*)). Our result also raises the possibility that other isotope systems with relatively long residence times might exhibit differences between different ocean basins during periods of reduced ocean mixing.

Ocean circulation, however, cannot account for the overall glacial-interglacial ~3‰ or more increase in $\delta^{234}U$ of both ocean basins (Fig. 3a). External ^{234}U inputs must have increased relative to ^{238}U during the early deglaciation. With 3 times the modern riverine U flux, a 3‰ shift in oceanic $\delta^{234}U$ is possible during HS1 (Fig. S4). However since the hydrological cycle was probably weaker during the late last glacial and early deglaciation than the present (*2*), increased dissolved U flux from global rivers alone as a driver for the $\delta^{234}U$ change is considered unlikely. An increase in $\delta^{234}U$ of the continental inputs is, therefore, likely to have been important in seawater $\delta^{234}U$ evolution. There are no direct measurements of the $\delta^{234}U$ of past watersheds, so here we compiled $\delta^{234}U$ data from speleothems that grew during the relevant time period. Although speleothem $\delta^{234}U$ does not necessarily reflect the primary

surface weathering signal, including influences such as the percolation of meteoric waters from the surface down into the cave, it may still provide a first order indication on the variability of hydrological cycle that controlled the overall ^{234}U budget available for weathering (*26*). The available data come from the mid to low latitudes (Fig. S5) and they do not exhibit any distinctive $\delta^{234}U$ shifts from 30-15 ka, suggesting that weathering variability in these areas was not large enough to account for the oceanic $\delta^{234}U$ observations.

Instead, high-latitude processes could have played a key role in driving global seawater $\delta^{234}U$ increase from the last glacial to 15 ka. In the early part of the last deglaciation, the base of North American ice sheets are thought to have become increasingly wetter (*10*). We propose that ^{234}U-enriched water was released from subglacial melt reservoirs with a prolonged residence time and from leaching of the previously frozen subglacial sediments by basal melt water over this period. In both cases, subglacial meltwaters are likely to be enriched in recoiled ^{234}U (*7, 11*). In addition, sediments (and their former pore waters) frozen within the base of icebergs might also contribute to releasing U and nutrients to the ocean (*27*) during these periods. The reconstructed number of ice streams based on field evidence (*8*) and the modelled subglacial melt rate (*10, 28*) (Fig. 2b) of the North American ice sheets were much higher during early deglaciation (before 15 ka) than later. It is notable that the modelled ice discharge (*29*) of the Laurentide Ice Sheet was also high during the glacial and early deglaciation, reaching a peak at the late HS1 (Fig. 2). This timing is consistent with the enhanced release and transport of excess ^{234}U to the ocean during the early deglaciation. In this case the peak oceanic $\delta^{234}U$ indicates that active basal water from the whole ice-sheet interior may have been active in exporting to the margin during HS1. In another modelling experiment (*19*), the sensitivity of oceanic responses to inputs with different $\delta^{234}U$ ratios was tested. With an average $\delta^{234}U$ of ~800‰ for the input to the upper Atlantic during HS1, the model result is able to reproduce the observed amplitude of $\delta^{234}U$ increase from the last glacial to 15 ka (Fig. 3b). A more realistic case might be an increase in both the U flux and the $\delta^{234}U$ of the high-latitude continental inputs, but de-convolving these two factors is difficult. There is a hint from the compiled data that the surface ocean has lower $\delta^{234}U$ than the intermediate depth ocean (Fig. S3). Our extended modelling experiments are unable to replicate this feature, even with all high-latitude excess ^{234}U routed to the intermediate ocean via the polar surface Atlantic and no deep-ocean overturning and mixing (*19*). These results indicate that other mechanisms such as local influences or diagenetic processes are responsible to those differences.

The transition from HS1 to B-A is marked by a distinct decrease in $\delta^{234}U$ of the low latitude Atlantic by ~3‰ from about 150‰ to the modern seawater signature. The Pacific $\delta^{234}U$ appears to rise at the same time, converging with the Atlantic $\delta^{234}U$ during mid B-A. We suggest this convergence is due to the abrupt increase in overturning of the Atlantic at the end of HS (*21, 23*) (Figs 2c and 3a), although the depletion of subglacial excess ^{234}U pool might also have played a role (*19*). Stabilized Holocene seawater $\delta^{234}U$ afterwards implies that U cycle in the modern ocean is likely close to a steady state (*30*). Nevertheless, perturbation of oceanic U isotopes by polar processes might still be active even during the climatically and oceanographically more stable late Holocene period. For example, widespread collapse of the Ross Ice Shelf and export of old materials from inland of Antarctica was inferred to occur at ~5-1.5 ka in response to the regional warming (*31*). These may be accompanied by a ^{234}U rich flux to the Southern Ocean, although a large shift in the whole ocean $\delta^{234}U$ was probably limited. On longer orbital time scales, seawater $\delta^{234}U$ is thought to be higher during past interglacial periods and lower during glacials (e.g., (*3, 16, 17*)) with the decreases potentially associated with low sea level (*16*). By comparison to the deglacial mechanism, our study implies that progressive NH glaciation could have reduced the weathering input from high latitude continents, leading to lower glacial oceanic $\delta^{234}U$.

The retreat of the NH ice sheets started at about 20 ka and continued through HS1 (Fig. 2a) (*1*), considerably earlier than enhanced surface melting that dominated ice-sheet mass loss and sea level rise in the late deglaciation/early Holocene (*29*). Our data provide evidence for enhanced subglacial melt activity from the NH ice-sheet interior during the early deglaciation, supporting the notion that basal melting/sliding represents one of the feedbacks involved in enhancing early deglaciation as a result of the build-up of very large NH ice sheets (*10*). An interesting consequence of the basal melt inputs may be the associated release of nutrients to the ocean. Recent work from the Greenland Ice Sheet indicates dissolved phosphorus yields are at least equal to those associated with the Mississippi or Amazon rivers (*32*). In this regard, nutrients from direct subglacial weathering should be considered in the future as a potential source to fuel productivity in the North Atlantic during HS1.

References and Notes:

1. G. Denton *et al.*, The last glacial termination. *Science* **328**, 1652-1656 (2010).
2. P. U. Clark *et al.*, Global climate evolution during the last deglaciation. *Proc. Nat. Acad. Sci. U.S.A.* **109**, E1134-E1142 (2012).
3. L. F. Robinson, G. M. Henderson, L. Hall, I. Matthews, Climatic control of riverine and Seawater uranium-isotope ratios. *Science* **305**, 851-854 (2004).

4. M. B. Andersen, C. H. Stirling, B. Zimmermann, A. N. Halliday, Precise determination of the open ocean U-234/U-238 composition. *Geochem. Geophys. Geosyst.* **11**, (2010).
5. K. Kigoshi, Alpha-recoil thorium-234: dissolution into water and the uranium-234/uranium-238 disequilibrium in nature. *Science* **173**, 47-48 (1971).
6. F. Chabaux, J. Riotte, O. Dequincey, U-Th-Ra fractionation during weathering and river transport. *Rev. Mineral. Geochem.* **52**, 533-576 (2003).
7. M. B. Andersen, Y. Erel, B. Bourdon, Experimental evidence for U-234-U-238 fractionation during granite weathering with implications for U-234/U-238 in natural waters. *Geochim. Cosmochim. Acta* **73**, 4124-4141 (2009).
8. C. Stokes, M. Margold, C. Clark, L. Tarasov, Ice stream activity scaled to ice sheet volume during Laurentide Ice Sheet deglaciation. *Nature* **530**, 322-326 (2016).
9. A. M. Le Brocq *et al.*, Evidence from ice shelves for channelized meltwater flow beneath the Antarctic Ice Sheet. *Nat. Geosci.* **6**, 945-948 (2013).
10. S. J. Marshall, P. U. Clark, Basal temperature evolution of North American ice sheets and implications for the 100-kyr cycle. *Geophys. Res. Lett.* **29**, (2002).
11. G. M. Henderson, B. L. Hall, A. Smith, L. F. Robinson, Control on (U-234/U-238) in lake water: A study in the Dry Valleys of Antarctica. *Chem. Geol.* **226**, 298-308 (2006).
12. J. A. Mikucki *et al.*, Deep groundwater and potential subsurface habitats beneath an Antarctic dry valley. *Nat. Commun.* **6**, (2015).
13. G. M. Henderson, Seawater (U-234/U-238) during the last 800 thousand years. *Earth Planet. Sci. Lett.* **199**, 97-110 (2002).
14. R. M. Dunk, R. A. Mills, W. J. Jenkins, A reevaluation of the oceanic uranium budget for the Holocene. *Chem. Geol.* **190**, 45-67 (2002).
15. K. B. Cutler *et al.*, Radiocarbon calibration and comparison to 50 kyr BP with paired C-14 and Th-230 dating of corals from Vanuatu and Papua New Guinea. *Radiocarbon* **46**, 1127-1160 (2004).
16. T. M. Esat, Y. Yokoyama, Variability in the uranium isotopic composition of the oceans over glacial-interglacial timescales. *Geochim. Cosmochim. Acta* **70**, 4140-4150 (2006).
17. W. G. Thompson, H. A. Curran, M. A. Wilson, B. White, Sea-level oscillations during the last interglacial highstand recorded by Bahamas corals. *Nat. Geosci.* **4**, 684-687 (2011).
18. T. M. Esat, Y. Yokoyama, Coupled uranium isotope and sea-level variations in the oceans. *Geochim. Cosmochim. Acta* **74**, 7008-7020 (2010).
19. Materials and methods are available as supplementary materials on Science Online.
20. S. L. Jaccard, E. D. Galbraith, Large climate-driven changes of oceanic oxygen concentrations during the last deglaciation. *Nat. Geosci.* **5**, 151-156 (2012).
21. J. F. McManus, R. Francois, J. M. Gherardi, L. D. Keigwin, S. Brown-Leger, Collapse and rapid resumption of Atlantic meridional circulation linked to deglacial climate changes. *Nature* **428**, 834-837 (2004).
22. A. Ganopolski, S. Rahmstorf, Rapid changes of glacial climate simulated in a coupled climate model. *Nature* **409**, 153-158 (2001).
23. E. Bohm *et al.*, Strong and deep Atlantic meridional overturning circulation during the last glacial cycle. *Nature* **517**, 73-U170 (2015).
24. J. Lynch-Stieglitz *et al.*, Muted change in Atlantic overturning circulation over some glacial-aged Heinrich events. *Nat. Geosci.***7**, 144-150 (2014).

25. M. H. Simon *et al.*, Salt exchange in the Indian-Atlantic Ocean Gateway since the Last Glacial Maximum: A compensating effect between Agulhas Current changes and salinity variations? *Paleoceanography* **30**, 1318-1327 (2015).
26. J. Z. Zhou *et al.*, Geochemistry of speleothem records from southern Illinois: Development of (U-234)/(U-238) as a proxy for paleoprecipitation. *Chem. Geol.* **221**, 1-20 (2005).
27. R. Raiswell, L. G. Benning, M. Tranter, S. Tulaczyk, Bioavailable iron in the Southern Ocean: the significance of the iceberg conveyor belt. *Geochem. Trans.* **9**, 9 (2008).
28. L. J. Gregoire, A. J. Payne, P. J. Valdes, Deglacial rapid sea level rises caused by ice-sheet saddle collapses. *Nature* **487**, 219-U1506 (2012).
29. D. J. Ullman, A. E. Carlson, F. S. Anslow, A. N. LeGrande, J. M. Licciardi, Laurentide ice-sheet instability during the last deglaciation. *Nat. Geosci.***8**, 534-U140 (2015).
30. F. L. H. Tissot, N. Dauphas, Uranium isotopic compositions of the crust and ocean: Age corrections, U budget and global extent of modern anoxia. *Geochim. Cosmochim. Acta* **167**, 113-143 (2015).
31. Y. Yokoyama *et al.*, Widespread collapse of the Ross Ice Shelf during the late Holocene. *Proc. Nat. Acad. Sci. U.S.A.* **113**, 2354-2359 (2016).
32. J. Hawkings *et al.*, The Greenland Ice Sheet as a hotspot of phosphorus weathering and export in the Arctic. *Global Biogeochem. Cycles* (2016).
33. W. R. Peltier, D. F. Argus, R. Drummond, Space geodesy constrains ice age terminal deglaciation: The global ICE-6G_C (VM5a) model. *J. Geophys. Res. Solid Earth* **120**, 450-487 (2015).
34. K. Lambeck, H. Rouby, A. Purcell, Y. Y. Sun, M. Sambridge, Sea level and global ice volumes from the Last Glacial Maximum to the Holocene. *Proc. Nat. Acad. Sci. U.S.A.* **111**, 15296-15303 (2014).
35. L. F. Robinson, "RRS James Cook Cruise JC094, October 13–November 30 2013, Tenerife-Trinidad. TROPICS, Tracing Oceanic Processes using Corals and Sediments. Reconstructing abrupt Changes in Chemistry and Circulation of the Equatorial Atlantic Ocean: Implications for global Climate and deep-water Habitats.," (University of Bristol, 2014).
36. T. Chen *et al.*, Synchronous centennial abrupt events in the ocean and atmosphere during the last deglaciation. *Science* **349**, 1537-1541 (2015).
37. E. Mittelstaedt, A. S. Soule, K. S. Harpp, D. Fornari, Variations in Crustal Thickness, Plate Rigidity, and Volcanic Processes Throughout the Northern Galápagos Volcanic Province, in *The Galápagos*. John Wiley & Sons, Inc. p. 263-284 (2014)
38. S. Carey *et al.*, Exploring the Undersea World of the Galápagos Islands. *Oceanography Magazine* **29**, 32-34 (2016).
39. H. Cheng, J. Adkins, R. L. Edwards, E. A. Boyle, U-Th dating of deep-sea corals. *Geochim. Cosmochim. Acta* **64**, 2401-2416 (2000).
40. H. Cheng *et al.*, The half-lives of uranium-234 and thorium-230. *Chem. Geol*. **169**, 17-33 (2000).
41. A. K. Singh, F. Marcantonio, M. Lyle, Water column Th-230 systematics in the eastern equatorial Pacific Ocean and implications for sediment focusing. *Earth Planet. Sci. Lett.* **362**, 294-304 (2013).
42. R. Edwards, C. Gallup, H. Cheng, Uranium-series dating of marine and lacustrine carbonates. *Rev. Mineral. Geochem.* **52**, 363-405 (2003).
43. J. Marshall, K. Speer, Closure of the meridional overturning circulation through Southern Ocean upwelling. *Nat. Geosci.* **5**, 171-180 (2012).

44. A. Gnanadesikan, A simple predictive model for the structure of the oceanic pycnocline. *Science* **283**, 2077-2079 (1999).
45. M. Nikurashin, G. Vallis, A Theory of the Interhemispheric Meridional Overturning Circulation and Associated Stratification. *J. Phys. Oceanogr.* **42**, 1652-1667 (2012).
46. M. P. Hain, D. M. Sigman, G. H. Haug, Carbon dioxide effects of Antarctic stratification, North Atlantic Intermediate Water formation, and subantarctic nutrient drawdown during the last ice age: Diagnosis and synthesis in a geochemical box model. *Global Biogeochem. Cycles* **24**, (2010).
47. M. B. Andersen, D. Vance, A. R. Keech, J. Rickli, G. Hudson, Estimating U fluxes in a high-latitude, boreal post-glacial setting using U-series isotopes in soils and rivers. *Chem. Geol.* **354**, 22-32 (2013).
48. P. J. Reimer *et al.*, Intcal09 and Marine09 Radiocarbon Age Calibration Curves, 0-50,000 Years Cal Bp. *Radiocarbon* **51**, 1111-1150 (2009).
49. L. F. Robinson *et al.*, Deep-sea scleractinian coral age and depth distributions in the northwest Atlantic for the last 225,000 years. *Bull. Mar. Sci.* **81**, 371-391 (2007).
50. M. Gutjahr *et al.*, Structural limitations in deriving accurate U-series ages from calcitic cold-water corals contrast with robust coral radiocarbon and Mg/Ca systematics. *Chem. Geol.* **355**, 69-87 (2013).
51. L. F. Robinson *et al.*, Primary U distribution in scleractinian corals and its implications for U series dating. *Geochem. Geophys. Geosyst.* **7**, (2006).
52. A. Dutton, K. Lambeck, Ice Volume and Sea Level During the Last Interglacial. *Science* **337**, 216-219 (2012).
53. C. D. Gallup, R. L. Edwards, R. G. Johnson, The Timing of High Sea Levels over the Past 200,000 Years. *Science* **263**, 796-800 (1994).
54. C. H. Stirling, M. B. Andersen, Uranium-series dating of fossil coral reefs: Extending the sea-level record beyond the last glacial cycle. *Earth Planet. Sci. Lett.* **284**, 269-283 (2009).
55. W. G. Thompson, M. W. Spiegelman, S. L. Goldstein, R. C. Speed, An open-system model for U-series age determinations of fossil corals. *Earth Planet. Sci. Lett.* **210**, 365-381 (2003).
56. D. Scholz, A. Mangini, T. Felis, U-series dating of diagenetically altered fossil reef corals. *Earth Planet. Sci. Lett.* **218**, 163-178 (2004).
57. B. Villemant, N. Feuillet, Dating open systems by the 238U–234U–230Th method: application to Quaternary reef terraces. *Earth Planet. Sci. Lett.* **210**, 105-118 (2003).
58. P. J. Tomiak *et al.*, The role of skeletal micro-architecture in diagenesis and dating of Acropora palmata. *Geochim. Cosmochim. Acta* **183**, 153-175 (2016).
59. R. Schlitzer. (2015).
60. E. Bard, B. Hamelin, D. Delanghe-Sabatier, Deglacial Meltwater Pulse 1B and Younger Dryas Sea Levels Revisited with Boreholes at Tahiti. *Science* **327**, 1235-1237 (2010).
61. A. Burke, L. F. Robinson, The Southern Ocean's Role in Carbon Exchange During the Last Deglaciation. *Science* **335**, 557-561 (2012).
62. K. M. Cobb, C. D. Charles, H. Cheng, M. Kastner, R. L. Edwards, U/Th-dating living and young fossil corals from the central tropical Pacific. *Earth Planet. Sci. Lett.* **210**, 91-103 (2003).
63. L. B. Collins, J.-X. Zhao, H. Freeman, A high-precision record of mid–late Holocene sea-level events from emergent coral pavements in the Houtman Abrolhos Islands, southwest Australia. *Quat. Int.* **145–146**, 78-85 (2006).
64. E. R. M. Druffel *et al.*, Low reservoir ages for the surface ocean from mid-Holocene Florida corals. *Paleoceanography* **23**, (2008).

65. N. Durand *et al.*, Comparison of 14C and U-Th ages in corals from IODP# 310 cores offshore Tahiti. *Radiocarbon* **55**, 1947-1974 (2013).
66. R. G. Fairbanks *et al.*, Radiocarbon calibration curve spanning 0 to 50,000 years BP based on paired 230 Th/234 U/238 U and 14 C dates on pristine corals. *Quat. Sci. Rev.* **24**, 1781-1796 (2005).
67. N. Frank *et al.*, Northeastern Atlantic cold-water coral reefs and climate. *Geology* **39**, 743-746 (2011).
68. S. K. Hines, J. R. Southon, J. F. Adkins, A high-resolution record of Southern Ocean intermediate water radiocarbon over the past 30,000 years. *Earth Planet. Sci. Lett.* **432**, 46-58 (2015).
69. A. Mangini *et al.*, Deep sea corals off Brazil verify a poorly ventilated Southern Pacific Ocean during H2, H1 and the Younger Dryas. *Earth Planet. Sci. Lett.* **293**, 269-276 (2010).
70. H. G. Multer, E. Gischler, J. Lundberg, K. Simmons, E. Shinn, Key Largo Limestone revisited: Pleistocene shelf-edge facies, Florida Keys, USA. *Facies* **46**, 229-271 (2002).
71. L. F. Robinson, N. S. Belshaw, G. M. Henderson, U and Th concentrations and isotope ratios in modern carbonates and waters from the Bahamas. *Geochim. Cosmochim. Acta* **68**, 1777-1789 (2004).
72. C.-C. Shen *et al.*, Variation of initial 230 Th/232 Th and limits of high precision U–Th dating of shallow-water corals. *Geochim. Cosmochim. Acta* **72**, 4201-4223 (2008).
73. C. Stirling, T. Esat, M. McCulloch, K. Lambeck, High-precision U-series dating of corals from Western Australia and implications for the timing and duration of the Last Interglacial. *Earth Planet. Sci. Lett.* **135**, 115-130 (1995).
74. C. Wienberg *et al.*, Glacial cold-water coral growth in the Gulf of Cadiz: Implications of increased palaeo-productivity. *Earth Planet. Sci. Lett.* **298**, 405-416 (2010).
75. Y. Yokoyama, T. M. Esat, K. Lambeck, Coupled climate and sea-level changes deduced from Huon Peninsula coral terraces of the last ice age. *Earth Planet. Sci. Lett.* **193**, 579-587 (2001).
76. Y. J. Cai *et al.*, The variation of summer monsoon precipitation in central China since the last deglaciation. *Earth Planet. Sci. Lett.* **291**, 21-31 (2010).
77. H. Cheng *et al.*, Climate change patterns in Amazonia and biodiversity. *Nat. Commun.* **4**, (2013).
78. F. W. Cruz *et al.*, Insolation-driven changes in atmospheric circulation over the past 116,000 years in subtropical Brazil. *Nature* **434**, 63-66 (2005).
79. F. W. Cruz *et al.*, Orbitally driven east-west antiphasing of South American precipitation. *Nat. Geosci.* **2**, 210-214 (2009).
80. C. A. Dykoski *et al.*, A high-resolution, absolute-dated Holocene and deglacial Asian monsoon record from Dongge Cave, China. *Earth Planet. Sci. Lett.* **233**, 71-86 (2005).
81. W. M. Feng *et al.*, Changing amounts and sources of moisture in the U.S. southwest since the Last Glacial Maximum in response to global climate change (vol 401, pg 47, 2014). *Earth Planet. Sci. Lett.* **407**, 234-234 (2014).
82. D. Fleitmann *et al.*, Timing and climatic impact of Greenland interstadials recorded in stalagmites from northern Turkey. *Geophys. Res. Lett.* **36**, (2009).
83. J. Hellstrom, M. McCulloch, J. Stone, A detailed 31,000-year record of climate and vegetation change, from the isotope geochemistry of two New Zealand speleothems. *Quat. Res.* **50**, 167-178 (1998).

84. J. W. Partin, K. M. Cobb, J. F. Adkins, B. Clark, D. P. Fernandez, Millennial-scale trends in west Pacific warm pool hydrology since the Last Glacial Maximum. *Nature* **449**, 452-U453 (2007).
85. P. J. Rowe *et al.*, Speleothem isotopic evidence of winter rainfall variability in northeast Turkey between 77 and 6 ka. *Quat. Sci. Rev.* **45**, 60-72 (2012).
86. J. D. Shakun *et al.*, A high-resolution, absolute-dated deglacial speleothem record of Indian Ocean climate from Socotra Island, Yemen. *Earth Planet. Sci. Lett.* **259**, 442-456 (2007).
87. J. D. M. Wagner *et al.*, Moisture variability in the southwestern United States linked to abrupt glacial climate change. *Nat. Geosci.* **3**, 110-113 (2010).
88. X. F. Wang *et al.*, Millennial-scale precipitation changes in southern Brazil over the past 90,000 years. *Geophys. Res. Lett.* **34**, (2007).
89. A. Dai, K. E. Trenberth, in *Proceedings of the Symposium on Observing and Understanding the Variability of Water in Weather and Climate, 83rd Annual American Meteorological Society Meeting, Long Beach, CA*. (2003), pp. 1-18.
90. E. Y. Kwon *et al.*, Global estimate of submarine groundwater discharge based on an observationally constrained radium isotope model. *Geophys. Res. Lett.* **41**, 8438-8444 (2014).

Figure Captions:

Figure 1 Seawater $\delta^{234}U$ evolution reconstructed from corals over the last 30 ky. (A) Compilation of published coral initial $\delta^{234}U$ within the range of 135‰ to 155‰ and with 2 sigma error <3‰ (*19*). Data outside of this range have been truncated. **(B)** Low latitude North Atlantic records with ± 2 sigma confidence lines. Also shown are the initial $\delta^{234}U$ of low latitude Pacific reconstructed from Galápagos deep-sea corals. One data point of Galápagos coral during B-A with initial $\delta^{234}U$ higher than 155‰ has likely experienced diagenesis and is not shown. Black dotted line marks the modern seawater signature.

Figure 2 Seawater $\delta^{234}U$ evolution compared with other climate records. (A) Retreat rate of the northern and southern hemisphere ice sheets (*33*). (**B)** Basal melting rate of the North American ice sheets (*28*) and the ice discharge of the Laurentide ice sheet (*29*). **(C)** $^{231}Pa/^{230}Th$ of North Atlantic deep sediment core (*21, 23*). **(D)** Sea-level history (*34*). **(E)** Our reconstructed $\delta^{234}U$ evolution in the upper Atlantic and Pacific. Black dotted line denotes modern seawater $\delta^{234}U$.

Figure 3 Sensitivity experiment for seawater $\delta^{234}U$ response to ocean circulation and external inputs. (**A**) Effect of ocean mixing slowdown alone. (**B**) Effect of variable $\delta^{234}U$ of inputs to the upper Atlantic, applying 50% reduction of the glacial exchange flux during HS1. The area between the dash-dot curves is the range of low latitude Atlantic $\delta^{234}U$. External U fluxes through time in both experiments are kept as the modern inputs.

Acknowledgements Data of this work are available from the Supporting Online Material. Insightful comments from two anonymous reviewers helped us improving the manuscript. We thank C. Taylor and C. Coath for help in the lab. This study was funded by the European Research Council, the Natural Environment Research Council, Philip Leverhulme Trust, the National Science Foundation and a Marie Curie Reintegration Grant, NOAA Ocean Exploration Trust. We also thank Charles Darwin Foundation, Galápagos National Park, and INOCAR for making the sampling on Galápagos possible.

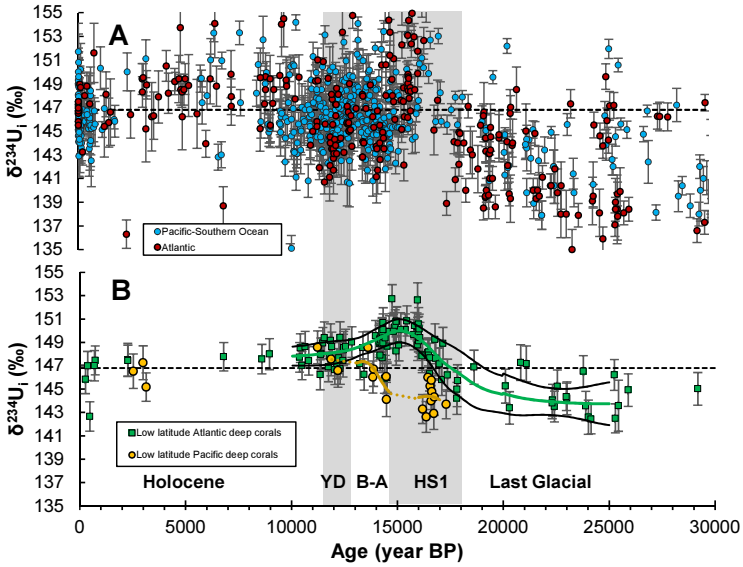
A
B
δ234Ui (‰)
Pacific-Southern Ocean
Atlantic
Low latitude Atlantic deep corals
Low latitude Pacific deep corals
Holocene
YD
B-A
HS1
Last Glacial
Age (year BP)

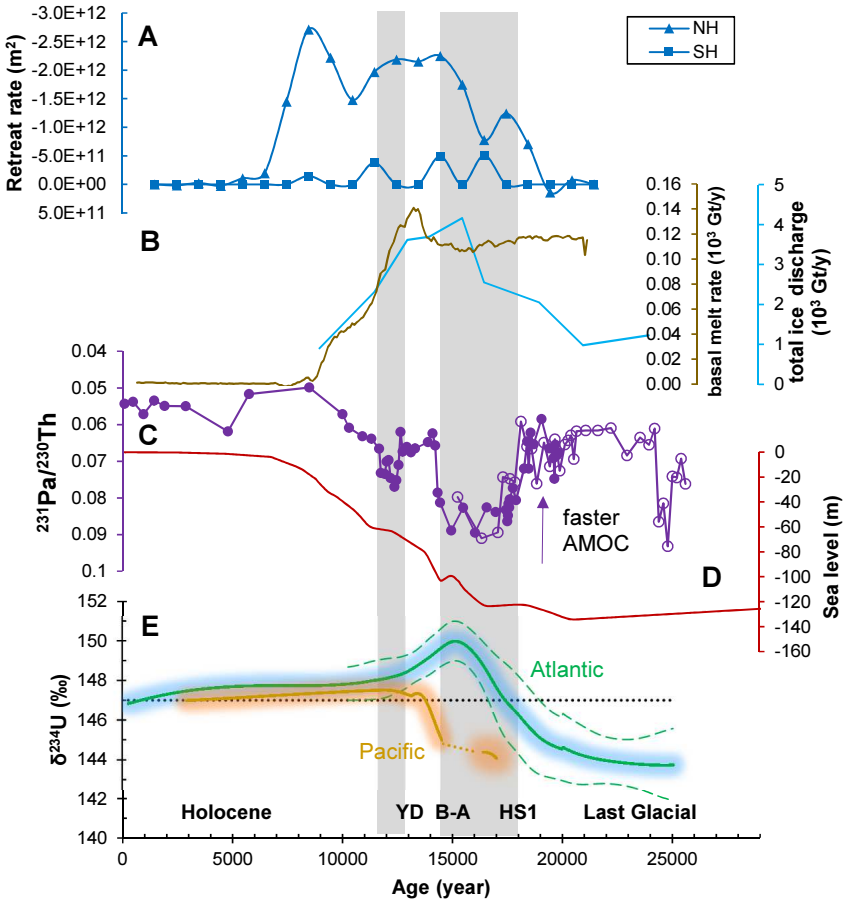
A
B
C
D
E
NH
SH
Retreat rate (m²)
-3.0E+12
-2.5E+12
-2.0E+12
-1.5E+12
-1.0E+12
-5.0E+11
0.0E+00
5.0E+11
basal melt rate (10³ Gt/y)
total ice discharge (10³ Gt/y)
231Pa/230Th
faster AMOC
Sea level (m)
δ234U (‰)
Atlantic
Pacific
Holocene
YD
B-A
HS1
Last Glacial
Age (year)
0
5000
10000
15000
20000
25000

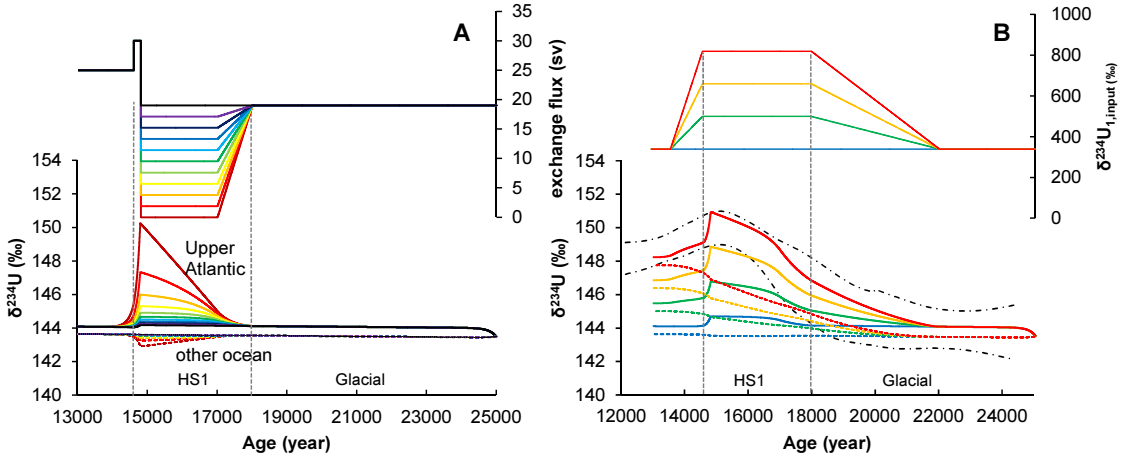
A
B
exchange flux (sv)
δ234U (‰)
δ234U1,input (‰)
Upper
Atlantic
other ocean
HS1
Glacial
Age (year)

Supplementary Materials for

Ocean mixing and ice-sheet control of last deglacial seawater $^{234}U/^{238}U$ evolution

Tianyu Chen*, Laura F. Robinson, Matthew P. Beasley, Louis M. Claxton, Morten B. Andersen, Lauren J. Gregoire, Jemma Wadham, Daniel J. Fornari, Karen S. Harpp

*correspondence to: tc14502@bristol.ac.uk

This PDF file includes:

Materials and Methods

Seawater $\delta^{234}U$ reconstruction

The low latitude North Atlantic deep-sea coral samples (Table S3, S4) were recovered during the JC094 cruise (*35, 36*) on seamounts away from the continental margin, from water depths of 700-2100 m. The majority of these samples are *Caryophyllia* and *Enallopsamia,* which were very well preserved with minimal internal bio-erosion. The Pacific deep-sea corals were recovered from the Galápagos platform in the Eastern Equatorial Pacific during MV1007 (*37*) and NA064 (*38*) with water depths of 419-627 m (Table S5, S6). The deglacial Galápagos corals reported in this study were mostly large colonial coral fragments from 589-627m. These corals were first cut and physically cleaned with a Dremel tool to remove visible ferromanganese and organic coatings or re-calcified areas. These samples were then chemically cleaned through oxidative and reductive stages (*39*). As outlined in Chen et al. (*36*), approximately 0.2 gram of cleaned sample was dissolved and spiked with ~ 0.06 g of the gravimetric weighed ^{236}U-^{229}Th mixed spike. U and Th isotopes were separated by anion-exchange columns and were measured by standard bracketing method (international U standard: U112a; and in house Th standard: SGS) on a Neptune Multi-Collector-Inductively Coupled Plasma-Mass Spectrometer (MC-ICP-MS) in the Bristol Isotope Group at the University of Bristol. The ^{229}Th, ^{230}Th, ^{234}U were measured using secondary electron multipliers (SEM), while other isotopes were measured with Faraday cups. Half-lives of ^{234}U and ^{230}Th are adopted from Cheng et al. (*40*) (245,250 and 75,690 years, respectively). To correct the initial ^{230}Th for age determination, we assume an initial atomic $^{232}Th/^{230}Th$ ratio of 12,500 ± 12,500 (2σ) in the low latitude Atlantic (*36*) and 2,025 ± 2,025 (2σ) in the low latitude Pacific (*41*), respectively. With the measured $\delta^{234}U$ and U-Th dated age of the coral sample, the initial $\delta^{234}U$ at the time of coral growth (i.e., initial seawater ratio) can be calculated by applying the radioactive decay equation (*42*). Final age and initial $\delta^{234}U$ uncertainties were propagated applying a Monte Carlo technique. Seventy-six out of 119 of the Atlantic coral initial $\delta^{234}U$ data were presented in Chen et al. (*36*) in a discussion of radiocarbon evolution in the low latitude North Atlantic. The smoothed lines in Fig. 2d (including the ± 2 sigma confidence lines) were generated using MATLAB functions. We use a Monte Carlo approach that first randomly samples a data point from an age window of 0.5 ky during 10-20 ka and 1 ky in other periods (since deglacial data are more dense). Analytical errors of the data points were not incorporated in the Monte Carlo simulation. A LOESS function (i.e. local regression method) was applied to smooth the data. This procedure was done 10,000 times and the ± 2 sigma confidence lines of the scatter of these data points were calculated accordingly. Thus the confidence lines only represent the degree of scatter of the available data. Two glacial corals around 21 ka (Fig. 1b) with initial $\delta^{234}U$ higher than the modern seawater were not included in the data smoothing. Inclusion of these data do not affect the conclusions of the study, and potentially point to a more rapid increase in $\delta^{234}U$ from the last glacial maximum to HS1 transition.

Seawater $\delta^{234}U$ box model: the upper Atlantic and the rest of the ocean

The magnitude of exchange between the Atlantic and the Pacific is controlled by the northward meridional flux derived from the circumpolar water (e.g., mode water and intermediate water subduction/advection, upwelling of AABW, Fig S1), plus leakage of the subtropical gyres (i.e., Agulhas leakage) (*43*). With a greatly reduced NADW formation, the northward flow from the ACC to the Atlantic would be reduced accordingly due to increased Southern Ocean eddy return flow (*44, 45*). During HS1, a reduced Gulf Stream (*24*) and Agulhas leakage (*25*) have also been suggested. Moreover, the shallow sill of Bering Strait makes it unlikely as an important passage for water mass exchange during the glacial and early

deglaciation when the sea level was low (*34*). These changes in the ocean may have contributed to reduce the exchange between Atlantic and the Pacific-Indian Ocean during the early deglaciation, with implication for geochemical mixing. Our box model assumes an interglacial and glacial exchange flux between the upper Atlantic/Arctic (box 1) and the rest of the ocean (box 2) of 25 Sv and 19 sv (1 Sv = 10^6 m^3/s), respectively (adopted from a more complex box model (*46*)). During the interglacial period, 6.5 Sv of the surface Indian waters flow to the surface Atlantic via a Agulhas leakage, while 15 Sv of intermediate waters originating from mid-depth South Pacific waters (via the Drake passage) and sub-Antarctic zone flow into the mid-depth Atlantic. Additional mixing between upper Atlantic and deep Atlantic is about 3.5 Sv (*46*).

The governing equations for ^{234}U and ^{238}U concentrations in the upper Atlantic – Arctic box (box 1) can be written as:

$$d^{234}U_1 / dt = -k \times {}^{234}U_1 - \lambda_{234} \times {}^{234}U_1 + \lambda_{238} \times {}^{238}U_1 + {}^{234}U_{1,input}/Mass_1 + Ex \times {}^{234}U_2 / Mass_1 - Ex \times {}^{234}U_1 / Mass_1 \quad (1)$$

$$d^{238}U_1 / dt = -k \times {}^{238}U_1 - \lambda_{238} \times {}^{238}U_1 + {}^{238}U_{1,input} / Mass_1 + Ex \times {}^{238}U_2 / Mass_1 - Ex \times {}^{238}U_1 / Mass_1 \quad (2)$$

where $^{234}U_{1,input}$, $^{238}U_{1,input}$ are the input fluxes of ^{234}U and ^{238}U respectively to box 1. k (2.5×10^{-6}) is the removal constant of U in seawater. λ_{234}, λ_{238} are the decay constants of ^{234}U and ^{238}U, respectively. Ex is the exchange flux between the two boxes. Similarly, the governing equations for ^{234}U and ^{238}U can be written for the other ocean (box 2). Given the initial conditions and input fluxes, these equations can be solved numerically. Table S1 gives the modern budget of the U cycle, which can maintain the seawater $\delta^{234}U$ at equilibrium of ~147‰. With the modern budget and an exchange flux of 25 Sv, difference of $\delta^{234}U$ between the 2 boxes are about 0.4‰ at steady state, which is consistent with observations suggesting homogenous modern $\delta^{234}U$ (within analytical error (*4*)) of the global ocean. Unless otherwise stated, the glacial and deglacial U flux and $\delta^{234}U$ of the continental inputs to the two boxes are kept as those of modern time.

The first experiment tests the response of $\delta^{234}U$ in the upper Atlantic (e.g., shallower than ~2000m) to changes in ocean circulation alone, while the modern inputs that can maintain an equilibrium seawater $\delta^{234}U$ of 147‰ are kept unchanged (Table S1). Note the riverine flux to the upper Atlantic has significantly higher $\delta^{234}U$ (321‰) than the other ocean box (Pacific and Indian Ocean, 188‰) (*47*). Implementing this modern input to the glacial ocean (initial $\delta^{234}U$ of 142.5‰) results in a negligible overall $\delta^{234}U$ increase of less than 1‰ in either box over a period of 10 ky (Fig. 3a). In this regard, the model experiment results are not critically dependent on the accurate modern flux estimation. The second experiment tests the effects of changing riverine U flux without changing its $\delta^{234}U$ (Fig. S4), while the third experiment tests the sensitivity of seawater $\delta^{234}U$ to a changing $\delta^{234}U$ of the input to the upper Atlantic (Fig. 3b).

<u>The $\delta^{234}U$ in surface and intermediate oceans</u>

The new data raise the possibility that intermediate waters had higher $\delta^{234}U$ than the surface waters when compared to published datasets (Fig. S3) during the glacial period. As the isopycnals of the intermediate ocean (i.e., shallower than 2 km) outcrop in the high latitude North Atlantic (Fig. S1), it is reasonable to assume that high $\delta^{234}U$ continental input into the polar North Atlantic/Arctic surface waters (Table S1) would directly supply the low latitude intermediate waters, providing a potential mechanism for decoupling surface and subsurface $\delta^{234}U$. To explore this possibility we applied a two box model containing an Atlantic-Indian-

Pacific surface layer (100 m) box and an intermediate box (the upper 2 km) connecting with the polar North Atlantic surface.

To simulate the maximum effect of the $\delta^{234}U$ difference between the surface and intermediate waters, we assume no abyssal upwelling and allow all excess ^{234}U to be supplied to the intermediate ocean box via the polar North Atlantic surface. For simplicity we did not separate the global oceans in different boxes, as our major interest here is to investigate the first order potential vertical $\delta^{234}U$ differences. In the absence of any deep ocean overturning and mixing, wind-driven gyre circulation is still able to actively mix the surface and intermediate oceans with an exchange flux of about 12.1 Sv (*46*). Model inputs to the two boxes are shown in Table S2 and Fig. S6. This simple model suggests that the $\delta^{234}U$ difference between the surface and intermediate waters are always less than 1‰ (Figure S6), and therefore not be resolvable with the typical analytical precision and data scatter (1-2‰). The results suggest that upper ocean wind-driven mixing can effectively homogenize $\delta^{234}U$ between the surface and subsurface oceans. However, in contrast to the expectation inferred from Fig. S3, the modelled $\delta^{234}U$ of the intermediate waters is actually slightly lower than the surface ocean (Fig. S6) resulting from two main reasons. First, in our model the surface box is 18 times smaller than the intermediate box (Table S2) so the intermediate ocean is much less sensitive to the external sources than the surface ocean (refer to equation (2) above). Second, when calculating the excess-^{234}U flux unsupported by ^{238}U, the surface ocean input is still higher than the intermediate box for the first two sensitivity experiments and only slightly lower for the other two experiments, since the surface box continues to receive a high U flux from rivers and groundwater (Table S2). Therefore even in this extreme scenario, our modelling is unable to reproduce a higher $\delta^{234}U$ in the intermediate ocean than the surface ocean. We conclude that ocean circulation is unlikely to cause a higher $\delta^{234}U$ in the intermediate ocean than the in the surface ocean. Instead, the observed surface-intermediate ocean $\delta^{234}U$ difference most likely reflects some other mechanisms such as local influences or diagenesis.

Supplementary Text

Preservation of seawater $^{234}U/^{238}U$ in relatively recent corals

The potential for millennial oceanic $\delta^{234}U$ variability during the last deglaciation and possibly the last glacial period (e.g., (*18*)) implies a more nuanced approach may be needed for judging the degree of coral diagenesis by using initial $\delta^{234}U$ (*3, 17, 48*). However with the current state of knowledge, including the large scatter of $\delta^{234}U$ data (0.5% or more, Figure S3) and potential for oceanic isotope heterogeneity, it is not possible to provide a single curve for past ocean $\delta^{234}U$ evolution. Indeed it remains likely that a large amount of scatter is caused by diagenesis.

Several processes that affect the initial $\delta^{234}U$ have been observed in deep-sea corals. External organic or ferromanganese coatings containing ^{230}Th can cause the apparent age (and calculated $\delta^{234}U_i$) to be high (e.g. (*39*)). Efforts to correct for this initial ^{230}Th include removing the coatings through physical and chemical procedures, and making corrections based on the ^{232}Th concentration and an assumed $^{232}Th/^{230}Th$ ratio (e.g. (*39*)). Bio-erosion produce endolithic boring holes within the coral skeletons (*49*), which may lead to dissolution or re-crystallization within the aragonite, or to organic/ferromanganese oxide residues in those holes. These residues may have higher U concentration than corals, leading to recoiled ^{234}U transfer from coatings into the coral skeleton, effectively elevating $\delta^{234}U$ in the coral fossils (*50, 51*).

Diagenesis in surface coral reefs likely follows different processes as those corals are often porous and might have experienced subaerial weathering associated with meteoric waters. Loss of recoiled ^{234}U for the last glacial and deglacial corals has the potential to result in averagely

lower $\delta^{234}U$ than deep water corals. However, elevated initial $^{234}U/^{238}U$ has often been seen in surface corals from the last and older interglacials (e.g., (*17, 52-54*)), which has been attributed to α-recoil related radionuclide re-distribution with ^{234}U-^{230}Th addition, rather than loss. Nevertheless, different diagenetic trends in fossil corals appear to be dictated by particular environmental regimes, and there is no single process that fully explains the pattern of surface coral diagenesis (*53-58*). As such it is challenging to select which corals in the compiled dataset represent the primary signatures of past seawater.

The deep-sea corals of this study were recovered from different water depths and different seamounts across the low latitude North Atlantic and Pacific. It is remarkable to note the consistency of our reconstructed deglacial $\delta^{234}U$, which indicates little diagenetic influence on most of the corals. The new data are also generally within the range constrained by the published deep and surface coral data (Fig. S3) in each ocean basin.

Several factors might be important in accounting for the small diagenetic influence of our samples. In the Pacific the Galápagos corals have exceptionally low ^{232}Th concentrations (Table S6), so the correction for initial ^{230}Th, and potential for diagenesis from high U concentration coatings is lower than in other settings. In addition, most of the samples analyzed were from large branching scleractinian corals which may be less susceptible to internal uranium isotopic reorganization. Our Atlantic deep-sea corals were collected in situ by remotely operation vehicle (ROV) on seamounts away from the continental margin (*35*), and were well preserved with minimal or no noticeable internal bio-erosion. We surmise the good preservation condition is related to the overall low export productivity in this region, which may limit coral bio-erosion. Second, the solitary coral specimens were generally small (length <5cm), and thus a large portion of the sample needs to be cut for U series analysis. This sampling approach might have effectively averaged the potential intra-skeleton heterogeneity, such as between the low and high U concentration parts of the samples (*51*).

The $\delta^{234}U$ decrease in the HS1 to B-A transition

Our modelling suggests that increasing the exchange between the upper Atlantic and the rest of the ocean could be the mechanism that explains the reduction in the low latitude North Atlantic $\delta^{234}U$ (Fig. 3a). It is likely that a decrease in $\delta^{234}U$ of the Atlantic inputs also contributed to the observed seawater $\delta^{234}U$ evolution. Note the seawater $\delta^{234}U$ in both the Pacific and Atlantic stopped increasing after 14 ka (Fig. 1), indicating the pool of excess ^{234}U under the NH ice sheets should have been depleted by active basal waters during HS1. The NH ice sheet retreat rate reached a plateau during B-A (Fig. 2a), which would have exposed large areas of subglacial terrains to a warmer climate. Intensified chemical weathering of the exposed continent might therefore have led to the dissolved $\delta^{234}U$ signature approaching the modern level. If the $\delta^{234}U$ of Atlantic inputs were reset to the modern level during B-A (Fig. 3b), our model is able reproduce the observed decrease in Atlantic $\delta^{234}U$ with a moderate reduction of exchange flux between the upper Atlantic and other ocean (i.e., 50%) during HS1.

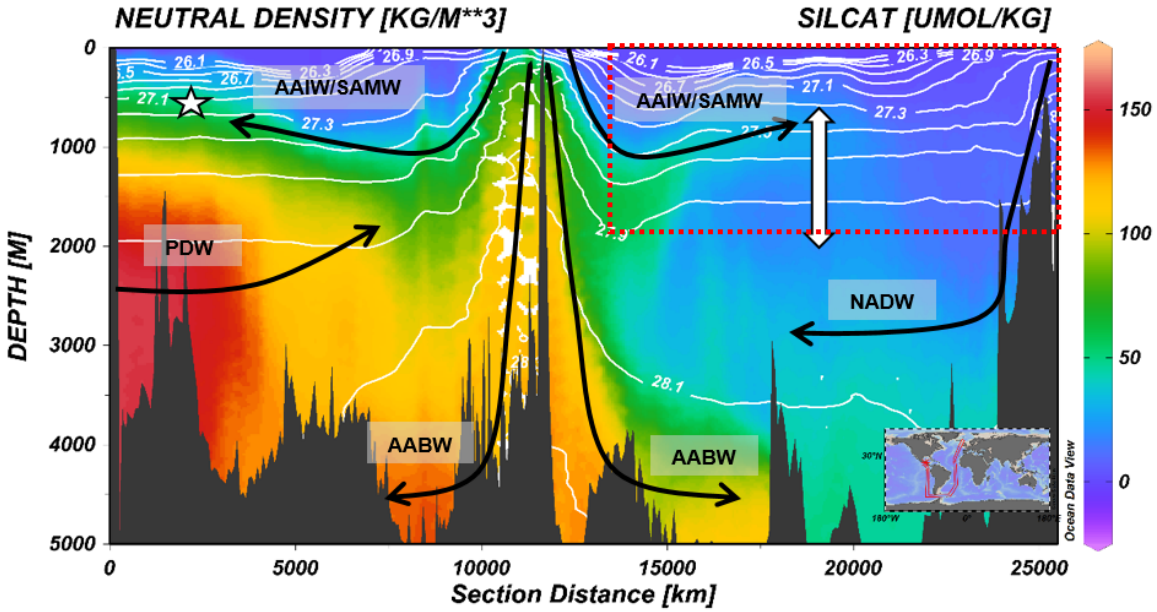

Fig. S1

Deep water circulation across the Atlantic and Pacific basin (from GLODAP bottle data ODV collection, see lower inset map for the section *(59)*) and locations of corals in this study. Star: Galapagos Islands; double-headed arrow: depth range of the low latitude North Atlantic samples. The color map shows the silicate concentration as a water mass tracer. Overlying contours are the seawater neutral density. PDW: Pacific Deep Water; SAMW/AAIW: Subantarctic Mode Water/Antarctic Intermediate Water; NADW: North Atlantic Deep Water; AABW: Antarctic Bottom Water. The red dashed line defines the upper Atlantic in the box model.

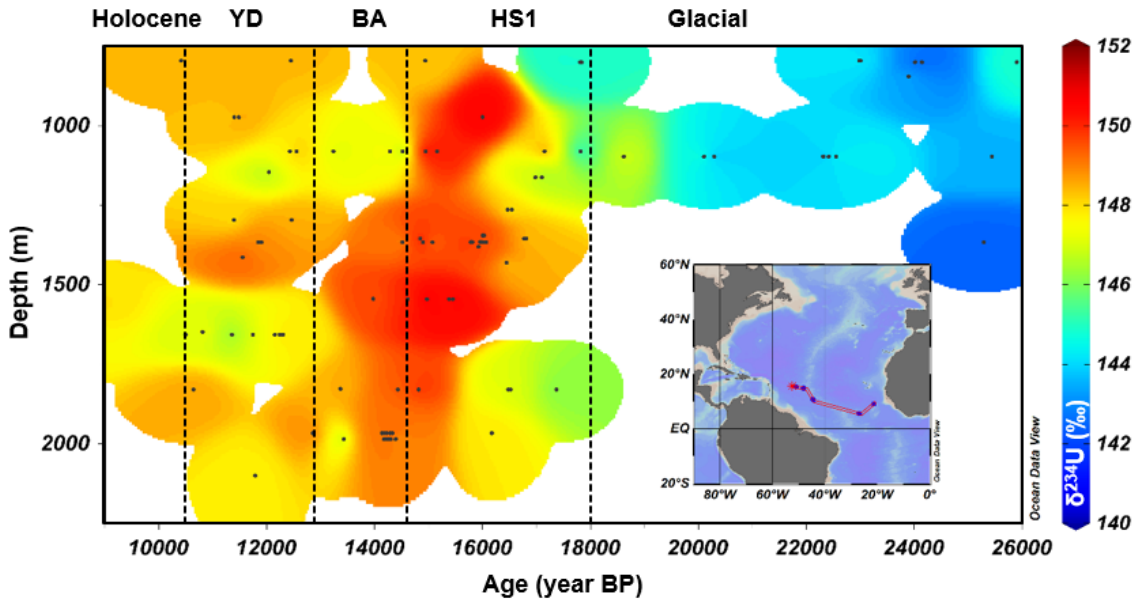

Fig. S2

$\delta^{234}U$ evolution at different depths in the low latitude North Atlantic (see lower inset map) based on deep-sea corals of this study.

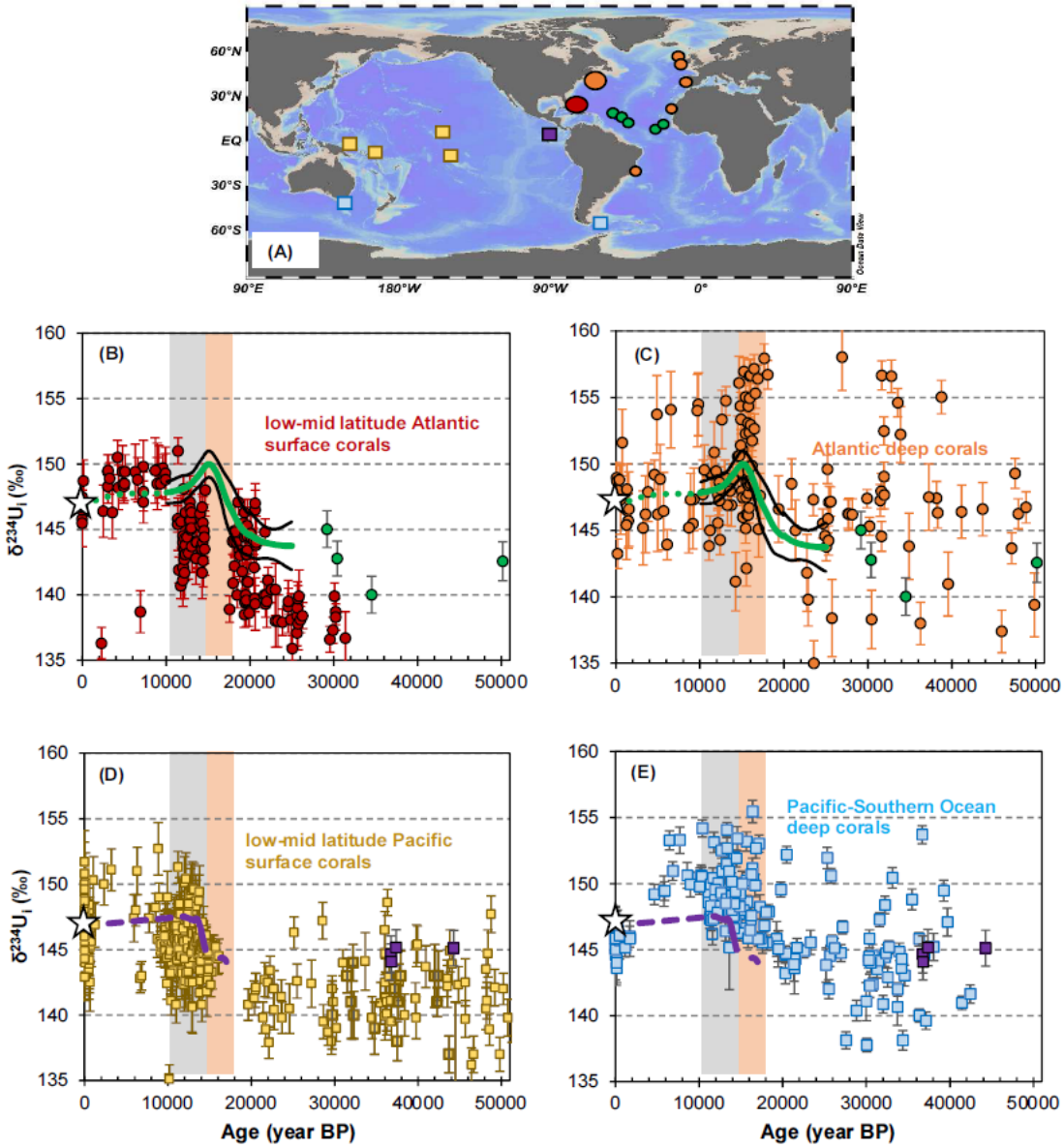

Fig. S3

Compilation of published coral initial $\delta^{234}U$ in comparison with this study over the last 50 ka *(15, 17, 36, 39, 49, 60-75)*. (**A**) Sampling sites of the corals. Symbols are consistent with the following plots. (**B**) Records of published low-mid latitude Atlantic surface corals, overlain by the smoothed curves based on our low latitude North Atlantic deep-sea corals with a few samples (green circles) from the earlier glacial period. (**C**) Same as (B) but showing the published Atlantic deep corals. (**D**) Same as (B) but showing the published low-mid latitude Pacific surface corals (purple curve and squares). (**E**) Same as (D) but showing the published Pacific-Southern Ocean deep-sea corals. Stars in (B) to (E) shows the modern seawater $\delta^{234}U$. Light brown shade indicates the early deglaciation while the grey shade indicates the late deglaciation.

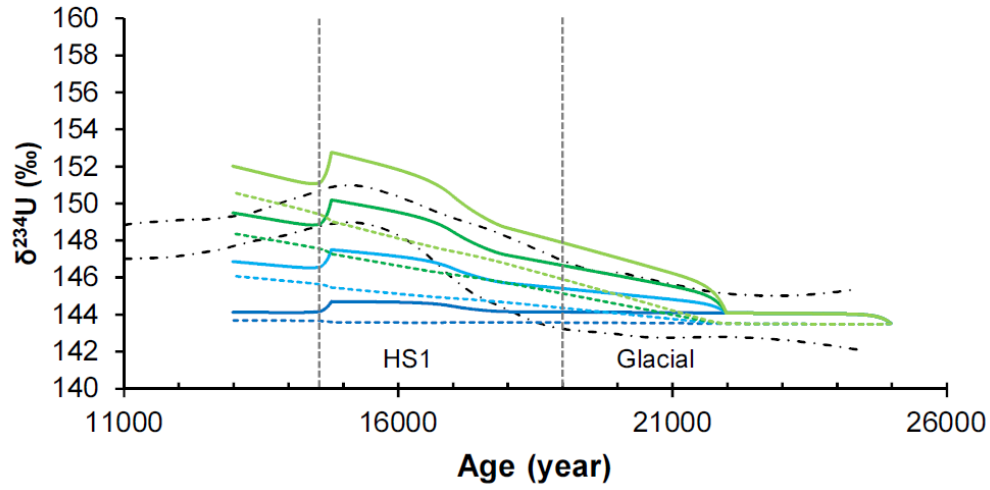

Fig. S4

Sensitivity experiment on the riverine flux variation. Solid lines represent the upper Atlantic $\delta^{234}U$ evolution and dashed lines represent the results of the other ocean. Different colors from bottom to top: $\delta^{234}U$ response to 1, 2, 3, and 4 times of the total modern riverine flux, respectively, during 22-13 ka. Exchange flux between the upper Atlantic and the other ocean applies a 50% reduction of glacial flux (19 Sv) during HS1 as shown in Fig. 3A. For comparison, the area between the black dash-dot curves is the smoothed range of low latitude North Atlantic $\delta^{234}U$. The $\delta^{234}U$ of the riverine and other inputs are kept constant.

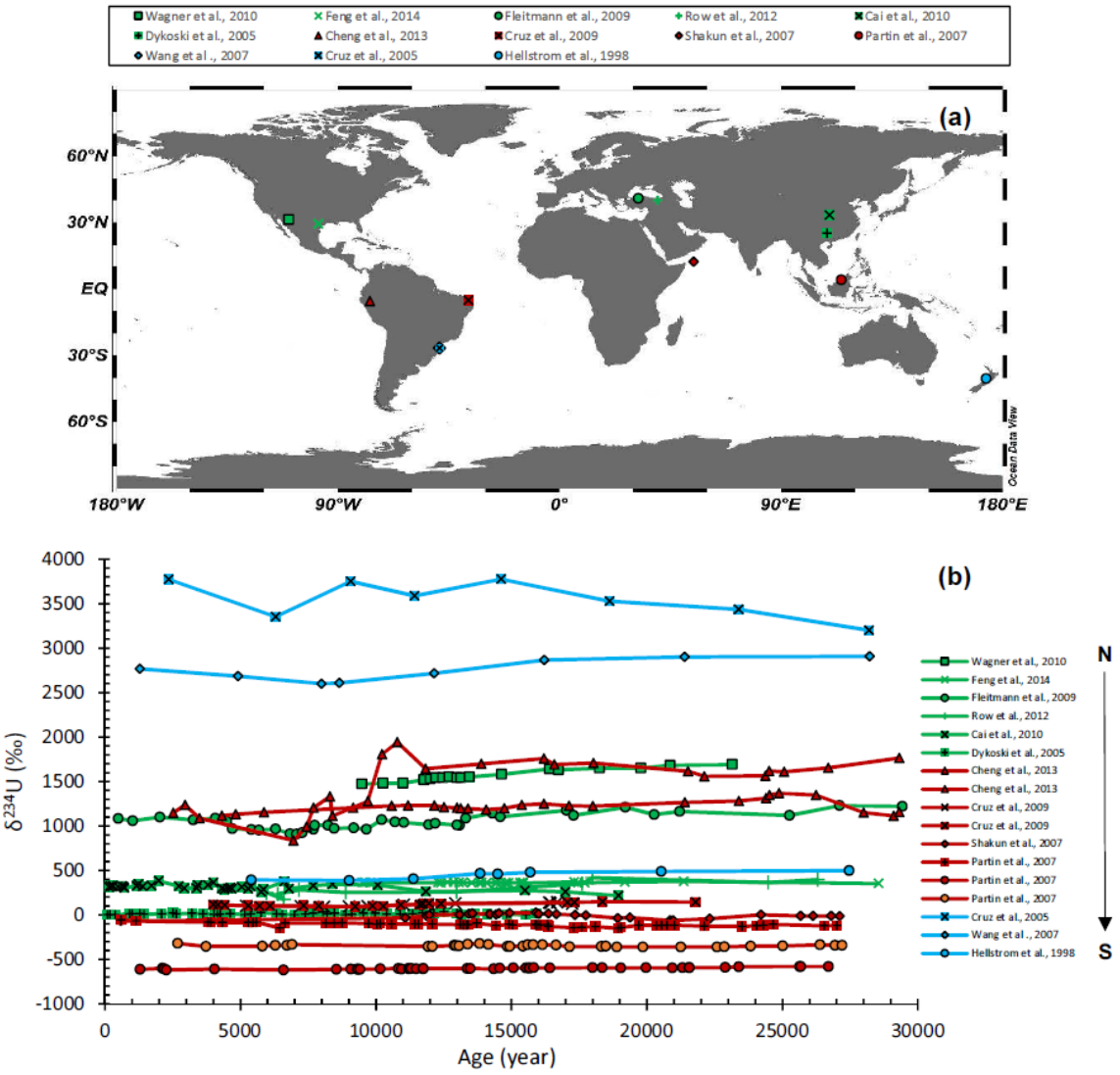

Fig. S5

Compiled low to mid latitude speleothem initial $\delta^{234}U$ records during the last glacial to interglacial transition (*76-88*)**. a,** Map of the speleothem locations. **b,** $\delta^{234}U$ evolution. Note most of the records do not show any distinct change through the transition.

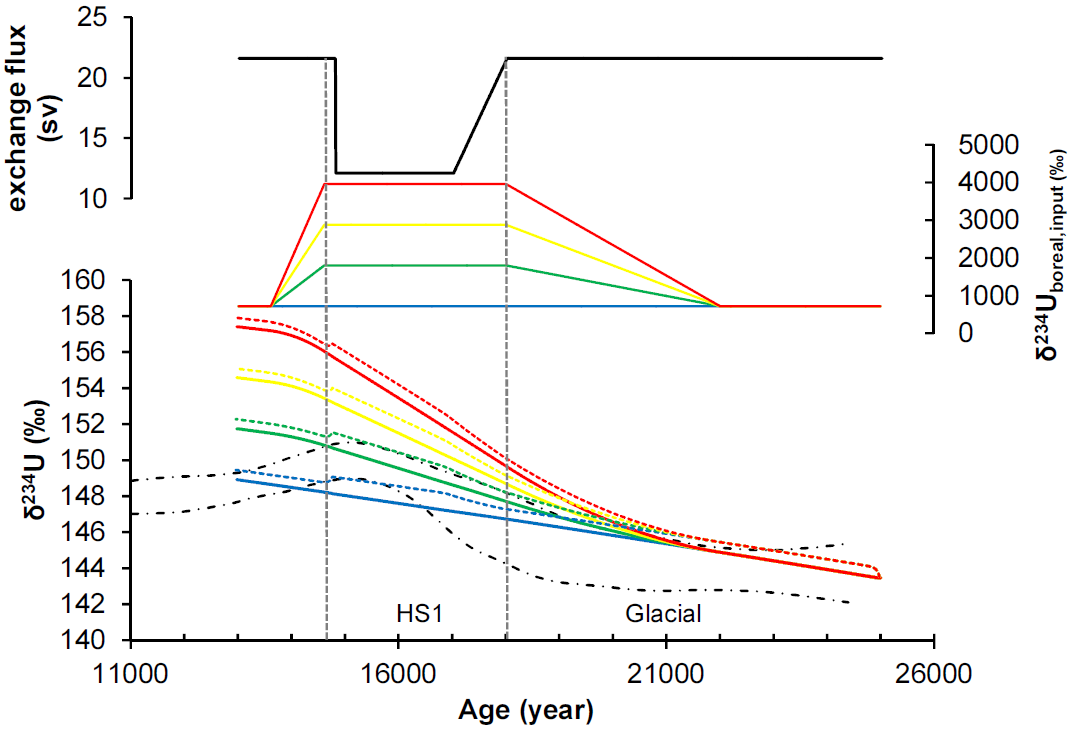

Fig. S6

Sensitivity experiment on surface and intermediate oceanic $\delta^{234}U$ response to complete shutdown of abyssal overturning/mixing during HS1, with variable $\delta^{234}U$ inputs to the polar North Atlantic that directly connects with the intermediate oceans. Solid lines represent the intermediate ocean and dashed lines represent the surface ocean. Each experiment corresponds to the same U inputs shown in Fig. 3B, except all the 'excess' ^{234}U is supplied to the intermediate oceans (Table S2). For reference, the area between the black dash-dot curves is the smoothed range of low latitude North Atlantic $\delta^{234}U$. The $\delta^{234}U$ and U flux of the low latitude riverine inputs are kept constant.

Table S1.

The modern budgets of U in the box model of this study

Box	Input	$^{234}U/^{238}U$	U flux ($\times 10^6$ mol/year)
Upper Atlantic-Arctic 1.4×10^{20} kg[a]			
	High latitude river	1.721[b]	4.1[c]
	Mid-low latitude River	1.247[b]	22.2[c]
	River average	1.321	26.3[c]
	Ground water/other	1.695[d]	1.4[d]
	model input	*1.339*	*27.6*
Other Ocean 1.26×10^{21} kg[a]			
	River	1.188[b]	15.7[c]
	Ground water/other	1.695[d]	3.2[d]
	model input	*1.273*	*18.9*
Total	River	1.271	42.0[c]
	Ground Water/other	1.695[d]	4.6[d]

a. Upper Atlantic-Arctic box is taken as 10% of the global oceanic volume, the approximate volume of the upper ~2.0 km of the Atlantic. Total inventory of oceanic U applied in the model is 1.86×10^{13} mol.

b. Estimated based on the compilation of Andersen et al. (*47*).

c. Riverine U flux was based on Dunk et al. (*14*), Tissot and Dauphas (*30*), but was scaled to the two boxes based on the fresh water discharge estimate of Dai and Trenberth (*89*), assuming U concentration of the rivers to the two model boxes are the same.

d. The U flux and $\delta^{234}U$ of ground water discharge/other was calculated assuming the modern ocean is in equilibrium of U cycling with a U residence time of 400 ky, which is well within the range of Dunk et al. (*14*) estimation for ground water discharge. The U input was scaled to the two boxes based on the ground water estimation of Kwon et al. (*90*), assuming U concentration of the ground water to the two model boxes are the same.

Table S2.

Inputs of U in the surface-intermediate ocean box model

Box	Input	$[^{234}U/^{238}U]^a$	U flux[a] ($\times 10^6$ mol/year)
Polar North surface Atlantic-Intermediate ocean 6.3×10^{20} kg			
	high latitude Atlantic River	1.721	4.1
		(EX1 1.721; EX2 2.98;	
		EX3 4.24;	
	model input	*EX4 5.50)*	*4.1*
Surface Atlantic-Pacific-Indian Ocean 3.5×10^{19} kg			
	mid-low latitude Atlantic River	1.247	22.2
	Other River	1.188	15.7
	Ground water/other	1.695	4.6
	model input	*1.274*	*42.5*

a. Based on the estimation from Table S1.

Table S3.

Geographical information of the deep-sea corals from the low latitude North Atlantic

sample name	Latitude (°N)	Longitude (°E)	Depth (m)
f0047carcs020	9.207	-21.300	1366
f0160enansm001c	10.755	-44.602	1657
f0001carcs027	9.216	-21.316	1080
f0001carcs039	9.216	-21.316	1080
f0061carnm008	5.602	-26.966	1966
f0060carnm029	5.602	-26.967	1985
f0061carnm003	5.602	-26.966	1966
f0060carnm014	5.602	-26.967	1985
f0060carnm021	5.602	-26.967	1985
f0061carnm002	5.602	-26.966	1966
f0060carnm016	5.602	-26.967	1985
f0061carnm001	5.602	-26.966	1966
f0061carnm012	5.602	-26.966	1966
f0061carnm004	5.602	-26.966	1966
f0019enacs005d	9.199	-21.289	1829
f0001carcs013	9.216	-21.316	1080
f0001carcs016	9.216	-21.316	1080
f0048carcs002	9.208	-21.301	1365
f0044carcsm003	9.206	-21.299	1345
f0052carcsm042L	9.220	-21.310	972.8
f0047carcs022	9.207	-21.300	1366
f0059carcs001	9.205	-21.299	1354
f0094descm005	5.620	-26.959	1162
f0054carcm023	9.222	-21.312	800
f0115solnm002c02	10.742	-44.558	1097
f0230descs001	15.422	-51.087	1478
f0115solnm002f02	10.742	-44.558	1097
f0076carcs005	5.626	-26.950	845
f0053carcsm019	9.222	-21.312	800
f0054carns014	9.222	-21.312	800
f0115solnm002g	10.742	-44.558	1097
f0053carcsm018	9.222	-21.312	800
f0076carcs010	5.626	-26.950	845
f0065carcs006	5.608	-26.961	1574
f0183carcm001	14.891	-48.151	840

f0216carcs002	14.865	-48.247	1569

Table S4.

U-Th dating of the deep-sea corals from the low latitude Atlantic

sample name	Age (year BP) corrected	2 sigma	Age (year BP) before correction	2 sigma	$\delta^{234}U_i$	2 sigma	^{238}U (ppm)	2 sigma	^{232}Th (ppt)	2 sigma	$[^{230}Th/^{238}U]$	2 sigma
f0047carcs020	11844	345	12186	60	149.2	1.4	2.60	0.01	1928	7.5	0.1217	0.0005
f0047carcs020	11906	365	12263	69	148.6	1.3	2.52	0.01	1956	8.9	0.1224	0.0006
f0160enansm001c	12300	54	12324	49	146.8	1.3	3.85	0.01	198	0.8	0.1227	0.0004
f0001carcs027	12428	304	12726	65	147.4	1.4	4.88	0.01	3156	13.1	0.1265	0.0006
f0001carcs039	12555	310	12857	66	148.6	1.5	4.34	0.01	2847	11.9	0.1279	0.0006
f0061carnm008	14136	110	14156	108	149.1	1.4	4.27	0.01	194	1.4	0.1399	0.0010
f0060carnm029	14186	99	14215	94	147.9	1.3	4.33	0.01	273	1.3	0.1403	0.0009
f0061carnm003	14222	72	14264	58	149.2	1.4	4.14	0.01	381	1.2	0.1409	0.0005
f0061carnm003	14245	83	14266	81	149.5	1.3	4.23	0.01	184	1.0	0.1410	0.0007
f0060carnm014	14249	87	14276	83	149.5	1.4	4.17	0.01	247	1.4	0.1411	0.0007
f0060carnm021	14276	82	14301	78	149.8	1.3	3.80	0.01	205	1.0	0.1414	0.0007
f0061carnm002	14285	88	14295	87	149.6	1.4	3.84	0.01	86	0.6	0.1413	0.0008
f0060carnm016	14301	92	14329	87	149.4	1.4	4.31	0.01	269	1.5	0.1416	0.0008
f0061carnm001	14326	111	14362	105	149.0	1.3	4.55	0.02	361	1.8	0.1418	0.0010
f0061carnm012	14327	89	14352	85	150.1	1.4	4.49	0.01	242	1.2	0.1419	0.0008
f0061carnm004	14327	103	14372	93	150.7	1.3	4.51	0.02	434	1.9	0.1421	0.0008
f0019enacs005d	14428	97	14481	82	149.4	1.5	4.60	0.01	530	2.4	0.1430	0.0007
f0001carcs013	14943	219	15146	82	150.8	1.2	3.58	0.01	1583	6.9	0.1492	0.0007
f0001carcs016	15157	230	15371	84	150.1	1.4	4.33	0.01	2011	8.9	0.1512	0.0007
f0048carcs002	15811	273	16070	85	150.4	1.1	4.82	0.01	2714	11.6	0.1576	0.0008
f0048carcs002	15983	373	16346	90	149.5	1.3	4.95	0.01	3886	15.3	0.1599	0.0008
f0044carcsm003	16001	256	16240	92	149.9	1.3	4.59	0.01	2385	10.7	0.1590	0.0008
f0044carcsm003	16030	234	16244	94	150.1	1.3	4.13	0.01	1922	7.9	0.1591	0.0008
f0052carcsm042L	16001	243	16227	92	150.6	1.4	3.68	0.01	1806	7.8	0.1590	0.0008
f0047carcs022	16009	310	16304	92	149.1	1.3	3.85	0.01	2472	10.8	0.1595	0.0008
f0047carcs022	16064	265	16311	97	149.4	1.3	3.62	0.01	1937	8.9	0.1596	0.0009
f0059carcs001	16773	229	16981	97	149.2	1.3	4.26	0.01	1919	8.7	0.1656	0.0009
f0059carcs001	16810	268	17060	96	147.6	1.5	4.31	0.01	2335	10.2	0.1661	0.0008
f0094descm005	16980	144	17094	87	147.2	1.4	4.77	0.01	1182	4.9	0.1663	0.0008
f0054carcm023	17806	292	18079	105	144.2	1.4	3.99	0.01	2350	10.1	0.1746	0.0009
f0054carcm023	17837	293	18111	98	145.7	1.4	3.99	0.01	2373	9.6	0.1751	0.0008
f0115solnm002c02	20294	193	20445	120	143.4	1.4	4.88	0.01	1598	6.8	0.1951	0.0010
f0230descs001	20818	159	20919	123	147.3	1.5	3.90	0.01	855	4.3	0.1998	0.0010
f0115solnm002f02	22551	172	22659	132	145.2	1.4	5.62	0.01	1320	5.6	0.2143	0.0011

f0076carcs005	23894	312	24170	143	143.6	1.3	4.94	0.01	2955	12.4	0.2266	0.0012
f0053carcsm019	24016	263	24242	134	142.6	1.5	4.01	0.01	1958	8.1	0.2270	0.0011
f0053carcsm019	24144	297	24406	139	142.4	1.3	3.92	0.01	2218	9.4	0.2284	0.0011
f0054carns014	25244	203	25382	148	146.2	1.3	3.65	0.01	1097	4.8	0.2372	0.0012
f0115solnm002g	25437	269	25646	170	143.6	2.2	5.32	0.02	2405	10.3	0.2388	0.0013
f0053carcsm018	25898	194	26011	157	144.9	1.4	4.06	0.01	989	4.2	0.2421	0.0013
f0076carcs010	29182	266	29390	168	145.0	1.4	3.91	0.01	1750	7.4	0.2693	0.0013
f0065carcs006	30393	275	30597	184	142.8	1.3	4.88	0.02	2150	11.6	0.2782	0.0014
f0183carcm001	34504	223	34608	198	140.0	1.4	5.02	0.01	1117	5.1	0.3082	0.0015
f0216carcs002	50140	344	50263	321	142.6	1.5	4.95	0.01	1313	5.7	0.4181	0.0021

Table S5.

Geographical information of the deep-sea corals from the Galápagos platform

sample name	Latitude (°N)	Longitude (°E)	Depth (m)
NA064-118-1-C-2A	-0.371	-90.815	419
NA064-117-01-C-2B	-0.371	-90.815	421
NA064-118-1-C-2B	-0.371	-90.815	419
MV1007-DO3-4-37	0.459	-90.712	627
MV1007-DO9-2	0.787	-91.304	589
MV1007-DO3-5-16	0.459	-90.712	627
MV1007-DO3-4-53	0.459	-90.712	627
MV1007-DO3-4-27	0.459	-90.712	627
MV1007-DO3-4-55	0.459	-90.712	627
MV1007-DO3-2-4	0.459	-90.712	627
MV1007-DO3-4-60	0.459	-90.712	627
MV1007-DO3-4-51	0.459	-90.712	627
MV1007-DO3-4-59	0.459	-90.712	627
MV1007-DO3-4-20	0.459	-90.712	627
MV1007-DO3-2-2	0.459	-90.712	627
MV1007-DO3-2-3	0.459	-90.712	627
MV1007-DO3-2-1	0.459	-90.712	627
MV1007-DO3-4-52	0.459	-90.712	627
MV1007-DO3-2-13	0.459	-90.712	627
MV1007-DO3-2-15	0.459	-90.712	627
MV1007-DO3-5-37	0.459	-90.712	627
MV1007-DO3-4-42	0.459	-90.712	627
MV1007-DO3-1-12	0.459	-90.712	627
MV1007-DO3-1-8	0.459	-90.712	627
MV1007-DO3-5-5	0.459	-90.712	627
MV1007-DO3-1-7	0.459	-90.712	627

Table S6.

U-Th dating of the deep-sea corals from the Galápagos platform

sample name	Age (year BP) corrected	2 sigma	Age (year BP) before correction	2 sigma	$\delta^{234}U_i$	2 sigma	^{238}U (ppm)	2 sigma	^{232}Th (ppt)	2 sigma	[$^{230}Th/^{238}U$]	2 sigma
NA064-118-1-C-2A	2517	21	2532	15	146.5	1.5	3.35	9.23E-03	17.9	0.21	0.0269	1.49E-04
NA064-117-01-C-2B	2942	55	2995	16	147.3	1.4	4.25	9.90E-03	79.5	0.36	0.0317	1.57E-04
NA064-118-1-C-2B	3101	41	3134	23	145.2	1.2	2.76	1.08E-02	32.8	0.26	0.0331	2.35E-04
MV1007-DO3-4-37	11231	63	11229	63	148.6	1.4	4.89	1.35E-02	-3.9	0.26	0.1126	5.80E-04
MV1007-DO9-2	11843	68	11865	65	147.6	1.4	4.43	1.03E-02	34.7	0.24	0.1185	5.88E-04
MV1007-DO3-5-16	12178	70	12194	69	146.6	1.4	4.28	9.22E-03	23.7	0.25	0.1217	6.27E-04
MV1007-DO3-4-53	13604	74	13609	74	148.6	1.4	4.10	9.59E-03	6.8	0.28	0.1349	6.66E-04
MV1007-DO3-4-27	13654	200	13840	71	146.0	1.4	4.13	8.63E-03	270.9	1.16	0.1367	6.43E-04
MV1007-DO3-4-55	13873	74	13873	74	146.7	1.5	4.34	9.71E-03	0.8	0.26	0.1371	6.65E-04
MV1007-DO3-2-4	14458	92	14480	89	144.1	1.5	4.37	1.09E-02	35.0	0.27	0.1425	7.99E-04
MV1007-DO3-4-60	14467	114	14478	113	146.1	1.5	4.11	1.23E-02	16.2	0.23	0.1427	1.03E-03
MV1007-DO3-4-51	15086	118	15101	117	155.1	1.6	3.93	1.11E-02	21.4	0.30	0.1496	1.06E-03
MV1007-DO3-4-59	16153	129	16186	125	143.3	1.2	4.35	1.08E-02	50.2	0.31	0.1578	1.11E-03
MV1007-DO3-4-20	16285	150	16359	130	142.6	1.3	4.44	1.27E-02	116.3	0.55	0.1593	1.16E-03
MV1007-DO3-2-2	16383	106	16439	90	146.0	1.5	4.25	1.05E-02	84.0	0.39	0.1603	7.90E-04
MV1007-DO3-2-3	16535	93	16545	92	145.3	1.4	4.56	1.16E-02	15.8	0.32	0.1611	8.07E-04
MV1007-DO3-2-1	16581	92	16594	91	144.0	1.3	4.61	1.04E-02	21.1	0.28	0.1614	8.00E-04
MV1007-DO3-4-52	16593	91	16608	89	145.7	1.4	4.18	9.61E-03	21.5	0.78	0.1618	7.79E-04
MV1007-DO3-2-13	16622	92	16624	92	144.8	1.5	4.52	1.09E-02	3.9	0.27	0.1618	8.02E-04
MV1007-DO3-2-15	16672	109	16717	101	142.9	1.4	4.06	8.72E-03	64.0	0.44	0.1625	8.83E-04
MV1007-DO3-5-37	16710	111	16741	107	144.3	1.6	4.19	1.39E-02	46.3	0.52	0.1628	9.31E-04
MV1007-DO3-4-42	17259	127	17301	120	143.7	1.2	4.40	1.67E-02	65.9	0.32	0.1679	1.06E-03
MV1007-DO3-1-12	36756	239	36811	233	144.6	1.4	4.10	1.24E-02	79.7	0.38	0.3259	1.69E-03
MV1007-DO3-1-8	36775	245	36880	220	144.1	1.4	4.34	1.04E-02	160.3	0.71	0.3266	1.60E-03
MV1007-DO3-5-5	37373	219	37396	218	145.2	1.4	3.68	7.91E-03	30.8	0.31	0.3303	1.57E-03
MV1007-DO3-1-7	44281	299	44367	287	145.1	1.4	4.41	1.10E-02	132.4	0.62	0.3797	1.95E-03

Table S7.

Compilation of published coral initial $\delta^{234}U$ from the last glacial to the Holocene

Reference	Location	Coral Type	Ocean	Age (year BP)	2s error	$\delta^{234}U_i$*	2s error
Bard et al. (*60*)	Tahiti	Surface	Pacific	9594	286	145.7	2.0
Bard et al.	Tahiti	Surface	Pacific	9632	47	145.6	2.0
Bard et al.	Tahiti	Surface	Pacific	9642	51	146.7	2.0
Bard et al.	Tahiti	Surface	Pacific	9656	45	144.9	2.0
Bard et al.	Tahiti	Surface	Pacific	9713	42	146.5	2.0
Bard et al.	Tahiti	Surface	Pacific	9883	62	144.4	2.0
Bard et al.	Tahiti	Surface	Pacific	9895	46	146.1	2.0
Bard et al.	Tahiti	Surface	Pacific	9951	216	149.0	2.0
Bard et al.	Tahiti	Surface	Pacific	9978	47	145.8	2.0
Bard et al.	Tahiti	Surface	Pacific	10179	31	146.0	2.0
Bard et al.	Tahiti	Surface	Pacific	10182	66	144.6	2.0
Bard et al.	Tahiti	Surface	Pacific	10262	41	146.9	1.0
Bard et al.	Tahiti	Surface	Pacific	10289	46	144.9	2.0
Bard et al.	Tahiti	Surface	Pacific	10314	47	143.2	2.0
Bard et al.	Tahiti	Surface	Pacific	10514	30	145.6	1.0
Bard et al.	Tahiti	Surface	Pacific	10670	122	147.0	2.0
Bard et al.	Tahiti	Surface	Pacific	10730	43	146.0	2.0
Bard et al.	Tahiti	Surface	Pacific	10790	32	145.8	2.0
Bard et al.	Tahiti	Surface	Pacific	10826	87	146.8	2.0
Bard et al.	Tahiti	Surface	Pacific	10971	230	147.2	2.0
Bard et al.	Tahiti	Surface	Pacific	11031	42	146.2	2.0
Bard et al.	Tahiti	Surface	Pacific	11059	48	144.6	2.0
Bard et al.	Tahiti	Surface	Pacific	11061	40	145.6	2.0
Bard et al.	Tahiti	Surface	Pacific	11062	39	145.4	2.0
Bard et al.	Tahiti	Surface	Pacific	11073	39	146.5	2.0
Bard et al.	Tahiti	Surface	Pacific	11090	42	144.2	2.0
Bard et al.	Tahiti	Surface	Pacific	11140	146	146.4	1.0
Bard et al.	Tahiti	Surface	Pacific	11321	53	145.0	1.0
Bard et al.	Tahiti	Surface	Pacific	11346	41	145.8	2.0
Bard et al.	Tahiti	Surface	Pacific	11386	54	148.5	2.0
Bard et al.	Tahiti	Surface	Pacific	11393	76	144.5	2.0
Bard et al.	Tahiti	Surface	Pacific	11563	42	144.5	2.0
Bard et al.	Tahiti	Surface	Pacific	11756	46	145.8	2.0
Bard et al.	Tahiti	Surface	Pacific	11902	43	145.6	2.0
Bard et al.	Tahiti	Surface	Pacific	12004	58	144.3	2.0

Bard et al.	Tahiti	Surface	Pacific	12004	45	150.1	2.0
Bard et al.	Tahiti	Surface	Pacific	12048	55	146.6	2.0
Bard et al.	Tahiti	Surface	Pacific	12060	67	146.4	2.0
Bard et al.	Tahiti	Surface	Pacific	12149	112	150.4	2.0
Bard et al.	Tahiti	Surface	Pacific	12279	54	146.8	2.0
Bard et al.	Tahiti	Surface	Pacific	12328	57	145.7	2.0
Bard et al.	Tahiti	Surface	Pacific	12340	46	147.5	2.0
Bard et al.	Tahiti	Surface	Pacific	12377	45	145.1	2.0
Bard et al.	Tahiti	Surface	Pacific	12486	89	147.9	2.0
Bard et al.	Tahiti	Surface	Pacific	12510	70	148.5	2.0
Bard et al.	Tahiti	Surface	Pacific	12559	44	147.2	2.0
Bard et al.	Tahiti	Surface	Pacific	12780	44	146.6	1.0
Bard et al.	Tahiti	Surface	Pacific	12785	62	144.8	2.0
Bard et al.	Tahiti	Surface	Pacific	12796	78	149.5	2.0
Bard et al.	Tahiti	Surface	Pacific	12875	46	146.4	2.0
Bard et al.	Tahiti	Surface	Pacific	12943	36	149.7	2.0
Bard et al.	Tahiti	Surface	Pacific	12945	61	142.5	2.0
Bard et al.	Tahiti	Surface	Pacific	12950	49	146.4	2.0
Bard et al.	Tahiti	Surface	Pacific	12956	57	146.2	2.0
Bard et al.	Tahiti	Surface	Pacific	12968	47	147.3	2.0
Bard et al.	Tahiti	Surface	Pacific	12981	63	145.3	2.0
Bard et al.	Tahiti	Surface	Pacific	13000	57	147.3	2.0
Bard et al.	Tahiti	Surface	Pacific	13086	247	147.2	2.0
Bard et al.	Tahiti	Surface	Pacific	13110	47	149.6	2.0
Bard et al.	Tahiti	Surface	Pacific	13146	47	145.3	2.0
Bard et al.	Tahiti	Surface	Pacific	13356	150	145.6	2.0
Bard et al.	Tahiti	Surface	Pacific	13398	47	146.2	2.0
Bard et al.	Tahiti	Surface	Pacific	13510	64	144.9	2.0
Bard et al.	Tahiti	Surface	Pacific	13743	47	148.7	2.0
Bard et al.	Tahiti	Surface	Pacific	13756	69	144.8	2.0
Bard et al.	Tahiti	Surface	Pacific	13767	68	149.4	2.0
Bard et al.	Tahiti	Surface	Pacific	13788	49	143.7	2.0
Bard et al.	Tahiti	Surface	Pacific	13801	36	141.7	1.0
Bard et al.	Tahiti	Surface	Pacific	13837	261	145.0	2.0
Bard et al.	Tahiti	Surface	Pacific	13856	66	143.4	2.0
Bard et al.	Tahiti	Surface	Pacific	13929	64	144.1	2.0
Burke and Robinson (*61*)	Drake Passage	Deep	Southern Ocean	9	78	145.9	0.7

Burke and Robinson	Drake Passage	Deep	Southern Ocean	66	11	146.8	0.7
Burke and Robinson	Drake Passage	Deep	Southern Ocean	468	21	146.1	0.7
Burke and Robinson	Drake Passage	Deep	Southern Ocean	1144	54	145.1	0.7
Burke and Robinson	Drake Passage	Deep	Southern Ocean	1708	28	146.0	0.8
Burke and Robinson	Drake Passage	Deep	Southern Ocean	1749	34	145.8	1.4
Burke and Robinson	Drake Passage	Deep	Southern Ocean	4643	169	149.2	0.8
Burke and Robinson	Drake Passage	Deep	Southern Ocean	5819	66	149.4	1.2
Burke and Robinson	Drake Passage	Deep	Southern Ocean	5883	53	149.4	0.7
Burke and Robinson	Drake Passage	Deep	Southern Ocean	6470	48	153.3	0.7
Burke and Robinson	Drake Passage	Deep	Southern Ocean	6858	69	151.0	0.7
Burke and Robinson	Drake Passage	Deep	Southern Ocean	7699	67	153.3	1.0
Burke and Robinson	Drake Passage	Deep	Southern Ocean	10144	62	150.5	0.7
Burke and Robinson	Drake Passage	Deep	Southern Ocean	10255	81	150.6	0.8
Burke and Robinson	Drake Passage	Deep	Southern Ocean	10304	79	150.5	0.7
Burke and Robinson	Drake Passage	Deep	Southern Ocean	11117	66	149.3	0.8
Burke and Robinson	Drake Passage	Deep	Southern Ocean	11142	69	148.6	0.7
Burke and Robinson	Drake Passage	Deep	Southern Ocean	11253	84	147.3	0.7
Burke and Robinson	Drake Passage	Deep	Southern Ocean	11365	135	149.9	0.8
Burke and Robinson	Drake Passage	Deep	Southern Ocean	11376	72	147.8	0.8
Burke and Robinson	Drake Passage	Deep	Southern Ocean	11405	94	148.3	0.7
Burke and Robinson	Drake Passage	Deep	Southern Ocean	11460	95	147.2	0.8
Burke and Robinson	Drake Passage	Deep	Southern Ocean	11608	131	146.2	0.8
Burke and Robinson	Drake Passage	Deep	Southern Ocean	11664	170	150.4	0.8
Burke and Robinson	Drake Passage	Deep	Southern Ocean	11699	129	147.4	0.8
Burke and Robinson	Drake Passage	Deep	Southern Ocean	11777	135	153.1	0.8

Burke and Robinson	Drake Passage	Deep	Southern Ocean	11911	125	149.1	0.8
Burke and Robinson	Drake Passage	Deep	Southern Ocean	12287	108	150.0	0.8
Burke and Robinson	Drake Passage	Deep	Southern Ocean	12798	122	148.5	0.7
Burke and Robinson	Drake Passage	Deep	Southern Ocean	13187	154	146.4	0.7
Burke and Robinson	Drake Passage	Deep	Southern Ocean	13397	76	151.3	0.7
Burke and Robinson	Drake Passage	Deep	Southern Ocean	13707	68	148.5	0.8
Burke and Robinson	Drake Passage	Deep	Southern Ocean	14710	95	148.1	0.7
Burke and Robinson	Drake Passage	Deep	Southern Ocean	15688	100	153.2	0.7
Burke and Robinson	Drake Passage	Deep	Southern Ocean	16402	310	155.5	0.9
Burke and Robinson	Drake Passage	Deep	Southern Ocean	20330	345	143.2	0.8
Burke and Robinson	Drake Passage	Deep	Southern Ocean	21524	220	144.3	0.8
Burke and Robinson	Drake Passage	Deep	Southern Ocean	25647	322	144.5	0.8
Chen et al. (*36*)	Drake Passage	Deep	Southern Ocean	12564	124	148.3	0.4
Chen et al.	Drake Passage	Deep	Southern Ocean	13113	131	147.6	0.4
Chen et al.	Drake Passage	Deep	Southern Ocean	13158	134	148.0	0.4
Chen et al.	Drake Passage	Deep	Southern Ocean	14063	121	148.7	0.4
Chen et al.	Drake Passage	Deep	Southern Ocean	14103	115	149.1	0.4
Chen et al.	Drake Passage	Deep	Southern Ocean	14177	243	152.0	0.5
Chen et al.	Drake Passage	Deep	Southern Ocean	14783	131	147.7	0.4
Chen et al.	Drake Passage	Deep	Southern Ocean	15221	145	148.3	0.4
Chen et al.	Drake Passage	Deep	Southern Ocean	15761	289	148.6	0.5
Chen et al.	Drake Passage	Deep	Southern Ocean	16176	115	147.0	0.4
Chen et al.	Drake Passage	Deep	Southern Ocean	20367	116	144.6	0.4
Chen et al.	Drake Passage	Deep	Southern Ocean	22578	162	144.9	0.5
Chen et al.	Drake Passage	Deep	Southern Ocean	25896	218	145.6	0.5

Chen et al.	Drake Passage	Deep	Southern Ocean	27159	244	146.7	0.5
Chen et al.	Low latitude Atlantic	Deep	Atlantic	269	99	145.8	1.2
Chen et al.	Low latitude Atlantic	Deep	Atlantic	371	58	147.0	1.2
Chen et al.	Low latitude Atlantic	Deep	Atlantic	474	60	142.6	1.3
Chen et al.	Low latitude Atlantic	Deep	Atlantic	692	17	147.0	1.3
Chen et al.	Low latitude Atlantic	Deep	Atlantic	731	128	147.5	1.2
Chen et al.	Low latitude Atlantic	Deep	Atlantic	2267	23	147.5	1.4
Chen et al.	Low latitude Atlantic	Deep	Atlantic	2273	21	147.4	1.3
Chen et al.	Low latitude Atlantic	Deep	Atlantic	6799	69	147.8	1.2
Chen et al.	Low latitude Atlantic	Deep	Atlantic	8602	35	147.6	1.3
Chen et al.	Low latitude Atlantic	Deep	Atlantic	8962	37	148.0	1.3
Chen et al.	Low latitude Atlantic	Deep	Atlantic	10383	49	147.7	1.3
Chen et al.	Low latitude Atlantic	Deep	Atlantic	10413	160	148.5	1.2
Chen et al.	Low latitude Atlantic	Deep	Atlantic	10499	44	147.0	1.2
Chen et al.	Low latitude Atlantic	Deep	Atlantic	10647	69	148.6	1.3
Chen et al.	Low latitude Atlantic	Deep	Atlantic	10812	50	147.4	1.2
Chen et al.	Low latitude Atlantic	Deep	Atlantic	11357	68	146.2	1.3
Chen et al.	Low latitude Atlantic	Deep	Atlantic	11391	115	148.0	1.4
Chen et al.	Low latitude Atlantic	Deep	Atlantic	11399	104	148.0	1.3
Chen et al.	Low latitude Atlantic	Deep	Atlantic	11482	133	148.9	1.3
Chen et al.	Low latitude Atlantic	Deep	Atlantic	11552	88	149.4	1.3
Chen et al.	Low latitude Atlantic	Deep	Atlantic	11743	53	146.9	1.3
Chen et al.	Low latitude Atlantic	Deep	Atlantic	11786	182	147.8	1.3
Chen et al.	Low latitude Atlantic	Deep	Atlantic	12042	102	146.7	1.3
Chen et al.	Low latitude Atlantic	Deep	Atlantic	12149	51	147.2	1.3

Chen et al.	Low latitude Atlantic	Deep	Atlantic	12239	57	147.7	1.3
Chen et al.	Low latitude Atlantic	Deep	Atlantic	12292	150	149.4	1.4
Chen et al.	Low latitude Atlantic	Deep	Atlantic	12450	111	148.4	1.3
Chen et al.	Low latitude Atlantic	Deep	Atlantic	12465	196	148.5	1.4
Chen et al.	Low latitude Atlantic	Deep	Atlantic	12850	85	149.0	1.3
Chen et al.	Low latitude Atlantic	Deep	Atlantic	13234	164	147.2	1.4
Chen et al.	Low latitude Atlantic	Deep	Atlantic	13368	123	148.5	1.4
Chen et al.	Low latitude Atlantic	Deep	Atlantic	13430	58	146.2	1.3
Chen et al.	Low latitude Atlantic	Deep	Atlantic	13972	93	149.6	1.3
Chen et al.	Low latitude Atlantic	Deep	Atlantic	14173	86	149.3	1.4
Chen et al.	Low latitude Atlantic	Deep	Atlantic	14178	90	148.9	1.3
Chen et al.	Low latitude Atlantic	Deep	Atlantic	14222	95	149.0	1.3
Chen et al.	Low latitude Atlantic	Deep	Atlantic	14284	153	147.7	1.3
Chen et al.	Low latitude Atlantic	Deep	Atlantic	14389	55	145.9	1.3
Chen et al.	Low latitude Atlantic	Deep	Atlantic	14515	113	148.7	1.3
Chen et al.	Low latitude Atlantic	Deep	Atlantic	14516	104	146.0	1.2
Chen et al.	Low latitude Atlantic	Deep	Atlantic	14611	148	149.9	1.4
Chen et al.	Low latitude Atlantic	Deep	Atlantic	14753	161	152.7	1.2
Chen et al.	Low latitude Atlantic	Deep	Atlantic	14817	85	149.9	1.5
Chen et al.	Low latitude Atlantic	Deep	Atlantic	14846	144	150.2	1.3
Chen et al.	Low latitude Atlantic	Deep	Atlantic	14895	141	150.4	1.4
Chen et al.	Low latitude Atlantic	Deep	Atlantic	14937	101	148.3	1.2
Chen et al.	Low latitude Atlantic	Deep	Atlantic	14969	105	150.8	1.3
Chen et al.	Low latitude Atlantic	Deep	Atlantic	15071	189	148.8	1.4
Chen et al.	Low latitude Atlantic	Deep	Atlantic	15378	107	150.1	1.4

Chen et al.	Low latitude Atlantic	Deep	Atlantic	15450	103	150.8	1.3
Chen et al.	Low latitude Atlantic	Deep	Atlantic	15782	217	149.7	1.3
Chen et al.	Low latitude Atlantic	Deep	Atlantic	15924	173	150.3	1.2
Chen et al.	Low latitude Atlantic	Deep	Atlantic	15952	144	148.8	1.3
Chen et al.	Low latitude Atlantic	Deep	Atlantic	15956	119	152.6	1.5
Chen et al.	Low latitude Atlantic	Deep	Atlantic	16172	211	147.8	1.4
Chen et al.	Low latitude Atlantic	Deep	Atlantic	16175	148	147.9	1.3
Chen et al.	Low latitude Atlantic	Deep	Atlantic	16444	132	148.1	1.3
Chen et al.	Low latitude Atlantic	Deep	Atlantic	16465	227	148.2	1.2
Chen et al.	Low latitude Atlantic	Deep	Atlantic	16473	236	147.9	1.3
Chen et al.	Low latitude Atlantic	Deep	Atlantic	16521	174	146.3	1.5
Chen et al.	Low latitude Atlantic	Deep	Atlantic	16538	227	147.7	1.3
Chen et al.	Low latitude Atlantic	Deep	Atlantic	16980	144	147.2	1.4
Chen et al.	Low latitude Atlantic	Deep	Atlantic	17099	255	145.8	1.3
Chen et al.	Low latitude Atlantic	Deep	Atlantic	17151	179	148.9	1.4
Chen et al.	Low latitude Atlantic	Deep	Atlantic	17366	236	146.2	1.4
Chen et al.	Low latitude Atlantic	Deep	Atlantic	17818	156	145.0	1.5
Chen et al.	Low latitude Atlantic	Deep	Atlantic	18616	165	146.9	1.5
Chen et al.	Low latitude Atlantic	Deep	Atlantic	20105	213	145.2	1.4
Chen et al.	Low latitude Atlantic	Deep	Atlantic	21089	126	147.2	1.5
Chen et al.	Low latitude Atlantic	Deep	Atlantic	22308	168	143.8	1.3
Chen et al.	Low latitude Atlantic	Deep	Atlantic	22321	164	144.0	1.4
Chen et al.	Low latitude Atlantic	Deep	Atlantic	22415	161	143.5	1.3
Chen et al.	Low latitude Atlantic	Deep	Atlantic	22980	349	144.3	1.2
Chen et al.	Low latitude Atlantic	Deep	Atlantic	23006	315	144.2	1.4

Chen et al.	Low latitude Atlantic	Deep	Atlantic	23781	205	146.5	1.4
Chen et al.	Low latitude Atlantic	Deep	Atlantic	25288	174	142.5	1.2
Cheng et al. (*39*)	N. Atlantic	Deep	Atlantic	12951	120	149.0	1.3
Cheng et al.	N. Atlantic	Deep	Atlantic	13258	760	146.9	1.5
Cheng et al.	N. Atlantic	Deep	Atlantic	13556	488	148.1	1.4
Cheng et al.	N. Atlantic	Deep	Atlantic	13736	223	146.9	1.6
Cheng et al.	N. Atlantic	Deep	Atlantic	15058	1131	151.1	2.2
Cheng et al.	N. Atlantic	Deep	Atlantic	15406	396	147.6	1.4
Cheng et al.	Pacific	Deep	Pacific	8	5	145.1	1.5
Cheng et al.	Pacific	Deep	Pacific	11	12	144.6	1.9
Cheng et al.	Pacific	Deep	Pacific	13	6	145.8	1.6
Cheng et al.	Pacific	Deep	Pacific	17	6	147.2	1.1
Cheng et al.	Pacific	Deep	Pacific	26	7	146.0	2.2
Cheng et al.	Pacific	Deep	Pacific	33	4	145.0	1.2
Cheng et al.	Pacific	Deep	Pacific	80	11	146.6	1.4
Cheng et al.	Pacific	Deep	Pacific	117	9	146.4	1.5
Cheng et al.	Pacific	Deep	Pacific	123	6	145.1	1.7
Cheng et al.	Pacific	Deep	Pacific	140	9	143.6	1.3
Cheng et al.	Pacific	Deep	Pacific	150	7	144.6	1.2
Cheng et al.	Pacific	Deep	Pacific	156	9	144.0	1.5
Cheng et al.	Pacific	Deep	Pacific	158	9	145.5	1.3
Cheng et al.	Pacific	Deep	Pacific	225	5	146.8	1.2
Cheng et al.	Pacific	Deep	Pacific	265	14	146.4	1.2
Cheng et al.	Pacific	Deep	Pacific	275	6	145.8	1.1
Cheng et al.	Pacific	Deep	Pacific	536	14	145.7	1.4
Cobb et al. (*62*)	Palmyra	Surface	Pacific	6	2	145.1	1.8
Cobb et al.	Palmyra	Surface	Pacific	14	2	146.1	1.1
Cobb et al.	Palmyra	Surface	Pacific	14	2	145.4	1.2
Cobb et al.	Palmyra	Surface	Pacific	14	2	144.1	1.8
Cobb et al.	Palmyra	Surface	Pacific	62	3	146.0	1.3
Cobb et al.	Palmyra	Surface	Pacific	62	2	143.0	1.9
Cobb et al.	Palmyra	Surface	Pacific	489	7	148.2	1.5
Cobb et al.	Palmyra	Surface	Pacific	489	8	145.2	2.1
Cobb et al.	Palmyra	Surface	Pacific	503	5	146.7	1.1
Cobb et al.	Palmyra	Surface	Pacific	508	5	145.6	1.4
Cobb et al.	Palmyra	Surface	Pacific	517	8	146.4	1.6
Cobb et al.	Palmyra	Surface	Pacific	523	7	148.5	1.2

Cobb et al.	Palmyra	Surface	Pacific	523	5	143.5	2.3
Cobb et al.	Palmyra	Surface	Pacific	538	10	145.5	2.4
Cobb et al.	Palmyra	Surface	Pacific	543	5	146.1	1.1
Cobb et al.	Palmyra	Surface	Pacific	543	5	145.9	1.7
Cobb et al.	Palmyra	Surface	Pacific	545	4	145.8	1.3
Cobb et al.	Palmyra	Surface	Pacific	545	5	146.3	1.3
Cobb et al.	Palmyra	Surface	Pacific	547	4	146.1	1.0
Cobb et al.	Palmyra	Surface	Pacific	585	6	148.0	1.0
Cobb et al.	Palmyra	Surface	Pacific	598	5	146.7	1.3
Cobb et al.	Palmyra	Surface	Pacific	623	9	142.5	2.2
Cobb et al.	Palmyra	Surface	Pacific	626	5	145.2	1.2
Collins et al. (*63*)	Australia	Surface	Pacific	1058	10	150.3	1.8
Collins et al.	Australia	Surface	Pacific	2335	13	150.0	1.6
Collins et al.	Australia	Surface	Pacific	3226	56	151.1	1.6
Collins et al.	Australia	Surface	Pacific	5913	27	147.4	1.8
Collins et al.	Australia	Surface	Pacific	6323	23	151.0	1.8
Cutler et al. (*15*)	Huon	Surface	Pacific	6150	28	148.0	1.2
Cutler et al.	Huon	Surface	Pacific	6675	40	142.8	1.1
Cutler et al.	Huon	Surface	Pacific	6833	35	143.0	1.1
Cutler et al.	Huon	Surface	Pacific	7740	31	147.4	1.1
Cutler et al.	Huon	Surface	Pacific	8505	51	148.2	1.1
Cutler et al.	Huon	Surface	Pacific	8719	33	145.8	1.4
Cutler et al.	Huon	Surface	Pacific	8927	32	149.0	1.1
Cutler et al.	Huon	Surface	Pacific	9056	67	145.6	1.2
Cutler et al.	Huon	Surface	Pacific	9101	72	144.9	1.2
Cutler et al.	Huon	Surface	Pacific	9103	28	145.2	1.2
Cutler et al.	Huon	Surface	Pacific	9158	27	145.2	1.2
Cutler et al.	Huon	Surface	Pacific	9178	23	145.4	1.3
Cutler et al.	Huon	Surface	Pacific	9679	29	145.5	1.0
Cutler et al.	Huon	Surface	Pacific	9681	32	146.2	1.3
Cutler et al.	Huon	Surface	Pacific	9873	34	142.4	1.2
Cutler et al.	Huon	Surface	Pacific	10121	38	133.3	2.2
Cutler et al.	Huon	Surface	Pacific	10174	60	135.1	1.1
Cutler et al.	Huon	Surface	Pacific	10296	44	143.3	1.7
Cutler et al.	Huon	Surface	Pacific	10296	44	143.3	1.7
Cutler et al.	Huon	Surface	Pacific	10399	29	141.1	1.1
Cutler et al.	Huon	Surface	Pacific	10441	31	143.1	1.2
Cutler et al.	Huon	Surface	Pacific	10441	31	143.1	1.2

Cutler et al.	Huon	Surface	Pacific	10457	42	144.0	1.4
Cutler et al.	Huon	Surface	Pacific	10973	67	140.8	1.4
Cutler et al.	Huon	Surface	Pacific	11045	31	145.7	1.3
Cutler et al.	Huon	Surface	Pacific	11208	48	151.3	1.2
Cutler et al.	Huon	Surface	Pacific	11221	52	147.4	1.1
Cutler et al.	Huon	Surface	Pacific	11288	37	144.8	1.1
Cutler et al.	Huon	Surface	Pacific	11387	50	145.8	1.2
Cutler et al.	Huon	Surface	Pacific	11449	37	144.7	1.3
Cutler et al.	Huon	Surface	Pacific	11606	52	144.2	1.2
Cutler et al.	Huon	Surface	Pacific	11616	52	143.3	1.2
Cutler et al.	Huon	Surface	Pacific	11632	107	143.4	1.2
Cutler et al.	Huon	Surface	Pacific	11698	44	146.8	1.1
Cutler et al.	Huon	Surface	Pacific	12151	54	145.0	1.2
Cutler et al.	Huon	Surface	Pacific	12157	79	144.8	1.2
Cutler et al.	Huon	Surface	Pacific	12193	43	143.7	1.2
Cutler et al.	Huon	Surface	Pacific	12221	54	142.8	1.3
Cutler et al.	Huon	Surface	Pacific	12247	44	147.8	1.0
Cutler et al.	Huon	Surface	Pacific	12449	64	146.4	1.2
Cutler et al.	Huon	Surface	Pacific	12539	53	143.9	1.2
Cutler et al.	Huon	Surface	Pacific	12542	130	146.9	1.3
Cutler et al.	Huon	Surface	Pacific	12587	38	144.6	1.7
Cutler et al.	Huon	Surface	Pacific	12610	49	147.6	1.0
Cutler et al.	Huon	Surface	Pacific	12622	46	146.0	1.7
Cutler et al.	Huon	Surface	Pacific	12626	32	146.2	1.3
Cutler et al.	Huon	Surface	Pacific	12630	68	146.0	1.2
Cutler et al.	Huon	Surface	Pacific	12630	68	146.0	1.2
Cutler et al.	Huon	Surface	Pacific	12635	63	144.7	1.3
Cutler et al.	Huon	Surface	Pacific	12740	48	146.0	1.2
Cutler et al.	Huon	Surface	Pacific	12810	53	146.3	1.2
Cutler et al.	Huon	Surface	Pacific	12886	63	144.4	1.2
Cutler et al.	Huon	Surface	Pacific	13287	166	145.6	1.2
Cutler et al.	Huon	Surface	Pacific	13866	46	144.3	1.3
Cutler et al.	Huon	Surface	Pacific	13894	73	143.9	1.2
Cutler et al.	Huon	Surface	Pacific	13928	73	144.3	1.3
Cutler et al.	Huon	Surface	Pacific	13973	50	145.0	1.3
Cutler et al.	Huon	Surface	Pacific	14042	53	143.6	1.1
Cutler et al.	Huon	Surface	Pacific	14045	42	145.0	1.2
Cutler et al.	Huon	Surface	Pacific	14059	57	140.8	1.3

Cutler et al.	Huon	Surface	Pacific	14078	56	144.7	1.2
Cutler et al.	Huon	Surface	Pacific	14169	55	143.1	1.2
Cutler et al.	Huon	Surface	Pacific	14233	86	144.8	1.3
Cutler et al.	Huon	Surface	Pacific	14259	67	146.8	1.5
Cutler et al.	Huon	Surface	Pacific	14298	72	143.6	1.2
Cutler et al.	Huon	Surface	Pacific	14358	66	143.9	1.1
Cutler et al.	Huon	Surface	Pacific	14537	57	145.0	1.2
Cutler et al.	Huon	Surface	Pacific	14604	69	144.4	1.2
Cutler et al.	Huon	Surface	Pacific	14611	52	145.7	1.2
Cutler et al.	Huon	Surface	Pacific	14866	102	144.5	1.2
Cutler et al.	Huon	Surface	Pacific	14867	47	143.9	1.1
Cutler et al.	Huon	Surface	Pacific	14878	88	143.6	1.4
Cutler et al.	Huon	Surface	Pacific	15278	55	143.3	1.3
Cutler et al.	Huon	Surface	Pacific	15945	70	144.3	1.2
Cutler et al.	Huon	Surface	Pacific	19623	68	140.8	1.2
Cutler et al.	Huon	Surface	Pacific	20362	58	141.3	1.3
Cutler et al.	Huon	Surface	Pacific	20502	132	141.9	1.3
Cutler et al.	Huon	Surface	Pacific	20559	75	142.1	1.1
Cutler et al.	Huon	Surface	Pacific	21406	81	139.8	1.2
Cutler et al.	Huon	Surface	Pacific	21606	101	142.7	1.3
Cutler et al.	Huon	Surface	Pacific	21739	83	138.9	1.3
Cutler et al.	Huon	Surface	Pacific	21970	76	142.5	1.2
Cutler et al.	Huon	Surface	Pacific	22127	98	137.9	1.2
Cutler et al.	Huon	Surface	Pacific	22127	98	137.9	1.2
Cutler et al.	Huon	Surface	Pacific	22260	114	143.4	1.1
Cutler et al.	Huon	Surface	Pacific	22690	139	142.0	1.4
Cutler et al.	Huon	Surface	Pacific	22690	139	142.0	1.4
Cutler et al.	Huon	Surface	Pacific	22709	76	140.4	1.5
Cutler et al.	Huon	Surface	Pacific	23628	90	141.4	1.3
Cutler et al.	Huon	Surface	Pacific	23662	96	139.8	1.2
Cutler et al.	Huon	Surface	Pacific	24577	101	140.5	1.9
Cutler et al.	Huon	Surface	Pacific	25134	90	146.3	1.2
Cutler et al.	Huon	Surface	Pacific	25482	99	142.6	1.3
Cutler et al.	Huon	Surface	Pacific	27208	91	142.4	1.8
Cutler et al.	Huon	Surface	Pacific	28564	177	147.2	1.4
Cutler et al.	Huon	Surface	Pacific	28645	169	139.5	1.3
Druffel et al. (*64*)	Florida	Surface	Atlantic	3054	21	149.4	1.3
Druffel et al.	Florida	Surface	Atlantic	3065	16	148.3	1.3

Druffel et al.	Florida	Surface	Atlantic	3100	21	149.5	1.2
Druffel et al.	Florida	Surface	Atlantic	3265	17	148.9	1.2
Druffel et al.	Florida	Surface	Atlantic	4890	27	148.5	1.3
Druffel et al.	Florida	Surface	Atlantic	4947	32	148.3	1.3
Druffel et al.	Florida	Surface	Atlantic	5045	53	148.5	1.3
Druffel et al.	Florida	Surface	Atlantic	5099	31	149.4	1.3
Durand et al. [65]	Tahiti	Surface	Pacific	10029	18	147.4	0.6
Durand et al.	Tahiti	Surface	Pacific	11033	15	146.8	0.5
Durand et al.	Tahiti	Surface	Pacific	11488	29	147.7	0.5
Durand et al.	Tahiti	Surface	Pacific	11837	14	146.6	0.3
Durand et al.	Tahiti	Surface	Pacific	12370	36	147.7	0.7
Durand et al.	Tahiti	Surface	Pacific	12430	27	147.0	0.5
Durand et al.	Tahiti	Surface	Pacific	13163	44	147.0	1.0
Durand et al.	Tahiti	Surface	Pacific	13460	21	146.3	0.8
Durand et al.	Tahiti	Surface	Pacific	13577	23	146.0	0.5
Durand et al.	Tahiti	Surface	Pacific	13580	21	145.8	0.5
Durand et al.	Tahiti	Surface	Pacific	13724	57	147.1	1.9
Durand et al.	Tahiti	Surface	Pacific	13736	18	145.9	0.5
Durand et al.	Tahiti	Surface	Pacific	13784	31	145.9	0.8
Durand et al.	Tahiti	Surface	Pacific	13848	29	146.5	0.7
Durand et al.	Tahiti	Surface	Pacific	13988	16	145.4	0.6
Durand et al.	Tahiti	Surface	Pacific	14015	27	145.2	0.4
Durand et al.	Tahiti	Surface	Pacific	14116	43	145.6	0.5
Durand et al.	Tahiti	Surface	Pacific	14145	45	147.1	0.6
Durand et al.	Tahiti	Surface	Pacific	14221	56	145.9	0.7
Durand et al.	Tahiti	Surface	Pacific	14239	33	144.7	0.9
Durand et al.	Tahiti	Surface	Pacific	14273	63	146.5	0.7
Durand et al.	Tahiti	Surface	Pacific	14278	15	145.3	0.4
Durand et al.	Tahiti	Surface	Pacific	14284	27	145.5	0.4
Durand et al.	Tahiti	Surface	Pacific	14312	38	146.2	0.5
Durand et al.	Tahiti	Surface	Pacific	14338	27	145.1	0.6
Durand et al.	Tahiti	Surface	Pacific	14348	22	145.6	0.4
Durand et al.	Tahiti	Surface	Pacific	14350	22	145.4	0.5
Durand et al.	Tahiti	Surface	Pacific	14359	39	145.3	0.9
Durand et al.	Tahiti	Surface	Pacific	14418	26	145.5	0.5
Durand et al.	Tahiti	Surface	Pacific	14456	59	145.9	0.8
Durand et al.	Tahiti	Surface	Pacific	14478	24	145.1	0.5
Durand et al.	Tahiti	Surface	Pacific	14490	33	145.2	0.5

Durand et al.	Tahiti	Surface	Pacific	14516	19	145.2	0.6
Durand et al.	Tahiti	Surface	Pacific	14519	20	145.1	0.5
Durand et al.	Tahiti	Surface	Pacific	14531	45	145.2	0.4
Durand et al.	Tahiti	Surface	Pacific	14555	24	145.5	0.6
Durand et al.	Tahiti	Surface	Pacific	14582	52	145.1	1.0
Durand et al.	Tahiti	Surface	Pacific	14588	25	146.1	0.6
Durand et al.	Tahiti	Surface	Pacific	14609	26	145.2	0.5
Durand et al.	Tahiti	Surface	Pacific	14650	22	145.1	0.7
Durand et al.	Tahiti	Surface	Pacific	14663	61	141.8	1.9
Durand et al.	Tahiti	Surface	Pacific	14720	25	145.1	0.6
Durand et al.	Tahiti	Surface	Pacific	14734	57	144.6	0.9
Durand et al.	Tahiti	Surface	Pacific	14748	25	144.7	0.5
Durand et al.	Tahiti	Surface	Pacific	14769	37	142.7	0.9
Durand et al.	Tahiti	Surface	Pacific	14793	26	143.3	1.4
Durand et al.	Tahiti	Surface	Pacific	14801	32	144.8	0.6
Durand et al.	Tahiti	Surface	Pacific	14853	30	144.8	0.6
Durand et al.	Tahiti	Surface	Pacific	14901	22	145.4	0.5
Durand et al.	Tahiti	Surface	Pacific	14912	26	143.5	1.4
Durand et al.	Tahiti	Surface	Pacific	14994	25	145.3	0.4
Durand et al.	Tahiti	Surface	Pacific	15146	24	142.3	0.9
Durand et al.	Tahiti	Surface	Pacific	15147	31	145.4	0.7
Durand et al.	Tahiti	Surface	Pacific	15232	33	145.3	0.5
Durand et al.	Tahiti	Surface	Pacific	15310	23	145.3	0.8
Durand et al.	Tahiti	Surface	Pacific	15512	27	145.3	0.8
Durand et al.	Tahiti	Surface	Pacific	15744	29	145.2	0.5
Durand et al.	Tahiti	Surface	Pacific	16087	42	144.5	1.3
Durand et al.	Tahiti	Surface	Pacific	29209	51	138.7	1.0
Durand et al.	Tahiti	Surface	Pacific	29631	62	138.0	1.0
Durand et al.	Tahiti	Surface	Pacific	29666	58	142.0	1.0
Durand et al.	Tahiti	Surface	Pacific	29838	53	141.0	1.0
Fairbanks et al. (*66*)	Barbados	Surface	Atlantic	7289	38	149.8	2.0
Fairbanks et al.	Barbados	Surface	Atlantic	8934	59	148.5	2.0
Fairbanks et al.	Barbados	Surface	Atlantic	8936	44	149.6	2.0
Fairbanks et al.	Barbados	Surface	Atlantic	9155	36	149.4	2.0
Fairbanks et al.	Barbados	Surface	Atlantic	9330	34	148.5	1.0
Fairbanks et al.	Barbados	Surface	Atlantic	9618	45	149.7	1.0
Fairbanks et al.	Barbados	Surface	Atlantic	9922	41	149.3	2.0
Fairbanks et al.	Barbados	Surface	Atlantic	9941	66	148.8	2.0

Fairbanks et al.	Barbados	Surface	Atlantic	11390	27	145.8	1.0
Fairbanks et al.	Barbados	Surface	Atlantic	11393	60	145.4	2.0
Fairbanks et al.	Barbados	Surface	Atlantic	11429	32	151.0	1.0
Fairbanks et al.	Barbados	Surface	Atlantic	11512	34	141.9	1.0
Fairbanks et al.	Barbados	Surface	Atlantic	11756	106	140.7	1.0
Fairbanks et al.	Barbados	Surface	Atlantic	11791	57	145.6	2.0
Fairbanks et al.	Barbados	Surface	Atlantic	12002	49	141.1	2.0
Fairbanks et al.	Barbados	Surface	Atlantic	12015	48	144.5	1.0
Fairbanks et al.	Barbados	Surface	Atlantic	12017	64	142.1	1.0
Fairbanks et al.	Barbados	Surface	Atlantic	12029	60	144.0	1.0
Fairbanks et al.	Barbados	Surface	Atlantic	12091	56	148.1	1.0
Fairbanks et al.	Barbados	Surface	Atlantic	12103	78	143.5	1.0
Fairbanks et al.	Barbados	Surface	Atlantic	12170	30	143.5	1.0
Fairbanks et al.	Barbados	Surface	Atlantic	12179	66	142.7	1.0
Fairbanks et al.	Barbados	Surface	Atlantic	12186	83	141.7	2.0
Fairbanks et al.	Barbados	Surface	Atlantic	12203	75	143.1	1.0
Fairbanks et al.	Barbados	Surface	Atlantic	12239	173	144.3	1.0
Fairbanks et al.	Barbados	Surface	Atlantic	12290	55	143.8	1.0
Fairbanks et al.	Barbados	Surface	Atlantic	12303	28	146.3	1.0
Fairbanks et al.	Barbados	Surface	Atlantic	12327	89	143.1	2.0
Fairbanks et al.	Barbados	Surface	Atlantic	12533	51	144.4	1.0
Fairbanks et al.	Barbados	Surface	Atlantic	12680	149	143.2	2.0
Fairbanks et al.	Barbados	Surface	Atlantic	12816	74	145.7	2.0
Fairbanks et al.	Barbados	Surface	Atlantic	12844	58	147.1	2.0
Fairbanks et al.	Barbados	Surface	Atlantic	12873	48	145.6	1.0
Fairbanks et al.	Barbados	Surface	Atlantic	12883	38	146.6	2.0
Fairbanks et al.	Barbados	Surface	Atlantic	12907	108	145.7	2.0
Fairbanks et al.	Barbados	Surface	Atlantic	12919	33	145.0	1.0
Fairbanks et al.	Barbados	Surface	Atlantic	12926	98	145.0	2.0
Fairbanks et al.	Barbados	Surface	Atlantic	12996	60	145.1	2.0
Fairbanks et al.	Barbados	Surface	Atlantic	13013	45	146.3	2.0
Fairbanks et al.	Barbados	Surface	Atlantic	13066	34	143.7	2.0
Fairbanks et al.	Barbados	Surface	Atlantic	13555	37	142.8	2.0
Fairbanks et al.	Barbados	Surface	Atlantic	13574	51	142.8	1.0
Fairbanks et al.	Barbados	Surface	Atlantic	13578	51	144.1	2.0
Fairbanks et al.	Barbados	Surface	Atlantic	13632	31	144.0	2.0
Fairbanks et al.	Barbados	Surface	Atlantic	14064	58	146.2	2.0
Fairbanks et al.	Barbados	Surface	Atlantic	14100	54	145.3	1.0

Fairbanks et al.	Barbados	Surface	Atlantic	14222	36	143.7	2.0
Fairbanks et al.	Barbados	Surface	Atlantic	14259	40	143.5	1.0
Fairbanks et al.	Barbados	Surface	Atlantic	14283	44	146.7	1.0
Fairbanks et al.	Barbados	Surface	Atlantic	14295	58	141.7	2.0
Fairbanks et al.	Barbados	Surface	Atlantic	14394	37	145.5	2.0
Fairbanks et al.	Barbados	Surface	Atlantic	14397	33	144.0	1.0
Fairbanks et al.	Barbados	Surface	Atlantic	14408	39	142.6	2.0
Fairbanks et al.	Barbados	Surface	Atlantic	14539	45	144.9	2.0
Fairbanks et al.	Barbados	Surface	Atlantic	14573	30	144.4	2.0
Fairbanks et al.	Barbados	Surface	Atlantic	14596	51	143.5	2.0
Fairbanks et al.	Barbados	Surface	Atlantic	14685	44	148.0	2.0
Fairbanks et al.	Barbados	Surface	Atlantic	17580	137	138.9	1.0
Fairbanks et al.	Barbados	Surface	Atlantic	17935	51	144.1	1.0
Fairbanks et al.	Barbados	Surface	Atlantic	17996	69	140.9	1.0
Fairbanks et al.	Barbados	Surface	Atlantic	18116	73	144.0	1.0
Fairbanks et al.	Barbados	Surface	Atlantic	18174	65	142.2	1.0
Fairbanks et al.	Barbados	Surface	Atlantic	18176	112	144.9	2.0
Fairbanks et al.	Barbados	Surface	Atlantic	18218	88	144.8	2.0
Fairbanks et al.	Barbados	Surface	Atlantic	18408	52	144.0	1.0
Fairbanks et al.	Barbados	Surface	Atlantic	18494	71	140.0	1.0
Fairbanks et al.	Barbados	Surface	Atlantic	18617	42	147.1	1.0
Fairbanks et al.	Barbados	Surface	Atlantic	18716	56	143.4	2.0
Fairbanks et al.	Barbados	Surface	Atlantic	18806	65	143.0	2.0
Fairbanks et al.	Barbados	Surface	Atlantic	19075	110	141.8	2.0
Fairbanks et al.	Barbados	Surface	Atlantic	19203	74	145.5	1.0
Fairbanks et al.	Barbados	Surface	Atlantic	19337	45	138.5	1.0
Fairbanks et al.	Barbados	Surface	Atlantic	19345	106	146.3	1.0
Fairbanks et al.	Barbados	Surface	Atlantic	19434	59	139.4	1.0
Fairbanks et al.	Barbados	Surface	Atlantic	19438	50	139.5	1.0
Fairbanks et al.	Barbados	Surface	Atlantic	19443	60	144.4	2.0
Fairbanks et al.	Barbados	Surface	Atlantic	19450	72	144.4	2.0
Fairbanks et al.	Barbados	Surface	Atlantic	19455	80	143.3	1.0
Fairbanks et al.	Barbados	Surface	Atlantic	19483	53	140.0	1.0
Fairbanks et al.	Barbados	Surface	Atlantic	19581	52	139.6	2.0
Fairbanks et al.	Barbados	Surface	Atlantic	19595	88	143.1	2.0
Fairbanks et al.	Barbados	Surface	Atlantic	19627	67	143.1	1.0
Fairbanks et al.	Barbados	Surface	Atlantic	19638	50	141.0	2.0
Fairbanks et al.	Barbados	Surface	Atlantic	19677	128	143.4	1.0

Fairbanks et al.	Barbados	Surface	Atlantic	19678	66	145.3	2.0
Fairbanks et al.	Barbados	Surface	Atlantic	19684	78	144.5	2.0
Fairbanks et al.	Barbados	Surface	Atlantic	19770	64	141.0	1.0
Fairbanks et al.	Barbados	Surface	Atlantic	19913	67	138.6	1.0
Fairbanks et al.	Barbados	Surface	Atlantic	20082	54	144.4	2.0
Fairbanks et al.	Barbados	Surface	Atlantic	20085	68	144.7	2.0
Fairbanks et al.	Barbados	Surface	Atlantic	20469	64	144.1	1.0
Fairbanks et al.	Barbados	Surface	Atlantic	20504	78	142.1	2.0
Fairbanks et al.	Barbados	Surface	Atlantic	20575	62	139.7	1.0
Fairbanks et al.	Barbados	Surface	Atlantic	20614	180	146.5	2.0
Fairbanks et al.	Barbados	Surface	Atlantic	20632	61	139.3	2.0
Fairbanks et al.	Barbados	Surface	Atlantic	20634	78	147.0	1.0
Fairbanks et al.	Barbados	Surface	Atlantic	20714	86	143.8	1.0
Fairbanks et al.	Barbados	Surface	Atlantic	20734	62	144.0	2.0
Fairbanks et al.	Barbados	Surface	Atlantic	21714	81	140.0	1.0
Fairbanks et al.	Barbados	Surface	Atlantic	21802	82	144.8	1.0
Fairbanks et al.	Barbados	Surface	Atlantic	21858	81	139.3	1.0
Fairbanks et al.	Barbados	Surface	Atlantic	21922	82	140.0	1.0
Fairbanks et al.	Barbados	Surface	Atlantic	22010	72	139.5	2.0
Fairbanks et al.	Barbados	Surface	Atlantic	22160	123	141.1	1.0
Fairbanks et al.	Barbados	Surface	Atlantic	22536	91	140.4	1.0
Fairbanks et al.	Barbados	Surface	Atlantic	22574	95	140.4	1.0
Fairbanks et al.	Barbados	Surface	Atlantic	23039	75	138.0	2.0
Fairbanks et al.	Barbados	Surface	Atlantic	23044	73	140.4	2.0
Fairbanks et al.	Barbados	Surface	Atlantic	23296	121	138.0	2.0
Fairbanks et al.	Barbados	Surface	Atlantic	23867	88	137.9	1.0
Fairbanks et al.	Barbados	Surface	Atlantic	24549	62	139.1	2.0
Fairbanks et al.	Barbados	Surface	Atlantic	24579	81	139.5	1.0
Fairbanks et al.	Barbados	Surface	Atlantic	24883	109	138.1	2.0
Fairbanks et al.	Barbados	Surface	Atlantic	25045	59	135.9	1.0
Fairbanks et al.	Barbados	Surface	Atlantic	25622	126	137.1	1.0
Fairbanks et al.	Barbados	Surface	Atlantic	25639	90	138.4	1.0
Fairbanks et al.	Barbados	Surface	Atlantic	25645	80	139.0	2.0
Fairbanks et al.	Barbados	Surface	Atlantic	25741	105	139.7	1.0
Fairbanks et al.	Barbados	Surface	Atlantic	25743	122	137.8	2.0
Fairbanks et al.	Barbados	Surface	Atlantic	25866	105	139.9	2.0
Fairbanks et al.	Barbados	Surface	Atlantic	26044	80	138.1	1.0
Fairbanks et al.	Barbados	Surface	Atlantic	26278	99	138.4	1.0

Fairbanks et al.	Barbados	Surface	Atlantic	29540	82	136.6	1.0
Fairbanks et al.	Barbados	Surface	Atlantic	29898	149	137.3	1.0
Fairbanks et al.	Kiritimati	Surface	Pacific	8824	36	152.7	2.0
Fairbanks et al.	Kiritimati	Surface	Pacific	10612	33	145.2	2.0
Fairbanks et al.	Kiritimati	Surface	Pacific	10615	51	143.4	2.0
Fairbanks et al.	Kiritimati	Surface	Pacific	10642	37	145.0	2.0
Fairbanks et al.	Kiritimati	Surface	Pacific	11527	50	145.3	2.0
Fairbanks et al.	Kiritimati	Surface	Pacific	11548	42	147.4	2.0
Fairbanks et al.	Kiritimati	Surface	Pacific	11569	56	147.1	2.0
Fairbanks et al.	Kiritimati	Surface	Pacific	11571	48	145.4	2.0
Fairbanks et al.	Kiritimati	Surface	Pacific	11591	30	145.3	2.0
Fairbanks et al.	Kiritimati	Surface	Pacific	11612	43	148.5	2.0
Fairbanks et al.	Kiritimati	Surface	Pacific	11625	45	143.4	2.0
Fairbanks et al.	Kiritimati	Surface	Pacific	11697	49	143.2	2.0
Fairbanks et al.	Kiritimati	Surface	Pacific	11730	38	146.1	2.0
Fairbanks et al.	Kiritimati	Surface	Pacific	11805	75	146.9	2.0
Fairbanks et al.	Kiritimati	Surface	Pacific	11839	43	146.1	2.0
Fairbanks et al.	Kiritimati	Surface	Pacific	11859	52	145.2	2.0
Fairbanks et al.	Kiritimati	Surface	Pacific	11920	46	142.3	2.0
Fairbanks et al.	Kiritimati	Surface	Pacific	11925	23	144.3	2.0
Fairbanks et al.	Kiritimati	Surface	Pacific	11931	36	145.6	2.0
Fairbanks et al.	Kiritimati	Surface	Pacific	11949	41	144.6	2.0
Fairbanks et al.	Kiritimati	Surface	Pacific	11996	52	144.4	2.0
Fairbanks et al.	Kiritimati	Surface	Pacific	12081	83	142.6	2.0
Fairbanks et al.	Kiritimati	Surface	Pacific	12103	32	145.7	2.0
Fairbanks et al.	Kiritimati	Surface	Pacific	12172	59	144.6	2.0
Fairbanks et al.	Kiritimati	Surface	Pacific	12199	81	143.2	2.0
Fairbanks et al.	Kiritimati	Surface	Pacific	12223	50	145.5	2.0
Fairbanks et al.	Kiritimati	Surface	Pacific	12287	58	144.8	2.0
Fairbanks et al.	Kiritimati	Surface	Pacific	12304	45	144.7	2.0
Fairbanks et al.	Kiritimati	Surface	Pacific	12433	53	143.3	2.0
Fairbanks et al.	Kiritimati	Surface	Pacific	12461	45	145.4	2.0
Fairbanks et al.	Kiritimati	Surface	Pacific	12526	80	144.8	2.0
Fairbanks et al.	Kiritimati	Surface	Pacific	12553	93	142.5	2.0
Fairbanks et al.	Kiritimati	Surface	Pacific	12611	75	145.8	2.0
Fairbanks et al.	Kiritimati	Surface	Pacific	12716	55	149.2	2.0
Fairbanks et al.	Kiritimati	Surface	Pacific	12785	59	147.5	2.0
Fairbanks et al.	Kiritimati	Surface	Pacific	12836	50	146.5	2.0

Fairbanks et al.	Kiritimati	Surface	Pacific	12838	93	140.7	2.0
Fairbanks et al.	Kiritimati	Surface	Pacific	12942	96	140.6	2.0
Fairbanks et al.	Kiritimati	Surface	Pacific	12959	41	146.7	2.0
Fairbanks et al.	Kiritimati	Surface	Pacific	12961	60	147.4	2.0
Fairbanks et al.	Kiritimati	Surface	Pacific	12990	56	147.9	2.0
Fairbanks et al.	Kiritimati	Surface	Pacific	12995	56	146.4	2.0
Fairbanks et al.	Kiritimati	Surface	Pacific	13117	58	146.8	2.0
Fairbanks et al.	Kiritimati	Surface	Pacific	13365	42	148.7	2.0
Fairbanks et al.	Kiritimati	Surface	Pacific	13397	66	148.3	2.0
Fairbanks et al.	Kiritimati	Surface	Pacific	13650	90	144.6	2.0
Fairbanks et al.	Kiritimati	Surface	Pacific	13698	82	145.2	2.0
Fairbanks et al.	Kiritimati	Surface	Pacific	13709	47	142.6	2.0
Frank et al. (*67*)	NE Atlantic	Deep	Atlantic	750	70	151.6	2.5
Frank et al.	NE Atlantic	Deep	Atlantic	1456	100	145.7	2.1
Frank et al.	NE Atlantic	Deep	Atlantic	3510	91	146.2	2.9
Frank et al.	NE Atlantic	Deep	Atlantic	3831	27	147.9	2.2
Frank et al.	NE Atlantic	Deep	Atlantic	4961	77	146.2	2.8
Frank et al.	NE Atlantic	Deep	Atlantic	4869	42	153.7	2.9
Frank et al.	NE Atlantic	Deep	Atlantic	5270	110	148.9	2.6
Frank et al.	NE Atlantic	Deep	Atlantic	5670	38	146.5	2.9
Frank et al.	NE Atlantic	Deep	Atlantic	9290	210	147.3	2.4
Frank et al.	NE Atlantic	Deep	Atlantic	9810	220	154.5	2.4
Frank et al.	NE Atlantic	Deep	Atlantic	9700	350	154.0	2.7
Frank et al.	NE Atlantic	Deep	Atlantic	3230	110	145.2	2.8
Frank et al.	NE Atlantic	Deep	Atlantic	6520	140	154.1	2.9
Frank et al.	NE Atlantic	Deep	Atlantic	78790	490	140.3	2.9
Frank et al.	NE Atlantic	Deep	Atlantic	8890	160	147.3	2.0
Frank et al.	NE Atlantic	Deep	Atlantic	1540	160	146.6	2.8
Frank et al.	NE Atlantic	Deep	Atlantic	9170	150	145.5	1.9
Frank et al.	NE Atlantic	Deep	Atlantic	8680	160	145.2	1.9
Frank et al.	NE Atlantic	Deep	Atlantic	10350	90	147.7	2.6
Frank et al.	NE Atlantic	Deep	Atlantic	1321	12	148.1	1.9
Frank et al.	NE Atlantic	Deep	Atlantic	1244	38	145.4	2.6
Frank et al.	NE Atlantic	Deep	Atlantic	554	25	147.3	2.6
Hines et al. (*68*)	Tasmania	Deep	Southern Ocean	8587	216	150.6	1.0
Hines et al.	Tasmania	Deep	Southern Ocean	8981	107	149.9	0.9
Hines et al.	Tasmania	Deep	Southern Ocean	10084	192	149.8	0.6

Hines et al.	Tasmania	Deep	Southern Ocean	10387	399	154.2	0.7
Hines et al.	Tasmania	Deep	Southern Ocean	11951	67	149.5	0.6
Hines et al.	Tasmania	Deep	Southern Ocean	12205	131	147.8	0.8
Hines et al.	Tasmania	Deep	Southern Ocean	12615	86	149.3	0.9
Hines et al.	Tasmania	Deep	Southern Ocean	12682	33	152.5	0.6
Hines et al.	Tasmania	Deep	Southern Ocean	12782	134	150.9	0.6
Hines et al.	Tasmania	Deep	Southern Ocean	13183	264	148.9	0.6
Hines et al.	Tasmania	Deep	Southern Ocean	13199	39	148.5	0.7
Hines et al.	Tasmania	Deep	Southern Ocean	13306	130	151.5	1.1
Hines et al.	Tasmania	Deep	Southern Ocean	13311	70	148.8	1.4
Hines et al.	Tasmania	Deep	Southern Ocean	13347	25	154.1	0.6
Hines et al.	Tasmania	Deep	Southern Ocean	13354	90	152.7	0.8
Hines et al.	Tasmania	Deep	Southern Ocean	13593	78	150.9	0.9
Hines et al.	Tasmania	Deep	Southern Ocean	13620	79	147.9	1.7
Hines et al.	Tasmania	Deep	Southern Ocean	13817	63	147.8	1.6
Hines et al.	Tasmania	Deep	Southern Ocean	13852	139	150.0	1.5
Hines et al.	Tasmania	Deep	Southern Ocean	13891	72	150.2	0.7
Hines et al.	Tasmania	Deep	Southern Ocean	13916	59	148.0	0.7
Hines et al.	Tasmania	Deep	Southern Ocean	13922	79	149.1	0.8
Hines et al.	Tasmania	Deep	Southern Ocean	14134	240	147.5	0.6
Hines et al.	Tasmania	Deep	Southern Ocean	14161	82	146.6	0.8
Hines et al.	Tasmania	Deep	Southern Ocean	14210	43	148.5	0.9
Hines et al.	Tasmania	Deep	Southern Ocean	14289	48	148.6	0.6
Hines et al.	Tasmania	Deep	Southern Ocean	14347	66	149.4	0.8
Hines et al.	Tasmania	Deep	Southern Ocean	14390	80	147.1	0.6

Hines et al.	Tasmania	Deep	Southern Ocean	14464	52	151.9	0.6
Hines et al.	Tasmania	Deep	Southern Ocean	14578	80	153.4	0.9
Hines et al.	Tasmania	Deep	Southern Ocean	14831	35	146.3	0.6
Hines et al.	Tasmania	Deep	Southern Ocean	14869	53	148.3	0.6
Hines et al.	Tasmania	Deep	Southern Ocean	14898	132	149.2	1.2
Hines et al.	Tasmania	Deep	Southern Ocean	15056	67	146.6	0.7
Hines et al.	Tasmania	Deep	Southern Ocean	15172	62	150.0	1.0
Hines et al.	Tasmania	Deep	Southern Ocean	15312	76	148.0	0.7
Hines et al.	Tasmania	Deep	Southern Ocean	15683	104	150.2	0.6
Hines et al.	Tasmania	Deep	Southern Ocean	15837	65	145.9	0.7
Hines et al.	Tasmania	Deep	Southern Ocean	16129	71	146.5	0.7
Hines et al.	Tasmania	Deep	Southern Ocean	16238	76	147.6	0.6
Hines et al.	Tasmania	Deep	Southern Ocean	16279	523	150.7	0.5
Hines et al.	Tasmania	Deep	Southern Ocean	16398	102	151.2	0.8
Hines et al.	Tasmania	Deep	Southern Ocean	16485	50	150.3	0.7
Hines et al.	Tasmania	Deep	Southern Ocean	16722	64	149.9	0.8
Hines et al.	Tasmania	Deep	Southern Ocean	16804	202	152.7	0.7
Hines et al.	Tasmania	Deep	Southern Ocean	17065	46	145.8	0.5
Hines et al.	Tasmania	Deep	Southern Ocean	17189	73	153.0	0.7
Hines et al.	Tasmania	Deep	Southern Ocean	17279	109	148.2	0.9
Hines et al.	Tasmania	Deep	Southern Ocean	17328	74	145.8	0.5
Hines et al.	Tasmania	Deep	Southern Ocean	17608	164	145.5	0.8
Hines et al.	Tasmania	Deep	Southern Ocean	17805	88	146.8	0.5
Hines et al.	Tasmania	Deep	Southern Ocean	18001	65	147.8	0.5
Hines et al.	Tasmania	Deep	Southern Ocean	18102	65	145.5	0.6

Hines et al.	Tasmania	Deep	Southern Ocean	18333	38	147.9	0.6
Hines et al.	Tasmania	Deep	Southern Ocean	19274	57	145.8	1.3
Hines et al.	Tasmania	Deep	Southern Ocean	19457	108	145.0	1.4
Hines et al.	Tasmania	Deep	Southern Ocean	19483	61	145.3	1.2
Hines et al.	Tasmania	Deep	Southern Ocean	19789	185	149.6	0.6
Hines et al.	Tasmania	Deep	Southern Ocean	20367	109	144.7	0.6
Hines et al.	Tasmania	Deep	Southern Ocean	20471	147	152.2	0.6
Hines et al.	Tasmania	Deep	Southern Ocean	21344	153	143.9	1.3
Hines et al.	Tasmania	Deep	Southern Ocean	21399	183	144.3	0.7
Hines et al.	Tasmania	Deep	Southern Ocean	21408	57	143.6	1.9
Hines et al.	Tasmania	Deep	Southern Ocean	21704	164	145.1	0.7
Hines et al.	Tasmania	Deep	Southern Ocean	23338	75	145.6	0.9
Hines et al.	Tasmania	Deep	Southern Ocean	25198	144	143.8	1.3
Hines et al.	Tasmania	Deep	Southern Ocean	25324	333	151.9	0.8
Hines et al.	Tasmania	Deep	Southern Ocean	25526	209	142.0	0.7
Hines et al.	Tasmania	Deep	Southern Ocean	25769	378	150.6	0.6
Hines et al.	Tasmania	Deep	Southern Ocean	26191	57	145.1	0.7
Hines et al.	Tasmania	Deep	Southern Ocean	26980	96	144.7	0.7
Hines et al.	Tasmania	Deep	Southern Ocean	27579	92	138.1	0.7
Hines et al.	Tasmania	Deep	Southern Ocean	28832	163	140.4	0.8
Mangini et al. (*69*)	Brazil Margin	Deep	Atlantic	10532	190	149.5	1.9
Mangini et al.	Brazil Margin	Deep	Atlantic	11692	150	150.9	2.3
Mangini et al.	Brazil Margin	Deep	Atlantic	12612	335	153.3	2.2
Mangini et al.	Brazil Margin	Deep	Atlantic	16982	155	145.1	2.1
Mangini et al.	Brazil Margin	Deep	Atlantic	26932	265	158.0	2.5
Multer et al. (*70*)	Florida	Surface	Atlantic	2300	100	136.3	1.2
Multer et al.	Florida	Surface	Atlantic	2500	60	146.4	2.0

Multer et al.	Florida	Surface	Atlantic	3600	40	146.3	2.0
Multer et al.	Florida	Surface	Atlantic	4200	40	150.5	1.3
Multer et al.	Florida	Surface	Atlantic	4300	200	148.2	1.7
Multer et al.	Florida	Surface	Atlantic	4800	30	149.4	2.0
Multer et al.	Florida	Surface	Atlantic	6300	60	149.4	2.1
Multer et al.	Florida	Surface	Atlantic	6600	30	148.8	1.7
Multer et al.	Florida	Surface	Atlantic	6920	40	138.7	1.6
Multer et al.	Florida	Surface	Atlantic	7300	90	147.9	1.5
Multer et al.	Florida	Surface	Atlantic	7300	100	147.1	1.6
Multer et al.	Florida	Surface	Atlantic	8700	70	149.5	2.5
Robinson et al. (*71*)	Bahamas	Surface	Atlantic	0	0	145.8	0.7
Robinson et al.	Bahamas	Surface	Atlantic	0	0	146.5	0.7
Robinson et al.	Bahamas	Surface	Atlantic	0	0	146.7	0.7
Robinson et al. (*49*)	NW Atlantic	Deep	Atlantic	73	56	148.9	1.2
Robinson et al.	NW Atlantic	Deep	Atlantic	115	18	148.7	1.2
Robinson et al.	NW Atlantic	Deep	Atlantic	200	43	143.2	1.1
Robinson et al.	NW Atlantic	Deep	Atlantic	303	42	148.0	1.1
Robinson et al.	NW Atlantic	Deep	Atlantic	406	74	148.8	1.2
Robinson et al.	NW Atlantic	Deep	Atlantic	4599	682	149.2	1.1
Robinson et al.	NW Atlantic	Deep	Atlantic	6093	189	143.9	1.1
Robinson et al.	NW Atlantic	Deep	Atlantic	11086	144	143.8	1.1
Robinson et al.	NW Atlantic	Deep	Atlantic	11199	161	145.0	1.1
Robinson et al.	NW Atlantic	Deep	Atlantic	11326	242	149.2	1.4
Robinson et al.	NW Atlantic	Deep	Atlantic	11446	404	149.3	1.1
Robinson et al.	NW Atlantic	Deep	Atlantic	11926	316	149.5	1.1
Robinson et al.	NW Atlantic	Deep	Atlantic	12128	148	147.7	1.2
Robinson et al.	NW Atlantic	Deep	Atlantic	12150	119	145.5	1.1
Robinson et al.	NW Atlantic	Deep	Atlantic	12289	139	147.3	1.1
Robinson et al.	NW Atlantic	Deep	Atlantic	12310	114	147.2	1.1
Robinson et al.	NW Atlantic	Deep	Atlantic	12329	341	148.6	1.2
Robinson et al.	NW Atlantic	Deep	Atlantic	12411	128	144.3	1.1
Robinson et al.	NW Atlantic	Deep	Atlantic	12415	85	148.1	1.1
Robinson et al.	NW Atlantic	Deep	Atlantic	13096	149	154.7	1.1
Robinson et al.	NW Atlantic	Deep	Atlantic	13584	463	148.0	1.2
Robinson et al.	NW Atlantic	Deep	Atlantic	13948	159	148.9	1.1
Robinson et al.	NW Atlantic	Deep	Atlantic	14491	742	150.6	3.0
Robinson et al.	NW Atlantic	Deep	Atlantic	14680	212	150.6	1.1
Robinson et al.	NW Atlantic	Deep	Atlantic	14824	134	154.4	1.0

Robinson et al.	NW Atlantic	Deep	Atlantic	14866	348	151.4	1.2
Robinson et al.	NW Atlantic	Deep	Atlantic	14880	116	153.3	1.1
Robinson et al.	NW Atlantic	Deep	Atlantic	14969	163	149.4	1.1
Robinson et al.	NW Atlantic	Deep	Atlantic	14997	133	148.0	1.1
Robinson et al.	NW Atlantic	Deep	Atlantic	15050	133	147.5	1.2
Robinson et al.	NW Atlantic	Deep	Atlantic	15119	122	146.0	1.1
Robinson et al.	NW Atlantic	Deep	Atlantic	15226	196	156.9	1.1
Robinson et al.	NW Atlantic	Deep	Atlantic	15438	188	145.1	1.1
Robinson et al.	NW Atlantic	Deep	Atlantic	15444	390	152.3	1.1
Robinson et al.	NW Atlantic	Deep	Atlantic	15451	157	155.0	1.1
Robinson et al.	NW Atlantic	Deep	Atlantic	15519	163	147.5	1.1
Robinson et al.	NW Atlantic	Deep	Atlantic	15531	310	148.6	1.1
Robinson et al.	NW Atlantic	Deep	Atlantic	15542	275	142.1	1.3
Robinson et al.	NW Atlantic	Deep	Atlantic	15564	191	146.2	1.3
Robinson et al.	NW Atlantic	Deep	Atlantic	15617	162	163.7	1.1
Robinson et al.	NW Atlantic	Deep	Atlantic	15721	176	148.6	1.1
Robinson et al.	NW Atlantic	Deep	Atlantic	15724	180	153.1	1.1
Robinson et al.	NW Atlantic	Deep	Atlantic	15729	191	146.1	1.1
Robinson et al.	NW Atlantic	Deep	Atlantic	15740	169	149.0	1.2
Robinson et al.	NW Atlantic	Deep	Atlantic	15742	381	149.8	1.2
Robinson et al.	NW Atlantic	Deep	Atlantic	15746	151	149.6	1.1
Robinson et al.	NW Atlantic	Deep	Atlantic	15748	275	148.4	1.1
Robinson et al.	NW Atlantic	Deep	Atlantic	15776	352	149.4	1.1
Robinson et al.	NW Atlantic	Deep	Atlantic	15779	170	154.3	1.1
Robinson et al.	NW Atlantic	Deep	Atlantic	15801	179	147.8	1.1
Robinson et al.	NW Atlantic	Deep	Atlantic	15845	183	148.7	1.1
Robinson et al.	NW Atlantic	Deep	Atlantic	15857	214	146.7	1.1
Robinson et al.	NW Atlantic	Deep	Atlantic	15868	354	148.4	1.1
Robinson et al.	NW Atlantic	Deep	Atlantic	15904	194	152.4	1.1
Robinson et al.	NW Atlantic	Deep	Atlantic	15917	327	156.6	1.2
Robinson et al.	NW Atlantic	Deep	Atlantic	15930	227	154.9	1.1
Robinson et al.	NW Atlantic	Deep	Atlantic	16029	531	156.7	1.2
Robinson et al.	NW Atlantic	Deep	Atlantic	16030	527	152.9	1.1
Robinson et al.	NW Atlantic	Deep	Atlantic	16058	294	148.5	1.1
Robinson et al.	NW Atlantic	Deep	Atlantic	16200	579	149.9	1.1
Robinson et al.	NW Atlantic	Deep	Atlantic	16201	1298	151.7	1.2
Robinson et al.	NW Atlantic	Deep	Atlantic	16453	256	157.2	1.1
Robinson et al.	NW Atlantic	Deep	Atlantic	16490	822	152.6	1.1

Robinson et al.	NW Atlantic	Deep	Atlantic	16607	161	155.3	1.1
Robinson et al.	NW Atlantic	Deep	Atlantic	16900	218	156.4	1.0
Robinson et al.	NW Atlantic	Deep	Atlantic	17650	190	157.9	1.1
Robinson et al.	NW Atlantic	Deep	Atlantic	18074	223	156.7	1.1
Robinson et al.	NW Atlantic	Deep	Atlantic	24616	453	145.5	1.1
Robinson et al.	NW Atlantic	Deep	Atlantic	24903	830	144.6	1.1
Robinson et al.	NW Atlantic	Deep	Atlantic	25040	725	143.8	1.0
Robinson et al.	NW Atlantic	Deep	Atlantic	25176	294	149.6	1.1
Robinson et al.	NW Atlantic	Deep	Atlantic	25240	724	145.9	1.1
Robinson et al.	NW Atlantic	Deep	Atlantic	25305	734	144.2	1.1
Robinson et al.	NW Atlantic	Deep	Atlantic	25363	720	147.1	1.2
Robinson et al.	NW Atlantic	Deep	Atlantic	25562	422	147.2	1.1
Robinson et al.	NW Atlantic	Deep	Atlantic	27650	363	146.2	1.1
Robinson et al.	NW Atlantic	Deep	Atlantic	27753	1302	146.2	1.2
Robinson et al.	NW Atlantic	Deep	Atlantic	28130	297	146.2	1.2
Robinson et al.	NW Atlantic	Deep	Atlantic	29918	510	147.4	0.7
Robinson et al.	NW Atlantic	Deep	Atlantic	30135	499	162.0	1.2
Robinson et al.	NW Atlantic	Deep	Atlantic	30196	262	145.3	0.7
Robinson et al.	NW Atlantic	Deep	Atlantic	31475	817	147.2	1.2
Robinson et al.	NW Atlantic	Deep	Atlantic	31607	2020	148.0	1.3
Robinson et al.	NW Atlantic	Deep	Atlantic	31636	481	144.5	1.1
Robinson et al.	NW Atlantic	Deep	Atlantic	31661	620	156.7	1.1
Robinson et al.	NW Atlantic	Deep	Atlantic	31909	388	152.5	1.1
Robinson et al.	NW Atlantic	Deep	Atlantic	31929	534	149.0	1.1
Robinson et al.	NW Atlantic	Deep	Atlantic	31956	469	147.7	1.1
Robinson et al.	NW Atlantic	Deep	Atlantic	32818	482	156.6	1.2
Robinson et al.	NW Atlantic	Deep	Atlantic	33561	343	154.6	1.1
Robinson et al.	NW Atlantic	Deep	Atlantic	38182	284	147.4	1.3
Robinson et al.	NW Atlantic	Deep	Atlantic	38331	299	146.3	1.2
Robinson et al.	NW Atlantic	Deep	Atlantic	38762	1241	155.0	1.3
Robinson et al.	NW Atlantic	Deep	Atlantic	47131	426	143.6	1.2
Robinson et al.	NW Atlantic	Deep	Atlantic	47540	521	149.3	1.1
Robinson et al.	NW Atlantic	Deep	Atlantic	47906	463	146.3	1.1
Robinson et al.	NW Atlantic	Deep	Atlantic	48838	419	146.7	1.2
Robinson et al.	NW Atlantic	Deep	Atlantic	56530	496	142.4	1.1
Robinson et al.	NW Atlantic	Deep	Atlantic	56681	522	155.3	1.2
Robinson et al.	NW Atlantic	Deep	Atlantic	56831	590	148.3	1.2
Robinson et al.	NW Atlantic	Deep	Atlantic	56961	1844	168.2	1.4

Robinson et al.	NW Atlantic	Deep	Atlantic	57452	428	151.2	1.2
Robinson et al.	NW Atlantic	Deep	Atlantic	58309	622	150.4	1.2
Robinson et al.	NW Atlantic	Deep	Atlantic	58694	817	143.9	1.2
Robinson et al.	NW Atlantic	Deep	Atlantic	60122	1012	150.2	1.3
Robinson et al.	NW Atlantic	Deep	Atlantic	66837	4015	155.2	2.1
Robinson et al.	NW Atlantic	Deep	Atlantic	67654	1523	150.3	1.4
Robinson et al.	NW Atlantic	Deep	Atlantic	79486	741	151.8	1.2
Robinson et al.	NW Atlantic	Deep	Atlantic	85149	730	149.9	1.2
Robinson et al.	NW Atlantic	Deep	Atlantic	87274	1242	150.1	1.3
Robinson et al.	NW Atlantic	Deep	Atlantic	88025	897	149.2	1.2
Robinson et al.	NW Atlantic	Deep	Atlantic	140367	1534	174.5	1.4
Robinson et al.	NW Atlantic	Deep	Atlantic	144543	1764	173.6	1.5
Robinson et al.	NW Atlantic	Deep	Atlantic	152453	1827	150.2	1.3
Robinson et al.	NW Atlantic	Deep	Atlantic	153231	1713	163.7	1.4
Robinson et al.	NW Atlantic	Deep	Atlantic	154046	1922	154.9	1.4
Robinson et al.	NW Atlantic	Deep	Atlantic	155955	1854	159.4	1.5
Robinson et al.	NW Atlantic	Deep	Atlantic	157961	2345	157.5	1.6
Robinson et al.	NW Atlantic	Deep	Atlantic	158350	2057	157.0	1.5
Robinson et al.	NW Atlantic	Deep	Atlantic	196936	3196	168.6	1.9
Robinson et al.	NW Atlantic	Deep	Atlantic	204634	3153	146.0	1.7
Shen et al. (*72*)	Santo	Surface	Pacific	21	1	147.1	1.6
Shen et al.	Santo	Surface	Pacific	42	1	145.9	1.9
Shen et al.	Santo	Surface	Pacific	47	1	145.4	1.8
Shen et al.	Santo	Surface	Pacific	59	1	147.9	1.6
Shen et al.	Santo	Surface	Pacific	77	1	148.6	1.7
Shen et al.	Sumatra	Surface	Pacific	9	1	149.3	2.3
Shen et al.	Sumatra	Surface	Pacific	12	2	145.8	2.0
Shen et al.	Sumatra	Surface	Pacific	13	1	146.3	1.4
Shen et al.	Sumatra	Surface	Pacific	19	2	146.1	1.8
Shen et al.	Sumatra	Surface	Pacific	31	2	142.9	1.7
Shen et al.	Sumatra	Surface	Pacific	33	1	144.7	2.2
Shen et al.	Sumatra	Surface	Pacific	35	3	146.9	2.5
Shen et al.	Sumatra	Surface	Pacific	65	2	146.6	1.8
Shen et al.	Sumatra	Surface	Pacific	77	3	148.6	1.9
Shen et al.	Sumatra	Surface	Pacific	80	5	144.0	2.5
Shen et al.	Sumatra	Surface	Pacific	107	7	145.5	2.5
Shen et al.	Sumatra	Surface	Pacific	110	2	150.2	2.2
Shen et al.	Sumatra	Surface	Pacific	411	10	146.7	1.4

Shen et al.	Sumatra	Surface	Pacific	427	8	146.4	1.7
Shen et al.	Sumatra	Surface	Pacific	563	15	143.9	2.2
Shen et al.	Sumatra	Surface	Pacific	586	15	148.4	2.0
Shen et al.	Sumatra	Surface	Pacific	592	15	144.2	2.2
Shen et al.	Sumatra	Surface	Pacific	595	17	145.5	2.5
Shen et al.	Sumatra	Surface	Pacific	740	6	145.3	1.2
Shen et al.	Sumatra	Surface	Pacific	765	5	146.7	1.1
Shen et al.	Sumatra	Surface	Pacific	804	37	145.6	1.9
Shen et al.	Sumatra	Surface	Pacific	1249	53	146.9	1.7
Shen et al.	Taiwan	Surface	Pacific	4	0	146.0	2.4
Shen et al.	Taiwan	Surface	Pacific	5	3	147.1	2.0
Shen et al.	Taiwan	Surface	Pacific	7	1	145.6	1.5
Shen et al.	Taiwan	Surface	Pacific	7	2	148.1	1.9
Shen et al.	Taiwan	Surface	Pacific	8	1	147.5	1.5
Shen et al.	Taiwan	Surface	Pacific	8	1	147.2	2.2
Shen et al.	Taiwan	Surface	Pacific	9	1	150.0	2.0
Shen et al.	Taiwan	Surface	Pacific	9	1	147.1	2.2
Shen et al.	Taiwan	Surface	Pacific	10	1	148.9	2.2
Shen et al.	Taiwan	Surface	Pacific	10	1	146.6	2.1
Shen et al.	Taiwan	Surface	Pacific	10	1	151.7	2.4
Shen et al.	Taiwan	Surface	Pacific	10	1	146.7	1.6
Shen et al.	Taiwan	Surface	Pacific	12	1	150.8	2.4
Shen et al.	Taiwan	Surface	Pacific	12	1	147.5	2.1
Shen et al.	Taiwan	Surface	Pacific	13	1	145.3	2.1
Shen et al.	Taiwan	Surface	Pacific	13	1	146.7	2.2
Shen et al.	Taiwan	Surface	Pacific	13	1	146.9	2.0
Shen et al.	Taiwan	Surface	Pacific	13	1	146.3	2.1
Shen et al.	Taiwan	Surface	Pacific	13	1	147.3	2.3
Shen et al.	Taiwan	Surface	Pacific	14	1	146.7	1.7
Shen et al.	Taiwan	Surface	Pacific	14	1	147.9	2.2
Shen et al.	Taiwan	Surface	Pacific	14	0	145.9	1.6
Shen et al.	Taiwan	Surface	Pacific	17	1	145.4	2.0
Shen et al.	Taiwan	Surface	Pacific	17	1	145.8	1.7
Shen et al.	Taiwan	Surface	Pacific	17	1	149.6	2.1
Shen et al.	Taiwan	Surface	Pacific	18	0	146.7	2.2
Shen et al.	Taiwan	Surface	Pacific	20	1	146.8	2.4
Shen et al.	Taiwan	Surface	Pacific	23	1	145.0	2.0
Shen et al.	Taiwan	Surface	Pacific	24	1	145.6	1.9

Shen et al.	Taiwan	Surface	Pacific	42	1	144.9	2.0
Shen et al.	Taiwan	Surface	Pacific	47	1	144.3	1.9
Shen et al.	Vietnam	Surface	Pacific	11	2	146.4	2.5
Shen et al.	Vietnam	Surface	Pacific	14	1	147.5	2.5
Shen et al.	Vietnam	Surface	Pacific	14	1	146.3	2.4
Shen et al.	Vietnam	Surface	Pacific	24	1	148.7	2.5
Stirling[73]	Australia	Surface	Pacific	0	2	149.0	1.0
Stirling	Huon	Surface	Pacific	0	2	148.0	2.0
Stirling	Huon	Surface	Pacific	0	2	149.0	2.0
Thompson et al. (*17*)	Bahamas	Surface	Atlantic	0	0	147.3	0.2
Thompson et al.	Bahamas	Surface	Atlantic	0	0	147.5	0.5
Thompson et al.	Barbados	Surface	Atlantic	0	0	147.0	1.6
Thompson et al.	Barbados	Surface	Atlantic	0	0	145.5	1.8
Wienberg et al. (*74*)	NE Atlantic	Deep	Atlantic	23500	120	147.3	1.2
Wienberg et al.	NE Atlantic	Deep	Atlantic	36270	430	138.0	1.6
Wienberg et al.	NE Atlantic	Deep	Atlantic	45940	330	137.4	1.6
Wienberg et al.	NE Atlantic	Deep	Atlantic	17150	150	147.6	1.7
Wienberg et al.	NE Atlantic	Deep	Atlantic	23570	180	135.0	1.7
Wienberg et al.	NE Atlantic	Deep	Atlantic	20920	120	148.5	1.9
Wienberg et al.	NE Atlantic	Deep	Atlantic	14650	90	156.1	2.0
Wienberg et al.	NE Atlantic	Deep	Atlantic	22880	380	139.8	2.0
Wienberg et al.	NE Atlantic	Deep	Atlantic	41170	250	146.4	2.0
Wienberg et al.	NE Atlantic	Deep	Atlantic	43680	280	146.6	2.0
Wienberg et al.	NE Atlantic	Deep	Atlantic	30430	960	138.3	2.2
Wienberg et al.	NE Atlantic	Deep	Atlantic	21370	420	145.0	2.3
Wienberg et al.	NE Atlantic	Deep	Atlantic	49850	800	139.4	2.4
Wienberg et al.	NE Atlantic	Deep	Atlantic	19360	540	146.6	2.5
Wienberg et al.	NE Atlantic	Deep	Atlantic	34900	430	143.8	2.5
Wienberg et al.	NE Atlantic	Deep	Atlantic	37250	230	147.5	2.5
Wienberg et al.	NE Atlantic	Deep	Atlantic	57960	740	140.8	2.7
Wienberg et al.	NE Atlantic	Deep	Atlantic	22750	260	141.8	2.9
Wienberg et al.	NE Atlantic	Deep	Atlantic	25720	390	138.4	2.9
Yokoyama et al. (*75*)	Huon	Surface	Pacific	61400	600	139.0	2.0
Yokoyama et al.	Huon	Surface	Pacific	51800	800	136.0	9.0
Yokoyama et al.	Huon	Surface	Pacific	51800	1600	137.0	1.7
Yokoyama et al.	Huon	Surface	Pacific	53400	300	139.0	1.4
Yokoyama et al.	Huon	Surface	Pacific	51300	300	139.0	1.1
Yokoyama et al.	Huon	Surface	Pacific	44500	700	132.0	9.0

Yokoyama et al.	Huon	Surface	Pacific	42000	600	143.0	2.4
Yokoyama et al.	Huon	Surface	Pacific	42300	200	141.0	1.1
Yokoyama et al.	Huon	Surface	Pacific	43700	300	137.0	1.4
Yokoyama et al.	Huon	Surface	Pacific	34800	800	139.0	2.0
Yokoyama et al.	Huon	Surface	Pacific	33400	200	132.0	1.3
Yokoyama et al.	Huon	Surface	Pacific	37500	200	138.0	1.5
Yokoyama et al.	Huon	Surface	Pacific	37200	200	142.0	1.3
Yokoyama et al.	Huon	Surface	Pacific	37900	300	143.0	1.9
Yokoyama et al.	Huon	Surface	Pacific	32000	200	141.0	2.8
Yokoyama et al.	Huon	Surface	Pacific	42400	200	143.0	1.9
Yokoyama et al.	Huon	Surface	Pacific	37600	200	141.0	1.3
Yokoyama et al.	Huon	Surface	Pacific	29700	200	140.0	2.6
Yokoyama et al.	Huon	Surface	Pacific	32200	200	144.0	1.4
Yokoyama et al.	Huon	Surface	Pacific	32300	500	140.0	1.8
Yokoyama et al.	Huon	Surface	Pacific	31500	200	143.0	1.3

Table S8.

Compilation on speleothem initial $\delta^{234}U$ over the last 30 ky

Reference	Region	sample	Age (year BP)	2s error	initial $\delta^{234}U$*	2s error
Cai et al. (*76*)	central China	C996-1	160	230	311.0	4.0
Cai et al.	central China	C996-1	190	300	324.0	4.0
Cai et al.	central China	C996-2	270	50	316.0	2.0
Cai et al.	central China	C996-1	290	90	328.0	2.0
Cai et al.	central China	C996-1	480	20	318.0	2.0
Cai et al.	central China	C996-1	630	300	322.0	5.0
Cai et al.	central China	C996-2	680	60	315.0	3.0
Cai et al.	central China	C996-1	710	80	304.0	3.0
Cai et al.	central China	C996-2	1170	1290	324.0	5.0
Cai et al.	central China	C996-1	1230	110	345.0	3.0
Cai et al.	central China	C996-1	1390	20	320.0	2.0
Cai et al.	central China	C996-2	1710	110	328.0	3.0
Cai et al.	central China	C996-1	1980	420	382.0	4.0
Cai et al.	central China	C996-1	2730	80	321.0	3.0
Cai et al.	central China	C996-1	2920	410	300.0	4.0
Cai et al.	central China	C996-2	3380	1150	301.0	6.0
Cai et al.	central China	C996-1	3430	100	335.0	3.0
Cai et al.	central China	C996-1	3800	40	336.0	2.0
Cai et al.	central China	C996-1	4000	100	364.0	3.0
Cai et al.	central China	C996-2	4310	720	296.0	4.0
Cai et al.	central China	C996-2	4410	400	284.0	6.0
Cai et al.	central China	C996-2	4540	310	296.0	4.0
Cai et al.	central China	C996-1	4640	470	307.0	5.0
Cai et al.	central China	C996-1	4680	100	294.0	1.0
Cai et al.	central China	C996-1	5040	1410	314.0	5.0
Cai et al.	central China	C996-2	5280	790	294.0	8.0
Cai et al.	central China	C996-1	5380	530	320.0	4.0
Cai et al.	central China	C996-1	5760	370	258.0	5.0
Cai et al.	central China	C996-1	5850	250	288.0	3.0
Cai et al.	central China	C996-1	6620	800	377.0	10.0
Cai et al.	central China	C996-1	6790	1880	295.0	4.0
Cai et al.	central China	C996-1	7690	70	330.0	2.0
Cai et al.	central China	C996-2	8400	2040	344.0	4.0
Cai et al.	central China	C996-2	10070	190	336.0	3.0
Cai et al.	central China	C996-2	11840	240	263.0	3.0

Cai et al.	central China	C996-2	15500	100	273.0	3.0
Cai et al.	central China	C996-2	16990	90	259.0	2.0
Cai et al.	central China	C996-2	18960	180	216.0	3.0
Cheng et al. (*77*)	South America	NAR-C	2514	62	1148.0	2.7
Cheng et al.	South America	NAR-C	2952	161	1237.4	2.8
Cheng et al.	South America	NAR-C	3492	56	1086.1	2.6
Cheng et al.	South America	NAR-C	6951	90	835.6	2.5
Cheng et al.	South America	NAR-C	7433	45	989.1	2.8
Cheng et al.	South America	NAR-C	7694	48	1202.8	2.8
Cheng et al.	South America	NAR-C	8302	100	1331.7	2.8
Cheng et al.	South America	NAR-C	8398	66	1112.9	2.7
Cheng et al.	South America	NAR-C	9706	66	1276.0	2.5
Cheng et al.	South America	NAR-C	10223	61	1806.5	3.3
Cheng et al.	South America	NAR-C	10788	59	1941.0	2.9
Cheng et al.	South America	NAR-C	11838	148	1644.1	3.0
Cheng et al.	South America	NAR-C	13894	64	1698.4	2.2
Cheng et al.	South America	NAR-C	16202	247	1759.0	3.3
Cheng et al.	South America	NAR-C	16584	144	1691.5	3.2
Cheng et al.	South America	NAR-C	18027	107	1707.9	3.2
Cheng et al.	South America	NAR-C	21513	172	1613.1	3.3
Cheng et al.	South America	NAR-C	22117	86	1557.5	2.6
Cheng et al.	South America	NAR-C	24377	103	1564.2	2.8
Cheng et al.	South America	NAR-C	24507	80	1616.7	3.2
Cheng et al.	South America	NAR-C	25068	156	1607.5	3.5
Cheng et al.	South America	NAR-C	26689	72	1652.6	3.4
Cheng et al.	South America	NAR-C	29317	72	1765.1	3.0

Cheng et al.	South America	III	4314	66	1113.6	9.7
Cheng et al.	South America	III	4825	75	1131.2	11.0
Cheng et al.	South America	III	5871	119	1151.8	3.3
Cheng et al.	South America	III	9155	137	1202.5	2.2
Cheng et al.	South America	III	10580	167	1225.9	2.8
Cheng et al.	South America	III	11189	96	1229.1	2.4
Cheng et al.	South America	III	12158	141	1227.9	9.8
Cheng et al.	South America	III	12516	84	1211.8	3.0
Cheng et al.	South America	III	12988	82	1204.9	2.7
Cheng et al.	South America	III	13131	67	1196.4	2.7
Cheng et al.	South America	III	13399	62	1193.5	2.8
Cheng et al.	South America	III	14065	63	1183.2	2.9
Cheng et al.	South America	III	14736	127	1196.6	2.9
Cheng et al.	South America	III	15383	170	1234.6	10.8
Cheng et al.	South America	III	16202	223	1247.5	11.6
Cheng et al.	South America	III	17124	426	1226.0	2.9
Cheng et al.	South America	III	18001	347	1223.7	2.7
Cheng et al.	South America	III	21402	352	1262.9	11.1
Cheng et al.	South America	III	23395	113	1279.8	2.6
Cheng et al.	South America	III	24399	286	1312.0	2.9
Cheng et al.	South America	III	24524	182	1347.3	3.1
Cheng et al.	South America	III	24878	481	1368.0	9.2
Cheng et al.	South America	III	26244	106	1346.2	2.8
Cheng et al.	South America	III	28000	269	1150.0	10.7
Cheng et al.	South America	III	29111	117	1112.9	2.8

Cheng et al.	South America	III	29316	309	1157.4	12.6
Cruz et al. (*78*)	South America	Bt2	2350	130	3771.0	15.0
Cruz et al.	South America	Bt3	6300	70	3352.0	14.0
Cruz et al.	South America	Bt4	9070	460	3749.0	14.0
Cruz et al.	South America	Bt5	11430	470	3587.0	16.0
Cruz et al.	South America	Bt6	14620	260	3775.0	16.0
Cruz et al.	South America	Bt7	18620	630	3528.0	14.0
Cruz et al.	South America	Bt8	23380	320	3435.0	14.0
Cruz et al.	South America	Bt9	28200	1400	3199.0	20.0
Cruz et al. (*79*)	South America	RN1	4167	47	112.0	1.0
Cruz et al.	South America	RN1	4001	53	114.0	2.0
Cruz et al.	South America	RN1	4420	140	109.0	2.0
Cruz et al.	South America	RN1	5280	150	103.0	2.0
Cruz et al.	South America	RN1	5707	56	101.0	2.0
Cruz et al.	South America	RN1	6090	150	101.0	2.0
Cruz et al.	South America	RN1	7330	240	102.0	1.0
Cruz et al.	South America	RN1	7890	290	98.0	1.0
Cruz et al.	South America	RN1	9228	49	92.0	2.0
Cruz et al.	South America	RN1	9870	170	98.0	2.0
Cruz et al.	South America	RN1	10270	170	97.0	2.0
Cruz et al.	South America	RN1	10909	72	112.0	2.0
Cruz et al.	South America	RN1	11620	510	117.0	2.0
Cruz et al.	South America	RN1	11960	260	127.0	2.0
Cruz et al.	South America	RN1	11730	790	122.0	2.0
Cruz et al.	South America	RN1	12400	1100	126.0	3.0

Cruz et al.	South America	RN1	17063	85	140.0	2.0
Cruz et al.	South America	RN1	17329	62	141.0	1.0
Cruz et al.	South America	RN1	18360	620	148.0	1.0
Cruz et al.	South America	RN1	21800	900	143.0	1.0
Cruz et al.	South America	RN4	5210	160	101.0	3.0
Cruz et al.	South America	RN4	7230	150	96.0	2.0
Cruz et al.	South America	RN4	8080	500	91.0	2.0
Cruz et al.	South America	RN4	9000	570	94.0	3.0
Cruz et al.	South America	RN4	9690	250	96.0	2.0
Cruz et al.	South America	RN4	11030	260	113.0	4.0
Cruz et al.	South America	RN4	11920	130	117.0	2.0
Cruz et al.	South America	RN4	11830	620	117.0	3.0
Cruz et al.	South America	RN4	12930	340	129.0	17.0
Cruz et al.	South America	RN4	16440	150	132.0	1.0
Cruz et al.	South America	RN4	16400	1300	137.0	2.0
Cruz et al.	South America	RN4	16690	270	140.0	1.0
Cruz et al.	South America	RN4	17240	210	125.0	3.0
Dykoski et al. (*80*)	south China	D4	93	22	1.1	1.9
Dykoski et al.	south China	D4	183	21	5.2	3.3
Dykoski et al.	south China	D4	391	20	2.3	1.8
Dykoski et al.	south China	D4	914	33	11.8	1.5
Dykoski et al.	south China	D4	1003	41	8.9	4.8
Dykoski et al.	south China	D4	1294	32	14.4	1.5
Dykoski et al.	south China	D4	1442	70	7.3	2.4
Dykoski et al.	south China	D4	2088	47	10.8	1.7
Dykoski et al.	south China	D4	2519	59	20.0	1.5
Dykoski et al.	south China	D4	2627	138	8.9	1.4
Dykoski et al.	south China	D4	3218	56	16.3	1.7

Dykoski et al.	south China	D4	3625	60	11.4	2.2
Dykoski et al.	south China	D4	4034	84	2.5	1.2
Dykoski et al.	south China	D4	4152	51	2.1	1.6
Dykoski et al.	south China	D4	4260	50	6.0	1.3
Dykoski et al.	south China	D4	4629	87	14.2	1.8
Dykoski et al.	south China	D4	5167	57	0.8	1.3
Dykoski et al.	south China	D4	5383	109	11.1	2.2
Dykoski et al.	south China	D4	5769	53	25.0	1.3
Dykoski et al.	south China	D4	6324	60	9.5	2.0
Dykoski et al.	south China	D4	6549	64	2.9	1.6
Dykoski et al.	south China	D4	6998	38	1.1	1.2
Dykoski et al.	south China	D4	7399	62	8.2	1.3
Dykoski et al.	south China	D4	7687	44	16.3	1.3
Dykoski et al.	south China	D4	8056	74	28.9	1.6
Dykoski et al.	south China	D4	8197	75	8.9	1.6
Dykoski et al.	south China	D4	8472	64	15.8	2.3
Dykoski et al.	south China	D4	8890	73	0.4	1.6
Dykoski et al.	south China	D4	9105	416	2.9	4.7
Dykoski et al.	south China	D4	9542	78	16.3	14.0
Dykoski et al.	south China	D4	9977	112	16.2	1.9
Dykoski et al.	south China	D4	10397	77	7.3	1.5
Dykoski et al.	south China	D4	10890	118	7.3	1.9
Dykoski et al.	south China	D4	11368	88	9.1	1.3
Dykoski et al.	south China	D4	11723	88	19.4	2.5
Dykoski et al.	south China	D4	12149	81	16.2	1.9
Dykoski et al.	south China	D4	12514	91	28.7	3.3
Dykoski et al.	south China	D4	12995	90	18.2	1.7
Dykoski et al.	south China	D4	13169	95	5.0	1.6
Dykoski et al.	south China	D4	13165	98	1.5	1.7
Dykoski et al.	south China	D4	13638	104	9.8	3.2
Dykoski et al.	south China	D4	14117	103	8.6	1.8
Dykoski et al.	south China	D4	14835	114	5.6	1.9
Dykoski et al.	south China	D4	15541	95	0.0	1.5
Dykoski et al.	south China	D4	15918	108	11.0	1.4
Feng et al. (*81*)	North America	CWN-4	9500	400	364.0	1.4
Feng et al.	North America	CWN-5	9600	300	366.0	1.9
Feng et al.	North America	CWN-6	9800	400	362.0	1.9

Feng et al.	North America	CWN-7	12400	130	359.0	1.7
Feng et al.	North America	CWN-8	12290	250	364.0	2.1
Feng et al.	North America	CWN-9	12640	230	366.0	1.8
Feng et al.	North America	CWN-10	13210	130	365.0	1.3
Feng et al.	North America	CWN-11	12870	250	366.0	2.1
Feng et al.	North America	CWN-12	13060	290	364.0	2.1
Feng et al.	North America	CWN-13	13530	70	362.0	1.9
Feng et al.	North America	CWN-14	13820	40	360.0	1.7
Feng et al.	North America	CWN-15	13900	70	363.0	1.3
Feng et al.	North America	CWN-16	14090	50	360.0	1.7
Feng et al.	North America	CWN-17	14420	80	360.0	1.7
Feng et al.	North America	CWN-18	14460	50	359.0	1.5
Feng et al.	North America	CWN-19	14600	80	360.0	1.6
Feng et al.	North America	CWN-20	14810	80	358.0	1.6
Feng et al.	North America	CWN-21	14780	80	358.0	1.1
Feng et al.	North America	CWN-22	14890	50	360.0	1.7
Feng et al.	North America	CWN-23	15320	50	361.0	1.9
Feng et al.	North America	CWN-24	15410	50	359.0	1.7
Feng et al.	North America	CWN-25	15440	50	359.0	1.7
Feng et al.	North America	CWN-26	15420	80	357.0	1.4
Feng et al.	North America	CWN-27	17320	110	370.0	2.0
Feng et al.	North America	CWN-28	17460	60	360.0	1.9
Feng et al.	North America	CWN-29	17700	60	362.0	1.7
Feng et al.	North America	CWN-30	19190	50	370.0	2.0
Feng et al.	North America	CWN-31	21360	140	377.0	1.7

Feng et al.	North America	CWN-32	28550	170	353.0	1.9
Fleitmann et al. (*82*)	Turkey	So-1	494	12	1081.9	1.0
Fleitmann et al.	Turkey	So-1	1019	23	1057.9	1.0
Fleitmann et al.	Turkey	So-1	2025	34	1100.0	1.0
Fleitmann et al.	Turkey	So-1	3255	56	1066.9	1.0
Fleitmann et al.	Turkey	So-1	4072	78	1086.9	2.0
Fleitmann et al.	Turkey	So-1	4502	94	1051.9	2.0
Fleitmann et al.	Turkey	So-1	4704	80	968.0	2.0
Fleitmann et al.	Turkey	So-1	5398	76	959.7	1.0
Fleitmann et al.	Turkey	So-1	5678	85	953.1	3.0
Fleitmann et al.	Turkey	So-1	6299	139	964.7	1.0
Fleitmann et al.	Turkey	So-1	6833	121	911.6	1.0
Fleitmann et al.	Turkey	So-1	7075	90	907.8	1.0
Fleitmann et al.	Turkey	So-1	7279	81	924.2	1.0
Fleitmann et al.	Turkey	So-1	7698	132	962.2	1.0
Fleitmann et al.	Turkey	So-1	7734	125	1007.4	2.0
Fleitmann et al.	Turkey	So-1	8226	90	1007.1	2.0
Fleitmann et al.	Turkey	So-1	8456	76	970.5	1.0
Fleitmann et al.	Turkey	So-1	9183	122	978.7	1.0
Fleitmann et al.	Turkey	So-1	9645	127	962.8	1.0
Fleitmann et al.	Turkey	So-1	10211	173	1068.9	1.0
Fleitmann et al.	Turkey	So-1	10702	104	1046.0	1.0
Fleitmann et al.	Turkey	So-1	11025	156	1038.5	1.0
Fleitmann et al.	Turkey	So-1	11951	153	1012.9	3.0
Fleitmann et al.	Turkey	So-1	12184	148	1027.6	3.0
Fleitmann et al.	Turkey	So-1	13091	220	1005.9	1.0
Fleitmann et al.	Turkey	So-1	12994	126	1008.4	2.0
Fleitmann et al.	Turkey	So-1	13311	102	1085.0	2.0
Fleitmann et al.	Turkey	So-1	14295	162	1144.9	1.0
Fleitmann et al.	Turkey	So-1	14585	296	1101.9	16.0
Fleitmann et al.	Turkey	So-1	17032	178	1175.2	1.0
Fleitmann et al.	Turkey	So-1	17293	174	1119.1	2.0
Fleitmann et al.	Turkey	So-1	19204	234	1210.8	1.0
Fleitmann et al.	Turkey	So-1	20276	188	1128.5	2.0
Fleitmann et al.	Turkey	So-1	21208	213	1162.8	1.0
Fleitmann et al.	Turkey	So-1	25265	246	1116.9	1.0
Fleitmann et al.	Turkey	So-1	27114	267	1228.4	2.0

Fleitmann et al.	Turkey	So-1	29427	340	1221.3	2.0
Hellstrom et al. (*83*)	New Zealand	MD3	5401	275	391.0	44.0
Hellstrom et al.	New Zealand	MD3	9018	782	386.5	4.0
Hellstrom et al.	New Zealand	MD3	11382	1157	406.5	7.0
Hellstrom et al.	New Zealand	MD3	13850	878	466.0	13.0
Hellstrom et al.	New Zealand	MD3	14499	322	460.4	7.0
Hellstrom et al.	New Zealand	MD3	15699	145	476.8	5.0
Hellstrom et al.	New Zealand	MD3	20533	1868	488.2	5.0
Hellstrom et al.	New Zealand	MD3	27469	2417	497.3	57.0
Partin et al. (*84*)	Malaysia	BA04	1294	1843	-612.1	0.4
Partin et al.	Malaysia	BA04	2120	4458	-600.6	0.4
Partin et al.	Malaysia	BA04	2185	1805	-605.6	0.4
Partin et al.	Malaysia	BA04	2269	675	-620.2	0.2
Partin et al.	Malaysia	BA04	4039	1653	-611.3	0.5
Partin et al.	Malaysia	BA04	6589	104	-619.2	0.2
Partin et al.	Malaysia	BA04	8544	58	-613.2	1.3
Partin et al.	Malaysia	BA04	9078	254	-611.1	0.2
Partin et al.	Malaysia	BA04	9313	197	-611.2	0.1
Partin et al.	Malaysia	BA04	9332	73	-612.0	0.2
Partin et al.	Malaysia	BA04	9411	103	-612.5	0.2
Partin et al.	Malaysia	BA04	10160	407	-607.8	0.2
Partin et al.	Malaysia	BA04	10834	1032	-604.5	0.3
Partin et al.	Malaysia	BA04	10948	118	-609.1	0.2
Partin et al.	Malaysia	BA04	11203	45	-605.3	0.1
Partin et al.	Malaysia	BA04	11213	330	-607.4	0.2
Partin et al.	Malaysia	BA04	11238	71	-603.2	0.2
Partin et al.	Malaysia	BA04	11302	66	-604.8	0.1
Partin et al.	Malaysia	BA04	11490	42	-606.0	1.3
Partin et al.	Malaysia	BA04	11743	30	-606.3	0.2
Partin et al.	Malaysia	BA04	11744	247	-604.9	0.2
Partin et al.	Malaysia	BA04	13363	165	-604.8	1.2
Partin et al.	Malaysia	BA04	13487	661	-605.3	0.2
Partin et al.	Malaysia	BA04	14346	298	-606.8	1.3
Partin et al.	Malaysia	BA04	14564	106	-599.7	1.3
Partin et al.	Malaysia	BA04	15066	798	-597.0	0.2
Partin et al.	Malaysia	BA04	15545	363	-596.0	0.3
Partin et al.	Malaysia	BA04	15655	298	-597.4	0.2
Partin et al.	Malaysia	BA04	15673	93	-599.7	0.2

Partin et al.	Malaysia	BA04	15823	384	-594.1	0.2
Partin et al.	Malaysia	BA04	16415	241	-596.3	0.2
Partin et al.	Malaysia	BA04	17999	103	-595.7	1.2
Partin et al.	Malaysia	BA04	18349	222	-595.1	1.3
Partin et al.	Malaysia	BA04	19043	121	-596.4	0.2
Partin et al.	Malaysia	BA04	19968	293	-593.7	1.3
Partin et al.	Malaysia	BA04	20937	78	-598.2	0.2
Partin et al.	Malaysia	BA04	21313	188	-594.2	0.3
Partin et al.	Malaysia	BA04	21555	80	-595.2	0.3
Partin et al.	Malaysia	BA04	21571	99	-594.2	0.3
Partin et al.	Malaysia	BA04	22890	62	-589.7	0.2
Partin et al.	Malaysia	BA04	23391	50	-584.6	0.2
Partin et al.	Malaysia	BA04	25638	118	-580.8	0.2
Partin et al.	Malaysia	BA04	25683	65	-582.6	1.2
Partin et al.	Malaysia	BA04	26706	259	-580.8	0.4
Partin et al.	Malaysia	SCH02	2689	305	-320.8	0.5
Partin et al.	Malaysia	SCH02	3728	171	-355.9	0.4
Partin et al.	Malaysia	SCH02	5810	110	-353.7	0.3
Partin et al.	Malaysia	SCH02	6285	314	-342.8	0.2
Partin et al.	Malaysia	SCH02	6712	23	-342.2	0.2
Partin et al.	Malaysia	SCH02	6902	104	-333.3	0.3
Partin et al.	Malaysia	SCH02	11929	166	-355.8	0.3
Partin et al.	Malaysia	SCH02	12083	79	-355.5	0.2
Partin et al.	Malaysia	SCH02	12883	72	-343.0	0.3
Partin et al.	Malaysia	SCH02	12951	53	-347.0	0.2
Partin et al.	Malaysia	SCH02	13064	121	-349.2	0.3
Partin et al.	Malaysia	SCH02	13391	124	-331.1	0.3
Partin et al.	Malaysia	SCH02	13824	219	-324.8	0.3
Partin et al.	Malaysia	SCH02	14148	33	-334.4	0.3
Partin et al.	Malaysia	SCH02	14850	191	-354.1	0.2
Partin et al.	Malaysia	SCH02	14950	58	-354.7	0.2
Partin et al.	Malaysia	SCH02	15426	149	-353.9	0.2
Partin et al.	Malaysia	SCH02	15601	28	-337.8	0.2
Partin et al.	Malaysia	SCH02	15800	36	-337.9	0.2
Partin et al.	Malaysia	SCH02	16146	231	-337.1	0.2
Partin et al.	Malaysia	SCH02	16648	201	-338.5	0.3
Partin et al.	Malaysia	SCH02	17150	179	-359.1	0.2
Partin et al.	Malaysia	SCH02	18318	149	-356.3	0.3

Partin et al.	Malaysia	SCH02	18481	162	-352.7	0.4
Partin et al.	Malaysia	SCH02	18893	187	-360.5	0.3
Partin et al.	Malaysia	SCH02	19855	158	-362.2	0.2
Partin et al.	Malaysia	SCH02	21256	210	-360.5	0.3
Partin et al.	Malaysia	SCH02	22591	245	-360.7	0.2
Partin et al.	Malaysia	SCH02	22856	180	-358.7	0.3
Partin et al.	Malaysia	SCH02	23835	106	-352.3	0.2
Partin et al.	Malaysia	SCH02	25012	155	-350.7	0.3
Partin et al.	Malaysia	SCH02	26387	149	-335.4	0.4
Partin et al.	Malaysia	SCH02	26945	219	-342.0	0.4
Partin et al.	Malaysia	SCH02	27202	114	-341.5	0.3
Partin et al.	Malaysia	SSC01	593	118	-57.1	0.6
Partin et al.	Malaysia	SSC01	1145	280	-69.0	0.5
Partin et al.	Malaysia	SSC01	3802	2379	-81.5	0.5
Partin et al.	Malaysia	SSC01	3911	898	-83.6	0.5
Partin et al.	Malaysia	SSC01	4333	84	-86.3	0.5
Partin et al.	Malaysia	SSC01	5280	126	-85.7	1.1
Partin et al.	Malaysia	SSC01	5460	144	-85.2	1.3
Partin et al.	Malaysia	SSC01	5591	187	-82.6	0.4
Partin et al.	Malaysia	SSC01	6450	2007	-147.7	0.8
Partin et al.	Malaysia	SSC01	6648	183	-93.9	0.4
Partin et al.	Malaysia	SSC01	8156	545	-95.8	0.7
Partin et al.	Malaysia	SSC01	8462	443	-93.1	0.8
Partin et al.	Malaysia	SSC01	8747	113	-91.1	0.5
Partin et al.	Malaysia	SSC01	9729	96	-96.6	0.5
Partin et al.	Malaysia	SSC01	10043	533	-106.6	0.9
Partin et al.	Malaysia	SSC01	10165	532	-98.1	0.5
Partin et al.	Malaysia	SSC01	10581	362	-103.4	0.5
Partin et al.	Malaysia	SSC01	11438	161	-105.1	0.5
Partin et al.	Malaysia	SSC01	11569	143	-103.7	0.5
Partin et al.	Malaysia	SSC01	12080	1092	-105.5	0.5
Partin et al.	Malaysia	SSC01	13122	350	-111.9	0.4
Partin et al.	Malaysia	SSC01	13231	174	-112.5	0.5
Partin et al.	Malaysia	SSC01	13351	122	-113.1	0.5
Partin et al.	Malaysia	SSC01	13397	117	-112.0	0.4
Partin et al.	Malaysia	SSC01	13725	188	-94.5	0.5
Partin et al.	Malaysia	SSC01	14437	107	-120.5	0.5
Partin et al.	Malaysia	SSC01	14925	1297	-107.4	0.5

Partin et al.	Malaysia	SSC01	15049	76	-112.7	0.4
Partin et al.	Malaysia	SSC01	15892	85	-111.5	0.5
Partin et al.	Malaysia	SSC01	15906	109	-111.8	0.5
Partin et al.	Malaysia	SSC01	15977	78	-115.2	0.5
Partin et al.	Malaysia	SSC01	16075	65	-116.1	0.5
Partin et al.	Malaysia	SSC01	16336	128	-109.8	0.5
Partin et al.	Malaysia	SSC01	16369	730	-130.6	13.8
Partin et al.	Malaysia	SSC01	17306	142	-146.8	0.5
Partin et al.	Malaysia	SSC01	17598	279	-140.0	1.0
Partin et al.	Malaysia	SSC01	18102	878	-133.5	1.3
Partin et al.	Malaysia	SSC01	18947	918	-152.1	1.4
Partin et al.	Malaysia	SSC01	19052	123	-143.7	0.5
Partin et al.	Malaysia	SSC01	19712	91	-116.0	0.5
Partin et al.	Malaysia	SSC01	20353	866	-118.7	1.2
Partin et al.	Malaysia	SSC01	20538	1379	-117.7	1.8
Partin et al.	Malaysia	SSC01	20747	918	-118.5	1.3
Partin et al.	Malaysia	SSC01	21028	1088	-118.4	1.5
Partin et al.	Malaysia	SSC01	22120	123	-125.1	0.5
Partin et al.	Malaysia	SSC01	23510	149	-130.6	0.6
Partin et al.	Malaysia	SSC01	24055	270	-123.2	0.4
Partin et al.	Malaysia	SSC01	24307	979	-116.4	1.4
Partin et al.	Malaysia	SSC01	24668	172	-106.6	0.5
Partin et al.	Malaysia	SSC01	26552	1187	-124.6	1.7
Partin et al.	Malaysia	SSC01	27020	223	-119.6	0.6
Rowe et al. (*85*)	Turkey	K1	5960	160	250.5	4.2
Rowe et al.	Turkey	K1	6600	120	173.7	3.9
Rowe et al.	Turkey	K1	6380	130	236.6	4.8
Rowe et al.	Turkey	K1	7160	130	279.8	4.7
Rowe et al.	Turkey	K1	8890	200	251.9	4.0
Rowe et al.	Turkey	K1	12980	690	259.5	5.7
Rowe et al.	Turkey	K1	17620	330	351.9	5.8
Rowe et al.	Turkey	K1	17990	330	417.2	8.6
Rowe et al.	Turkey	K1	24480	440	364.6	5.8
Rowe et al.	Turkey	K1	26310	470	396.5	3.8
Shakun et al. (*86*)	Yemen	M1-5	588	15	-70.8	1.2
Shakun et al.	Yemen	M1-5	11086	122	-35.8	1.1
Shakun et al.	Yemen	M1-5	11864	107	-11.6	0.9
Shakun et al.	Yemen	M1-5	11971	137	-1.4	0.7

Shakun et al.	Yemen	M1-5	13085	137	1.4	0.6
Shakun et al.	Yemen	M1-5	13421	198	9.8	1.0
Shakun et al.	Yemen	M1-5	13558	183	10.9	0.8
Shakun et al.	Yemen	M1-5	13558	183	17.9	0.7
Shakun et al.	Yemen	M1-5	14199	183	6.6	0.8
Shakun et al.	Yemen	M1-5	14428	168	4.3	0.6
Shakun et al.	Yemen	M1-5	14534	122	16.4	1.2
Shakun et al.	Yemen	M1-5	14931	183	20.9	1.1
Shakun et al.	Yemen	M1-5	15908	214	25.2	0.6
Shakun et al.	Yemen	M1-5	15999	214	10.5	0.6
Shakun et al.	Yemen	M1-5	16365	153	13.0	0.9
Shakun et al.	Yemen	M1-5	16655	198	6.1	0.7
Shakun et al.	Yemen	M1-5	17342	214	-2.0	0.6
Shakun et al.	Yemen	M1-5	17739	183	-4.5	0.6
Shakun et al.	Yemen	M1-5	18929	214	-38.1	0.6
Shakun et al.	Yemen	M1-5	19371	198	-30.6	0.7
Shakun et al.	Yemen	M1-5	20852	229	-62.0	0.6
Shakun et al.	Yemen	M1-5	20974	244	-64.2	0.6
Shakun et al.	Yemen	M1-5	22316	275	-42.5	0.6
Shakun et al.	Yemen	M1-5	24208	275	1.9	0.8
Shakun et al.	Yemen	M1-5	25673	275	-11.1	0.6
Shakun et al.	Yemen	M1-5	26131	244	-12.7	0.6
Shakun et al.	Yemen	M1-5	26802	275	-10.4	0.6
Shakun et al.	Yemen	M1-5	27108	305	-15.1	0.8
Wagner et al. (*87*)	North America	COB-01-02	9487	138	1470.0	N.A.
Wagner et al.	North America	COB-01-02	10266	128	1480.0	N.A.
Wagner et al.	North America	COB-01-02	11009	56	1480.0	N.A.
Wagner et al.	North America	COB-01-02	11784	48	1520.0	N.A.
Wagner et al.	North America	COB-01-02	12013	94	1530.0	N.A.
Wagner et al.	North America	COB-01-02	12211	135	1540.0	N.A.
Wagner et al.	North America	COB-01-02	12469	207	1540.0	N.A.
Wagner et al.	North America	COB-01-02	12696	113	1550.0	N.A.
Wagner et al.	North America	COB-01-02	12997	218	1540.0	N.A.

Wagner et al.	North America	COB-01-02	13137	218	1540.0	N.A.
Wagner et al.	North America	COB-01-02	13456	232	1550.0	N.A.
Wagner et al.	North America	COB-01-02	14641	105	1580.0	N.A.
Wagner et al.	North America	COB-01-02	16406	81	1640.0	N.A.
Wagner et al.	North America	COB-01-02	16746	120	1630.0	N.A.
Wagner et al.	North America	COB-01-02	18255	123	1650.0	N.A.
Wagner et al.	North America	COB-01-02	19781	136	1650.0	N.A.
Wagner et al.	North America	COB-01-02	20868	76	1680.0	N.A.
Wagner et al.	North America	COB-01-02	23149	109	1690.0	N.A.
Wang et al. (*88*)	South America	BTV3A	1280	10	2766.0	6.0
Wang et al.	South America	BTV3A	4910	40	2684.0	4.0
Wang et al.	South America	BTV3A	7990	40	2599.0	5.0
Wang et al.	South America	BTV3A	8650	110	2609.0	8.0
Wang et al.	South America	BTV3A	12150	120	2715.0	9.0
Wang et al.	South America	BTV3A	16210	150	2867.0	13.0
Wang et al.	South America	BTV3A	21390	220	2899.0	12.0
Wang et al.	South America	BTV3A	28220	140	2907.0	5.0

* only those samples that covered the last deglacial period were compiled here

Supplementary References

35. L. F. Robinson, "RRS James Cook Cruise JC094, October 13–November 30 2013, Tenerife-Trinidad. TROPICS, Tracing Oceanic Processes using Corals and Sediments. Reconstructing abrupt Changes in Chemistry and Circulation of the Equatorial Atlantic Ocean: Implications for global Climate and deep-water Habitats.," (University of Bristol, 2014).
36. T. Chen *et al.*, Synchronous centennial abrupt events in the ocean and atmosphere during the last deglaciation. *Science* **349**, 1537-1541 (2015).

37. E. Mittelstaedt, A. S. Soule, K. S. Harpp, D. Fornari, Variations in Crustal Thickness, Plate Rigidity, and Volcanic Processes Throughout the Northern Galápagos Volcanic Province, in *The Galápagos*. John Wiley & Sons, Inc. p. 263-284 (2014)
38. S. Carey *et al.*, Exploring the Undersea World of the Galápagos Islands. *Oceanography Magazine* **29**, 32-34 (2016).
39. H. Cheng, J. Adkins, R. L. Edwards, E. A. Boyle, U-Th dating of deep-sea corals. *Geochim. Cosmochim. Acta* **64**, 2401-2416 (2000).
40. H. Cheng *et al.*, The half-lives of uranium-234 and thorium-230. *Chem. Geol*. **169**, 17-33 (2000).
41. A. K. Singh, F. Marcantonio, M. Lyle, Water column Th-230 systematics in the eastern equatorial Pacific Ocean and implications for sediment focusing. *Earth Planet. Sci. Lett.* **362**, 294-304 (2013).
42. R. Edwards, C. Gallup, H. Cheng, Uranium-series dating of marine and lacustrine carbonates. *Rev. Mineral. Geochem.* **52**, 363-405 (2003).
43. J. Marshall, K. Speer, Closure of the meridional overturning circulation through Southern Ocean upwelling. *Nat. Geosci.* **5**, 171-180 (2012).
44. A. Gnanadesikan, A simple predictive model for the structure of the oceanic pycnocline. *Science* **283**, 2077-2079 (1999).
45. M. Nikurashin, G. Vallis, A Theory of the Interhemispheric Meridional Overturning Circulation and Associated Stratification. *J. Phys. Oceanogr.* **42**, 1652-1667 (2012).
46. M. P. Hain, D. M. Sigman, G. H. Haug, Carbon dioxide effects of Antarctic stratification, North Atlantic Intermediate Water formation, and subantarctic nutrient drawdown during the last ice age: Diagnosis and synthesis in a geochemical box model. *Global Biogeochem. Cycles* **24**, (2010).
47. M. B. Andersen, D. Vance, A. R. Keech, J. Rickli, G. Hudson, Estimating U fluxes in a high-latitude, boreal post-glacial setting using U-series isotopes in soils and rivers. *Chem. Geol.* **354**, 22-32 (2013).
48. P. J. Reimer *et al.*, Intcal09 and Marine09 Radiocarbon Age Calibration Curves, 0-50,000 Years Cal Bp. *Radiocarbon* **51**, 1111-1150 (2009).
49. L. F. Robinson *et al.*, Deep-sea scleractinian coral age and depth distributions in the northwest Atlantic for the last 225,000 years. *Bull. Mar. Sci.* **81**, 371-391 (2007).
50. M. Gutjahr *et al.*, Structural limitations in deriving accurate U-series ages from calcitic cold-water corals contrast with robust coral radiocarbon and Mg/Ca systematics. *Chem. Geol.* **355**, 69-87 (2013).
51. L. F. Robinson *et al.*, Primary U distribution in scleractinian corals and its implications for U series dating. *Geochem. Geophys. Geosyst.* **7**, (2006).
52. A. Dutton, K. Lambeck, Ice Volume and Sea Level During the Last Interglacial. *Science* **337**, 216-219 (2012).
53. C. D. Gallup, R. L. Edwards, R. G. Johnson, The Timing of High Sea Levels over the Past 200,000 Years. *Science* **263**, 796-800 (1994).
54. C. H. Stirling, M. B. Andersen, Uranium-series dating of fossil coral reefs: Extending the sea-level record beyond the last glacial cycle. *Earth Planet. Sci. Lett.* **284**, 269-283 (2009).
55. W. G. Thompson, M. W. Spiegelman, S. L. Goldstein, R. C. Speed, An open-system model for U-series age determinations of fossil corals. *Earth Planet. Sci. Lett.* **210**, 365-381 (2003).
56. D. Scholz, A. Mangini, T. Felis, U-series dating of diagenetically altered fossil reef corals. *Earth Planet. Sci. Lett.* **218**, 163-178 (2004).
57. B. Villemant, N. Feuillet, Dating open systems by the 238U–234U–230Th method: application to Quaternary reef terraces. *Earth Planet. Sci. Lett.* **210**, 105-118 (2003).

58. P. J. Tomiak *et al.*, The role of skeletal micro-architecture in diagenesis and dating of Acropora palmata. *Geochim. Cosmochim. Acta* **183**, 153-175 (2016).
59. R. Schlitzer. (2015).
60. E. Bard, B. Hamelin, D. Delanghe-Sabatier, Deglacial Meltwater Pulse 1B and Younger Dryas Sea Levels Revisited with Boreholes at Tahiti. *Science* **327**, 1235-1237 (2010).
61. A. Burke, L. F. Robinson, The Southern Ocean's Role in Carbon Exchange During the Last Deglaciation. *Science* **335**, 557-561 (2012).
62. K. M. Cobb, C. D. Charles, H. Cheng, M. Kastner, R. L. Edwards, U/Th-dating living and young fossil corals from the central tropical Pacific. *Earth Planet. Sci. Lett.* **210**, 91-103 (2003).
63. L. B. Collins, J.-X. Zhao, H. Freeman, A high-precision record of mid–late Holocene sea-level events from emergent coral pavements in the Houtman Abrolhos Islands, southwest Australia. *Quat. Int.* **145–146**, 78-85 (2006).
64. E. R. M. Druffel *et al.*, Low reservoir ages for the surface ocean from mid-Holocene Florida corals. *Paleoceanography* **23**, (2008).
65. N. Durand *et al.*, Comparison of 14C and U-Th ages in corals from IODP# 310 cores offshore Tahiti. *Radiocarbon* **55**, 1947-1974 (2013).
66. R. G. Fairbanks *et al.*, Radiocarbon calibration curve spanning 0 to 50,000 years BP based on paired 230 Th/234 U/238 U and 14 C dates on pristine corals. *Quat. Sci. Rev.* **24**, 1781-1796 (2005).
67. N. Frank *et al.*, Northeastern Atlantic cold-water coral reefs and climate. *Geology* **39**, 743-746 (2011).
68. S. K. Hines, J. R. Southon, J. F. Adkins, A high-resolution record of Southern Ocean intermediate water radiocarbon over the past 30,000 years. *Earth Planet. Sci. Lett.* **432**, 46-58 (2015).
69. A. Mangini *et al.*, Deep sea corals off Brazil verify a poorly ventilated Southern Pacific Ocean during H2, H1 and the Younger Dryas. *Earth Planet. Sci. Lett.* **293**, 269-276 (2010).
70. H. G. Multer, E. Gischler, J. Lundberg, K. Simmons, E. Shinn, Key Largo Limestone revisited: Pleistocene shelf-edge facies, Florida Keys, USA. *Facies* **46**, 229-271 (2002).
71. L. F. Robinson, N. S. Belshaw, G. M. Henderson, U and Th concentrations and isotope ratios in modern carbonates and waters from the Bahamas. *Geochim. Cosmochim. Acta* **68**, 1777-1789 (2004).
72. C.-C. Shen *et al.*, Variation of initial 230 Th/232 Th and limits of high precision U–Th dating of shallow-water corals. *Geochim. Cosmochim. Acta* **72**, 4201-4223 (2008).
73. C. Stirling, T. Esat, M. McCulloch, K. Lambeck, High-precision U-series dating of corals from Western Australia and implications for the timing and duration of the Last Interglacial. *Earth Planet. Sci. Lett.* **135**, 115-130 (1995).
74. C. Wienberg *et al.*, Glacial cold-water coral growth in the Gulf of Cadiz: Implications of increased palaeo-productivity. *Earth Planet. Sci. Lett.* **298**, 405-416 (2010).
75. Y. Yokoyama, T. M. Esat, K. Lambeck, Coupled climate and sea-level changes deduced from Huon Peninsula coral terraces of the last ice age. *Earth Planet. Sci. Lett.* **193**, 579-587 (2001).
76. Y. J. Cai *et al.*, The variation of summer monsoon precipitation in central China since the last deglaciation. *Earth Planet. Sci. Lett.* **291**, 21-31 (2010).
77. H. Cheng *et al.*, Climate change patterns in Amazonia and biodiversity. *Nat. Commun.* **4**, (2013).

78. F. W. Cruz *et al.*, Insolation-driven changes in atmospheric circulation over the past 116,000 years in subtropical Brazil. *Nature* **434**, 63-66 (2005).
79. F. W. Cruz *et al.*, Orbitally driven east-west antiphasing of South American precipitation. *Nat. Geosci.* **2**, 210-214 (2009).
80. C. A. Dykoski *et al.*, A high-resolution, absolute-dated Holocene and deglacial Asian monsoon record from Dongge Cave, China. *Earth Planet. Sci. Lett.* **233**, 71-86 (2005).
81. W. M. Feng *et al.*, Changing amounts and sources of moisture in the U.S. southwest since the Last Glacial Maximum in response to global climate change (vol 401, pg 47, 2014). *Earth Planet. Sci. Lett.* **407**, 234-234 (2014).
82. D. Fleitmann *et al.*, Timing and climatic impact of Greenland interstadials recorded in stalagmites from northern Turkey. *Geophys. Res. Lett.* **36**, (2009).
83. J. Hellstrom, M. McCulloch, J. Stone, A detailed 31,000-year record of climate and vegetation change, from the isotope geochemistry of two New Zealand speleothems. *Quat. Res.* **50**, 167-178 (1998).
84. J. W. Partin, K. M. Cobb, J. F. Adkins, B. Clark, D. P. Fernandez, Millennial-scale trends in west Pacific warm pool hydrology since the Last Glacial Maximum. *Nature* **449**, 452-U453 (2007).
85. P. J. Rowe *et al.*, Speleothem isotopic evidence of winter rainfall variability in northeast Turkey between 77 and 6 ka. *Quat. Sci. Rev.* **45**, 60-72 (2012).
86. J. D. Shakun *et al.*, A high-resolution, absolute-dated deglacial speleothem record of Indian Ocean climate from Socotra Island, Yemen. *Earth Planet. Sci. Lett.* **259**, 442-456 (2007).
87. J. D. M. Wagner *et al.*, Moisture variability in the southwestern United States linked to abrupt glacial climate change. *Nat. Geosci.* **3**, 110-113 (2010).
88. X. F. Wang *et al.*, Millennial-scale precipitation changes in southern Brazil over the past 90,000 years. *Geophys. Res. Lett.* **34**, (2007).
89. A. Dai, K. E. Trenberth, in *Proceedings of the Symposium on Observing and Understanding the Variability of Water in Weather and Climate, 83rd Annual American Meteorological Society Meeting, Long Beach, CA*. (2003), pp. 1-18.
90. E. Y. Kwon *et al.*, Global estimate of submarine groundwater discharge based on an observationally constrained radium isotope model. *Geophys. Res. Lett.* **41**, 8438-8444 (2014).